ISTANBUL TECHNICAL UNIVERSITY ★ GRADUATE SCHOOL

A NEW ANTENNA DESIGN METHODOLOGY BASED ON PERFORMANCE ANALYSIS OF MIMO AND DEFINING NOVEL ANTENNA PARAMETERS

Ph.D. THESIS

Abubeker Abdulkerim YUSSUF

Department of Electronics and Communications Engineering

Telecommunications Engineering Programme

MAY 2024

ISTANBUL TECHNICAL UNIVERSITY ★ GRADUATE SCHOOL

A NEW ANTENNA DESIGN METHODOLOGY BASED ON PERFORMANCE ANALYSIS OF MIMO AND DEFINING NOVEL ANTENNA PARAMETERS

Ph.D. THESIS

Abubeker Abdulkerim YUSSUF
(504122305)

Department of Electronics and Communications Engineering

Telecommunications Engineering Programme

Thesis Advisor: Prof. Dr. Selcuk PAKER

MAY 2024

İSTANBUL TEKNİK ÜNİVERSİTESİ ★ LİSANSÜSTÜ EĞİTİM ENSTİTÜSÜ

MIMO PERFORMANS ANALIZINE VE ANTEN PARAMETRELERINI TANIMLAMAYA DAYALI YENI BIR ANTEN TASARIM METODOLOJISI

DOKTORA TEZİ

Abubeker Abdulkerim YUSSUF
(504122305)

Elektronık ve Haberleşme Mühendisliği Anabilim Dalı

Telekomŭnıkasyon Mühendisliği Programı

Tez Danışmanı: Prof. Dr. Selcuk PAKER

MAYIS 2024

Abubeker Abdulkerim YUSSUF, a Ph.D. student of ITU Graduate School student ID 504122305, successfully defended the dissertation entitled "A NEW ANTENNA DESIGN METHODOLOGY BASED ON PERFORMANCE ANALYSIS OF MIMO AND DEFINING NOVEL ANTENNA PARAMETERS", which he/she prepared after fulfilling the requirements specified in the associated legislations, before the jury whose signatures are below.

Thesis Advisor :	**Prof. Dr. Selcuk PAKER** Istanbul Technical University	.....
Jury Members :	**Prof. Dr. Mesut KARTAL** Istanbul Technical University	.....
	Assoc. Prof. Dr. Ertuğrul BAŞAR Koç University	.....
	Assoc. Dr. Mehmet Nuri AKINCI Istanbul Technical University	.....
	Prof. Dr. Mustafa Emre AYDEMIR Istanbul Arel University	.....

Date of Submission : 05 January 2024
Date of Defense : 08 May 2024

To my mother, Fatma, and my father, Abdulkerim,

FOREWORD

First and foremost, I would like to express my deep gratitude and praise to Allah Almighty, who has bestowed upon me the mental and physical strength, as well as His blessings and guidance, to complete this thesis. This thesis would not have been accomplished without the assistance and guidance of a number of individuals, without whom its completion would not have been possible.

There are no proper words to express my deep gratitude and respect for my academic and thesis supervisor, Prof. Dr. Selcuk PAKER, for offering me this opportunity. I am grateful for his kind support, incisive guidance, insightful advice, and encouragement, particularly for the generous time he has devoted to me during the whole time of my studies at Istanbul Technical University, Turkey.

Besides my advisor, I would like to express my gratitude to the members of my thesis committee: Assoc. Prof. Dr. Ertugrul BASAR, Prof. Dr. Mesut KARTAL, Prof. Dr. Mustafa Emre AYDEMIR, and Assoc. Dr. Mehmet Nuri AKINCI for their helpful and insightful feedback toward improving my work, which helped me develop a broader perspective on my thesis. Thank you for examining my work and for your valuable suggestions that helped improve the quality of this manuscript.

No research is possible without laboratory work and services. I appreciate the RF Laboratory group of the Electric and Electronics Engineering Faculty of ITU and particularly Dr. H. Bulent YAGCI for all the support and resources that gave me the opportunity to do my work.

Above all, none of this would have been possible without my family's love and patience, especially that of my father Abdulkerim and my mother Fatma. I also owe my deepest gratitude to people who have lent me encouragement and support in my PhD journey, such as Asst. Prof. Dr. Osman YUSSUF and Asst. Prof. Dr. Tewodros Assefa NIGUSSIE.

In summary, I would like to thank all the people and institutions that have supported me during my PhD journey, and I am grateful for their help and guidance in the completion of this thesis.

May 2024

Abubeker Abdulkerim YUSSUF

Telecommunication Engineering (Ph.D.)

TABLE OF CONTENTS

Page

ABBREVIATIONS

3GPP : 3rd Generation Partnership Project
4G : Fourth Generation
5G : Fifth Generation mobile networks
CCL : Channel Capacity Loss
CSI : Channel State Information
CSRR : Complementary Split Ring Resonator
CSRs : Complementary Spiral Rings
CST : Computer Simulation Technology
DN : Decoupling networks
DGS : Defected Ground structure
ECC : Envelope Correlation Coefficient
E field : Electric field
EM : Electromagnetic
FCC : Federal Communications Commission
H field : Magnetic field
HFSS : High Frequency Structure Simulator
i.i.d : ideal independent and identically distributed
LOS : Line of Sight
LTE : Long Term Evolution
MC : Mutual coupling
MEG : Mean Effective Gain
MIMO : Multiple-Input Multiple-Output
MTM : Metamaterial
NL : Neutralization Lines
NR : New Radio
OFDM : Orthogonal Frequency-Division Multiplexing
PCB : Printed Circuit Board
PEC : Perfect Electric Conductor
RF : Radio Frequency
SP : Scattering Parameters
SISO : Single-Input Single-Output
SNR : Signal to noise ratio
SRR : Split Ring Resonator
STBC : Space-Time Block Coding
TARC : Total Active Reflection Coefficient
TL : Transmission Line
UE : User Equipment
Wi-Fi : Wireless Fidelity
XPR : Cross Polarization power ratio

LIST OF TABLES

Page

LIST OF FIGURES

Page

A NEW ANTENNA DESIGN METHODOLOGY BASED ON PERFORMANCE ANALYSIS OF MIMO AND DEFINING NOVEL ANTENNA PARAMETERS

SUMMARY

The emergence of wireless technology has sparked significant interest in the design of MIMO (multiple-input multiple-output) antennas for wireless devices. MIMO antennas play a crucial role in meeting the requirements of current and future wireless standards. These antennas consist of multiple radiating elements at both the transmitter and receiver ends. The purpose of MIMO technology is to maximize data rates in wireless communication systems by utilizing multiple channels within the same bandwidth, especially in multipath environments. However, designing MIMO antennas for compact devices presents considerable challenges. The limited space between antennas leads to increased coupling and high correlation, which can negatively impact their performance.

Moreover, existing metrics used to evaluate conventional antenna systems are insufficient for fully assessing MIMO antenna performance. As a result, further performance characteristics need to be established to effectively evaluate the proposed MIMO antenna designs in this research. This thesis introduces a novel methodology for designing MIMO antennas that relies on crucial performance metrics and defining parameters. The focus is on key parameters that capture essential behaviors required for modern wireless standards, including the envelope correlation coefficient, diversity gain, and channel capacity.

The purpose of this thesis is to address these challenges by presenting a new approach to MIMO antenna design. The methodology integrates various performance measures and decoupling strategies to enhance antenna performance. By investigating coupling and interference effects among antenna components, this thesis also explores the use of decoupling strategies to mitigate these issues. Additionally, the technique emphasizes important criteria for MIMO antenna design within the LTE and sub-6 GHz 5G bands. These criteria encompass factors such as antenna spacing, slot dimensions, strip placements, and parasitic element sizes.

The thesis explores several MIMO antenna configurations suitable for 4G and 5G user equipment operating in the sub-6 GHz frequency range. Each design is tailored to meet specific requirements such as low profile, compactness, cost-effectiveness, and compatibility with multiple standards.

The first design focuses on a dual-band MIMO antenna utilizing a Vivaldi-shaped structure for Sub-6 GHz 5G wireless applications. This antenna aims to cover the 5G NR bands n78 (3.3-3.8 GHz) and n79 (4.4-5.0 GHz). With gains exceeding 7.63 dBi and 8.5 dBi respectively, the antenna offers simplicity in design, avoiding the

need for multilayer substrates and vias while maintaining mutual coupling below -30 dB. Performance evaluation includes analysis of S-parameters, envelope correlation coefficient (ECC), and channel capacity. Experimental measurements demonstrate an ECC below 0.01, aligning satisfactorily with simulation results.

The second design presents a concentric octagonal-shaped MIMO antenna specifically intended for 5G User Equipment (UE) applications in the sub-6 GHz bandwidth, specifically the 5G n38 band (2.57-2.62 GHz). This design emphasizes simplicity, avoiding multilayer substrates and vias, while achieving a gain of over 5 dBi and mutual coupling below -25 dB. Performance evaluation includes analysis of S-parameters, ECC, and Total Active Reflection Coefficient (TARC). Experimental results show an ECC below 0.01, indicating excellent performance consistent with simulations.

The third design proposes a compact quad-element MIMO antenna for LTE/Wi-Fi applications. This antenna consists of four dual-elliptically tapered elements arranged orthogonally, with cross-shaped stubs and ring-shaped stripes acting as decoupling elements. The prototype MIMO antenna operates in the 2.3 to 2.7 GHz frequency band, exhibiting high isolation exceeding 17 dB. Performance characterization involves measuring S-parameters. The results show an envelope correlation coefficient below 0.04 and a channel capacity loss lower than 0.6 b/s/Hz, reasonably aligning with simulated results.

The fourth design presents a wideband MIMO antenna suitable for LTE and Wi-Fi devices operating in the frequency bands of 2.1/2.3/2.6 GHz and 2.4 GHz respectively. This single-element MIMO antenna with quad-ports features a symmetrical four-port microstrip-fed monopole patch antenna and a frame-shaped partial ground plane. The design undergoes modeling, simulation, fabrication, and measurement. The results demonstrate reasonable agreement between simulations and measurements, with an operating bandwidth of 2-3.0 GHz, reflection coefficients below -10 dB, isolation under -12 dB, an ECC below 0.2, and diversity gain of approximately 10 dB.

Lastly, a quad-element MIMO antenna utilizing a modified Apollony fractal shape is designed for 5G mobile communications. This antenna comprises four radiating Apollony fractal elements positioned optimally with a partial ground plane. Each radiator element incorporates a microstrip feed with a quarter-wave transformer for improved impedance matching. Operating at 3.3-3.8 GHz, the antenna achieves S11 below or equal to -10 dB within the impedance bandwidth, with low mutual coupling below -20 dB. Performance evaluation includes S-parameters, ECC, and channel capacity analysis. Experimental measurements exhibit an envelope correlation coefficient below 0.05, and a channel capacity loss below 0.6, aligning reasonably well with simulation results.

In conclusion, this thesis showcases a range of MIMO antenna configurations for sub-6 GHz user equipment in 4G and 5G applications. Each design is carefully validated through the fabrication and testing of prototypes. Additionally, the thesis analyzes channel capacity in both LOS and NLOS fading environments for sub-6 GHz communications.

MIMO PERFORMANS ANALIZINE VE ANTEN PARAMETRELERINI TANIMLAMAYA DAYALI YENI BIR ANTEN TASARIM METODOLOJISI

ÖZET

Kablosuz teknolojinin ortaya çıkışı, kablosuz cihazlar için MIMO (çoklu giriş çoklu çıkış) antenlerin tasarımına olan ilgiyi önemli ölçüde artırmıştır. MIMO antenler, mevcut ve gelecekteki kablosuz standartların gereksinimlerini karşılamada çok önemli bir rol oynar. Bu antenler, hem verici hem de alıcı uçlarında birden fazla radyasyon elemanından oluşur. MIMO teknolojisinin amacı, özellikle çok yollu ortamlarda, aynı bant genişliği içinde birden fazla kanal kullanarak kablosuz iletişim sistemlerinde veri hızlarını en üst düzeye çıkarmaktır. Ancak, kompakt cihazlar için MIMO anten tasarlamak önemli zorluklar ortaya koymaktadır. Antenler arasındaki sınırlı alan, performanslarını olumsuz etkileyebilecek artan eşleşmeye ve yüksek korelasyona yol açmaktadır.

Dahası, geleneksel anten sistemlerini değerlendirmek için kullanılan mevcut ölçütler, MIMO anten performansını tam olarak değerlendirmek için yetersizdir. Sonuç olarak, bu araştırmada önerilen MIMO anten tasarımlarını etkili bir şekilde değerlendirmek için daha fazla performans özelliğinin belirlenmesi gerekmektedir. Bu tez, temel performans ölçütlerine ve tanımlayıcı parametrelere dayanan MIMO anten tasarımı için yeni bir metodoloji sunmaktadır. Odak noktası, zarf korelasyon katsayısı, çeşitlilik kazancı ve kanal kapasitesi dahil olmak üzere modern kablosuz standartlar için gerekli temel davranışları yakalayan temel parametrelerdir.

Bu tezin amacı, MIMO anten tasarımına yeni bir yaklaşım sunarak bu zorlukları ele almaktır. Metodoloji, anten performansını artırmak için çeşitli performans ölçümlerini ve eşleştirme çözme stratejilerini entegre etmektedir. Bu tez, anten bileşenleri arasındaki eşleşme ve girişim etkilerini inceleyerek, bu sorunları azaltmak için eşleştirme çözme stratejilerinin kullanımını da araştırmaktadır. Ek olarak, teknik, LTE ve 6 GHz altı 5G bantları içindeki MIMO anten tasarımı için önemli kriterleri vurgulamaktadır. Bu kriterler, anten aralığı, yuva boyutları, şerit yerleşimleri ve parazit eleman boyutları gibi faktörleri kapsamaktadır.

Tez, 6 GHz altı frekans aralığında çalışan 4G ve 5G kullanıcı ekipmanları için uygun birkaç MIMO anten konfigürasyonunu incelemektedir. Her tasarım, düşük profil, kompaktlık, uygun maliyetlilik ve çoklu standartlarla uyumluluk gibi özel gereksinimleri karşılamak üzere uyarlanmıştır.

Çift eliptik konik MIMO anteni, kullanıcı ekipmanı (UE) için tasarlanmıştır ve kompakt bir konfigürasyonda düzenlenmiş dört elementten oluşmaktadır. Yakın aralıklı anten elemanları arasındaki karşılıklı eşleşmeyi azaltmak için çeşitli ayırma teknikleri kullanılmıştır. Bu teknikler arasında parazit elemanlar, anten yerleşimi

ve yönlendirmesi, toprak üzerinde halka şeklinde şeritler ve 66 mm x 66 mm'lik bir genel boyut bulunmaktadır. Yakın aralıklı anten elemanları arasındaki karşılıklı eşleşmeyi etkili bir şekilde azaltmak için çeşitli ayırma teknikleri kullanılmıştır. Bu teknikler arasında radyatörleri stratejik olarak yerleştirme ve yönlendirmenin yanı sıra, substratın üstünde çapraz şekilli bir saplama paraziti ve altta halka şeklindeki şeritler bulunan kısmi bir toprak düzlemi gibi parazit yapıları eklemeyi içerir. Bu parazit elemanlar, radyan elemanlar arasındaki istenmeyen eşleşme etkilerini bastırmak için eşleşme akımları indükler ve yakın mesafede izolasyonu artırır. Özetle, çift eliptik konik MIMO anteni, 5G n40, n41 bandı için tasarlanmıştır ve ayrıca LTE (2.3-2.4GHz, 2.496-2.69GHz) ve Wi-Fi (2.412-2.484GHz) uygulamaları için de uygundur. MIMO anteni, 0,6 b/s/Hz'den düşük bir kapasite kaybı ve 0,04'lük bir ECC değeri ile arzu edilen performans özellikleri sergilemiştir, bu da onu LTE ve Wi-Fi uygulamaları için oldukça uygun hale getirir.

5G n78 bandı için modifiye edilmiş bir Apollonius fraktalı kullanan dört elemanlı MIMO anteni tasarlanmıştır. Anten konfigürasyonu, dört Apollonius fraktal anteni ve maksimum güç aktarımı ve yansımaları en aza indirmek için anten ile iletim hattı arasında eşleşme sağlamak üzere çeyrek dalga empedans eşleştirmesini kullanan bir ayırma tekniğinden oluşur. Ayırma teknikleri, eşleşme alanlarının gücünü azaltmak ve polarizasyon uyumsuzluğu yoluyla eşleşmeyi en aza indirmek için kullanılır. Ayrıca, $0,5\lambda$'lık bir eleman arası boşluğa sahip Apollonius şeklindeki bir fraktal MIMO antenin tasarımı ve karakterizasyonu da araştırılmıştır. Antenin genel boyutu 80 mm x 80 mm'dir. Antenin performansı, tam dalga elektromanyetik simülatörü kullanılarak yapılan simülasyonlar aracılığıyla değerlendirilmiştir. Daha sonra, Apollonius fraktal antenin bir prototipi üretilmiş ve MIMO anten sisteminin çeşitlilik performansını değerlendirmek için saçılma parametreleri ölçülmüştür. Apollonius şeklindeki MIMO antenin ölçülen yansıma katsayısı, -10dB'lik bir S11 ile 3,2 GHz ile 3,8 GHz arasında değişmiştir. Bu frekans aralığı, 5G ağlarının çalışma frekanslarıyla uyumludur. Ek olarak, bitişik anten elemanları arasındaki karşılıklı eşleşmenin -20dB'den düşük olduğu gözlemlenmiş olup, bu da girişimde önemli bir azalma olduğunu göstermektedir. Üretilen antenin ölçülen sonuçları, simüle edilen sonuçlarla oldukça uyumlu çıkmıştır. ECC ve kapasite kaybı ile karakterize edilen çeşitlilik performansı, sırasıyla 0,04 ve 0,5'ten düşük olan olumlu değerler göstermiştir. Bu bulgulara dayanarak, önerilen Apollonius şeklindeki MIMO antenin 5G taşınabilir iletişim cihazları için umut vadeden bir aday olduğu sonucuna varılabilir. Kompaktlığı, mükemmel performans parametreleriyle birleştiğinde, 5G iletişim sistemlerinin taleplerini karşılamak için onu çok uygun hale getirir.

Dual-band elipsel kesik Vivaldi MIMO anteni, 5G n78 ve n79 bantları için tasarlanmıştır. Bu anten, paylaşılan bir akıcı antena üzerinde dört elipsel kesik Vivaldi antenasından oluşan yapılandırmaya sahiptir ve dört porttan oluşur. Anten öğesi arasındaki izolasyonu artırmak için anten yapısına bir açıklama tekniği dahil edilmiştir. Bu teknik, anten yapraklarının ve kesiklerin stratejik yerleştirilmesi ve yönlendirilmesi şeklindedir. Antena genel boyutu 108 mm x 108 mm'dir. Vivaldi şeklindeki iki-bantlı MIMO antena, özellikle 5G uygulamaları için tasarlanmıştır ve 5G NR bantlarını kapsar n78 (3.3-3.8 GHz) ve n79 (4.4-5.0 GHz). Anten öğesi, n78 ve n79 iki frekans bantı için en az 7.63 dBi ve 8.5 dBi kazanç elde etmek istediğini ama keskinlik azaltılmıştır (-30 dB). Anten tasarımında karmaşık çok katmanlı ve via yapılandırmalarından kaçınılarak basitlik önceliklendirilmiştir. Önerilen antenin performansını değerlendirmek için S-parametreleri, ECC ve kanal kapasitesi gibi çeşitli performans

ölçütleri kullanılmıştır. Antenin performansını doğrulamak için deneysel ölçümler yapılmıştır. Değerlendirme, MIMO anten elemanları arasında yüksek bir çeşitlilik seviyesini gösteren 0,01'den düşük bir ECC değeri göstermiştir. Ölçümlerden elde edilen bulgular, önerilen anten tasarımının performansını desteklemek için doğrulama sağlayan simülasyon sonuçlarıyla uyumludur.

5G kullanıcı ekipmanı (UE) uygulamaları için tek katmanlı eşmerkezli sekizgen şekilli bir MIMO anteni tasarlanmıştır. Tasarım, iki koaksiyel besleme portu ile eşmerkezli bir sekizgen konfigürasyonu kullanarak kompaktlık ve eş yerleşim elde eder. Anten, 5G n38 bandında çalışır ve parazitik sekizgen halka elemanları, yuva ve yarık yapıları, optimize edilmiş besleme yerleşimi ve 60 mm x 60 mm'lik bir genel boyut kullanan bir ayırma tekniği kullanılmıştır. Tasarım, Hyperstudy kullanılarak araştırılmış ve optimize edilmiştir. Tasarım, 2,57 GHz ile 2,62 GHz arasında değişen n38 5G frekans bandında çalışma için anten elemanını optimize etmeye odaklanır. Bu tasarımın dikkat çekici bir özelliği, üretim sürecini basitleştiren ve üretim maliyetlerini azaltan tek bir katman kullanmasıdır. CST yazılımı, antenin elektromanyetik performansını simüle etmek için kullanılmıştır ve bu da antenin 5,5 dBi'lik bir tepe kazancı elde ettiğini ve karşılıklı eşleşmeyi -25 dB'nin altında tuttuğunu göstermektedir. Ek olarak, anten tüm frekans bandında 0,003 gibi son derece düşük bir ECC değerine sahiptir. Bu simülasyon sonuçları, simüle edilen performansla iyi bir uyum gösteren üretilmiş bir prototipten alınan ölçümlerle daha da doğrulanmıştır.

UE cihazları için geniş bantlı MIMO anteni, LTE b1, b40, b41, n1, n7, n40, n41 bantlarında çalışacak şekilde tasarlanmıştır. Anten konfigürasyonu, eşkenar dörtgen yapı yaması anteni, dört dengeli mikrostrip besleme hattı ve kısmi bir toprak düzlemi içinde bir nötrleştirme hattı içeren tek bir radyan elementten oluşur. Nötrleştirme, anten yerleşimi ve yönlendirmesi, portlar arasında 4 şerit adım kenarı ve ADS'de sentezlenmiş pi-ağları TL tabanlı ayırma ağı topolojisi kullanan bir ayırma tekniği kullanılmıştır. Antenin genel boyutu 108 mm x 108 mm'dir. Geniş bantlı kablosuz iletişim uygulamaları için dört portlu önerilen tek elemanlı MIMO anteni, tek bir radyan element içeren simetrik dört besleme hattı mikrostrip yama anteninden oluşur ve buna çerçeve şeklinde kısmen topraklanmış bir düzlem eşlik eder. Tasarlanan MIMO anteni, -10 dB'lik bir yansıma katsayısı ve yaklaşık 1,2 GHz'lik bir bant genişliği göstererek 2,0 GHz ile 3,0 GHz arasında değişmektedir. Ek olarak, kapsanan frekans bandında -12 dB'nin altında değerlerle kabul edilebilir bir izolasyon seviyesi elde eder.

Genel olarak, bu tezde sunulan araştırma, 5G ve ötesi kablosuz iletişim sistemlerinde kullanıcı ekipmanları için 6GHz altı frekanslarda MIMO anten tasarımı alanına önemli katkılar sağlamıştır. Özellikle tez, iyi performans gösteren beş anten tasarımı ve yeni bir anten tasarım metodolojisi önermektedir. Önerilen anten tasarımları, prototiplerin üretilmesi ve test edilmesi yoluyla dikkatlice doğrulanmaktadır. Ek olarak, tez, 6 GHz altı iletişim için hem LOS hem de NLOS solma ortamlarında kanal kapasitesini analiz eder.

1. INTRODUCTION

The advent of new wireless technologies has contributed to ongoing growth in the academic and industrial sectors throughout the decades. MIMO antenna systems are becoming more crucial owing to their potential to boost the data rate, capacity, and reliability of wireless communication systems. Nonetheless, enhancing MIMO antenna performance presents considerable design challenges. Maximizing throughput and minimizing errors require the careful manipulation of antenna parameters such as efficiency, isolation, correlation, and diversity. Finding a solution to this problem involves addressing the intricate balance between decoupling techniques, matching networks, spacing, placement and more.

The aim of the thesis is to overcome these challenges by providing a new approach to antenna design methodology that utilizes performance metrics for MIMO antenna systems. The proposed methodology intends to overcome the challenges presented by limited space portable devices by providing a complete approach to MIMO antenna design. It takes into account the need for compact and planar wideband antennas with high isolation and low correlation between elements, which are highly demanded in 4G LTE/5G wireless communication. This methodology also addresses the issue of large overall size, complex structures, and low radiation efficiency commonly found in MIMO antennas adopting isolation enhancement techniques.

This thesis examines the performance metrics of MIMO antenna systems in the LTE and sub-6 5G bands in depth. To verify the proposed methodology, several MIMO antenna prototypes were developed, simulated, built, and tested. The measured results indicate considerable improvements in port isolation, efficiency, and gain, demonstrating the effectiveness of the design process. This analysis examines crucial metrics, including capacity, diversity gain, and correlation coefficient, which play a vital role in evaluating system performance. By studying these metrics, valuable insights into the design requirements and trade-offs for MIMO antennas across different wireless applications were obtained.

1.1 Thesis Research Motivations

Due to the explosive growth of wireless communications devices, MIMO antennas are a key component of 4G and 5G technologies currently under research. Considerable study has been done on designing antennas for user equipment (UE) devices, but there is a continuous demand for antenna solutions to satisfy current and future generations of wireless technology.However, designing MIMO antennas for UE devices is very challenging for the following reasons: First, the antennas are more coupled due to their close proximity, resulting in high correlation. This significant correlation reduces MIMO antenna performance characteristics.

The primary objective of the research presented in this thesis is to investigate combining two decoupling strategies suitable for MIMO antennas to enhance isolation of closely spaced radiating patches within the configuration and thereby provide high diversity performance. Three decoupling techniques will be investigated: ground structure with defects (DGS), parasitic elements, and antenna positioning and orientation. Each approach will be combined with the others and applied to a recently constructed wideband MIMO antenna system to determine the effects of pairing each pair of methods on the antenna parameters. The research presents several UE antenna designs for 4G and 5G wireless networks operating at sub-6 GHz.

Thus, the proposed antennas should satisfy demands for low profile, compactness, affordability, and multistandard use. A prototype has been made, measured, and used to confirm each design. Also, a proper isolation approach should reduce correlation between MIMO antennas. MIMO antennas can be designed using standard antenna properties like reflection coefficient, bandwidth, radiation efficiency, and patterns. However, these are inadequate to characterize MIMO antenna performance. The channel capacity for sub-6 GHz communications in rich scattering environments based on Rayleigh and Rician fading channels will be examined. The effectiveness of the proposed MIMO antenna in this study can thus be evaluated using additional performance metrics. Therefore, a new antenna design methodology will be developed based on performance evaluation.

1.2 Thesis Objectives

1. To develop a new methodology for designing antennas that takes into account performance metrics for MIMO antennas. This will make it easier to design antennas with enhanced performance for wireless communication systems.

2. To identify key parameters that have a significant impact on antenna performance. The antenna design can then be optimized around these parameters, such as slot dimensions, strip positions, and parasitic element sizes.

3. To evaluate the performance of the designed antennas using established metrics such as channel capacity, ECC, diversity gain, TARC, scattering parameters, total efficiency, and 2D and 3D radiation patterns.

4. To examine existing decoupling strategies utilized in MIMO antenna systems. Implementing appropriate decoupling strategies improves both isolation and performance in MIMO antenna design. Decoupling methods, such as parasitic elements, defective grounds, and slots, can help minimize coupling between antennas in close proximity.

5. To propose a new antenna design methodology that incorporates MIMO performance analysis and defines antenna parameters.

6. To validate the effectiveness of the proposed methodology through simulations and experiments.

1.3 Literature Review

MIMO antenna technology has been widely utilized in current wireless communication systems due to boost data rates, spectrum efficiency, and link reliability [2, 3]. MIMO antenna technology has become increasingly popular, in communication systems because it can enhance system capacity without requiring transmission power or spectrum [4]. MIMO technology enables the use of antennas at both the transmitting and receiving ends allowing for utilization of the multipath propagation environment through spatial multiplexing and diversity techniques. This leads to improved channel

capacity, and overall system performance. However, designing MIMO antennas for gadgets poses challenges that want to be addressed [5]. Some of these challenges include establishing a compact size for the antennas, mitigation correlation between antenna elements to enhance channel capacity and providing strong isolation among the antennas. To address these challenges, various methodologies and decoupling techniques have been proposed in the literature. These include performance metrics, and decoupling techniques.

Despite the challenges associated with deploying MIMO antenna designs in close proximity areas, they have gained a lot of interest in the last decade. However, the limited area between the radiating elements in the portable device ends up with high mutual coupling and lower performance metrics. To solve this problem, several strategies have been proposed in the literature to reduce the mutual coupling and boost MIMO system performance.

In [6, 7], Defected Ground Structure (DGS) was designed to boost not just isolation but also bandwidth.The DGS was etched in the ground plane beneath the PCB board to provide strong isolation among the antenna ports.This bandwidth enhancement was notable at high frequencies in comparison to low frequencies. In addition, the DGS functioned as a bandpass filter in studies [8,9]. However, it is critical to note that DGS has barriers, including a reduced gain and a back-lobe pattern.

Metamaterial (MTM) techniques, as discussed in research [1, 10], has demonstrated the ability to create an electromagnetic band gap (EBG) that acts as a stop bands and band-pass filter in a selected frequency range. The utilization of a CRLH transmission line constructed with metamaterial has shown promising results in improving isolation between antenna elements [11]. Another proposed method for size discounting and insulation development is the use of split ring resonators (SRR) [12]. However, this technique may cause a decrease in antenna efficiency and bandwidth.

The decoupling approach defined in [13, 14] involves the use of metalized via walls, neutralized networks and short-circuited step impedances to reduce mutual coupling. In order for the network model to satisfy the substantial isolation requirements set by antenna impedances, it is crucial to determine the power transmission lengths and load reactance [15]. However, it is challenging to select the connecting sites,

and the bandwidth is narrow. Finally, this comprehensive study show that many decoupling techniques have complex structures, which creates a number of difficulties during the implementation phase. They still require adjustments to meet the demands of UE devices without impairing the performance of the other adjusting alterations. Combining more than one techniques can also provide attractive features for several latest gadgets, including good isolation, a lower coefficient, and a miniature design.

To satisfy the needs of contemporary wireless standards, that includes 4G LTE/5G, MIMO antennas need to contain high channel capacity, wideband, and gain [**?**]. However, addressing size and cost issues in MIMO systems often ends up in antenna miniaturization strategies that can compromise antenna bandwidth, performance, and gain. The crucial MIMO antenna metrics are isolation, correlation, diversity gain, total active reflection coefficient (TARC), mean effective gain (MEG) and capacity [16, 17].The maximum achievable data rate, known as channel capacity, is determined by the number of antennas as well as other factors including isolation between elements, and correlation. he maximum achievable data rate, known as channel capacity, is determined by the number of antennas as well as other factors including isolation between elements, and correlation. In order to enhance the performance of MIMO antenna systems for 4G LTE/5G wireless communication, it is important to mitigate the consequences of mutual coupling between the antenna elements [18].

To enhance capacity, emerging design methodologies focus on optimizing key performance metrics. Developing highly effective MIMO antennas requires a careful balance of multiple performance metrics. Important design parameters include element spacing, pattern diversity, decoupling structures, operating frequency, and array configuration [19, 20]. In order to mitigate the effects of mutual coupling and improve the performance of MIMO antenna systems for 5G wireless communication, it is crucial to adopt an effective methodology for antenna design. This methodology should consider various performance metrics, including mutual coupling reduction, channel capacity, data rate, gain, and bandwidth. New design methodologies leverage full-wave electromagnetic simulation and optimization techniques to fine-tune these parameters. This ensures that the antenna aligns with the desired frequency bands, adheres to physical device form factor constraints, and takes into account the characteristics of the wireless propagation environment [21]. By incorporating these

considerations, researchers can develop a comprehensive and systematic approach to MIMO antenna design, ultimately improving the performance of MIMO systems in 5G wireless communication.

1.4 Resarch Methodology

The research methodology for this PhD thesis is organized as follows:

1. Requirements and specifications definition:

The first stage involves defining the requirements and specifications for the MIMO antenna system, including the frequency range, bandwidth, gain, and polarization. The requirements are used to determine the optimal design parameters for the MIMO antenna system. The MIMO antennas include achieving high isolation between antenna elements to minimize correlation.

2. Antenna topology selection:

Once the key specifications are defined, the next step is to select an appropriate antenna topology for the MIMO system. Antenna topologies commonly used in wireless communication devices include monopoles, slot antennas, tapered antennas, and planar antennas. The design process involves selecting the appropriate types of antennas and determining their optimal geometry, including their size, shape, and orientation. Compact and low-profile designs are preferred to minimize their impact on portable devices. The antenna topology selection depends on the design constraints and requirements for performance metrics such as isolation, impedance bandwidth, and correlation.

3. MIMO antenna modeling and simulation:

Following the selection of the antenna topology, MIMO antenna modeling and simulation play a crucial stage in the design methodology and optimization process. This stage focuses on modeling MIMO antenna elements using electromagnetic simulation tools such as ANSYS HFSS and CST Microwave Studio. These simulation tools allow for the exploration and analysis of simulated MIMO antenna prototypes before physical implementation.

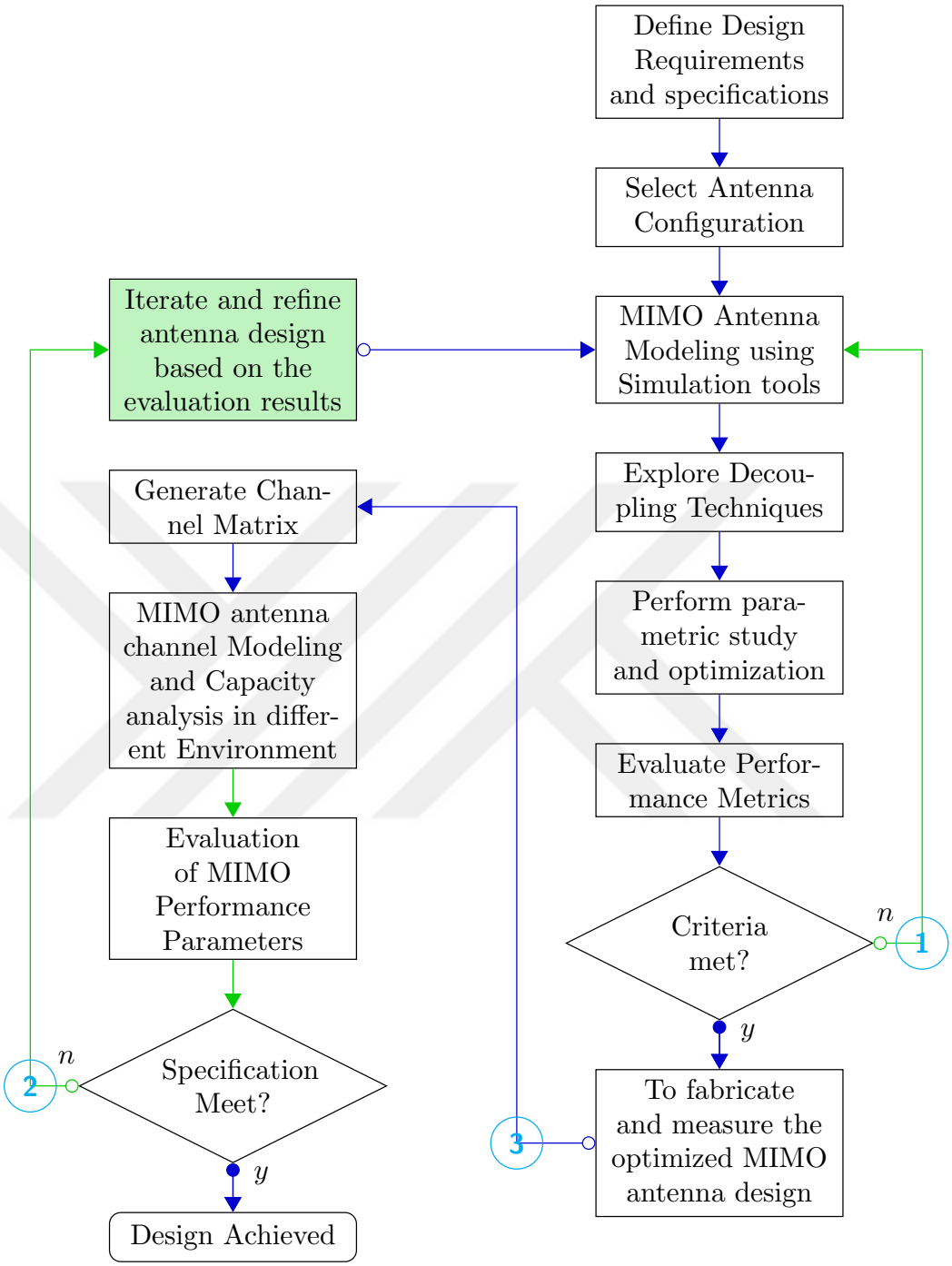

Figure 1.1 : Design methodology flow chart.

4. Decoupling techniques investigation:

High isolation between closely spaced MIMO antenna components is crucial for reducing envelope correlation and improving diversity performance. Therefore, this study investigates various decoupling techniques, including the use of parasitic elements, defected ground structures, slotted placement, and orientation, to enhance isolation between MIMO antenna elements in wireless applications.

5. Parametric simulations and optimization

This study runs parametric simulations to identify the crucial design parameters for optimizing MIMO antenna performance. Key parameters of the selected MIMO antenna geometry, such as antenna element length, width, separation distance, feed position, and decoupling features, can be swept across a range of values to evaluate their effects on key performance metrics. Hyper Study is also a tool for parametric variables and optimization. It can be used with a variety of DOE methods, ML algorithms, and optimization algorithms to find the optimal design for the problem.

6. Prototype fabrication and measurement:

After modeling and optimizing the MIMO antenna array through exhaustive simulations, the final designed antenna will be fabricated to validate the simulation results through measurements. Prototypes of the MIMO antenna will be constructed using standard printed circuit board (PCB) fabrication techniques. SMA connectors will be soldered to the feeding points to integrate with RF test equipment. The fabricated antennas will be measured in an anechoic chamber and a vector network analyzer (VNA) to characterize key performance parameters including S-parameters, isolation, correlation, radiation patterns, and efficiency.

7. MIMO channel modeling and capacity analysis:

MIMO antenna systems are widely used in modern wireless communications to increase channel capacity through spatial diversity. However, the performance of MIMO systems heavily relies on the underlying channel characteristics. Stochastic channel models provide a way to simulate different fading environments for MIMO analysis. This thesis investigates MIMO channel modeling and capacity using the stochastic models, including Rayleigh and Rician fading, for different wireless propagation environments.

8. Iterative refinement and optimization:

The iterative process of refining and optimizing the design is a crucial methodology stage, as results from prototyping and testing are fed back into the simulations. An initial antenna topology and design are first developed through simulation, modeling, and prototyping. However, the complex trade-offs between various MIMO performance metrics cannot be fully optimized in an initial design. This work takes an iterative approach to incrementally refine and re-optimize the MIMO antenna array design to achieve improved overall performance

1.5 Thesis Organization

The thesis is organized in the following manner:

Chapter 2 presents an overview of MIMO antennas, including their Systems and performance metrics. This chapter lays the foundation for the rest of the thesis and provides the necessary background information for understanding the proposed methodology.

Chapter 3 reviews existing isolation enhancement techniques that can be employed to enhance the performance of MIMO antennas. This chapter provides a comprehensive survey of the state-of-the-art techniques and identifies the limitations of the existing approaches.

Chapter 4 presents a compact MIMO antenna that was developed to validate the methodology. The design utilized dual-elliptically tapered radiating elements, arranged in a compact configuration. To effectively reduce mutual coupling between the closely spaced antenna elements, several decoupling techniques were employed, including the strategic placement and orientation of the radiators as well as the incorporation of parasitic structures.

Chapter 5 demonstrates the validation of the proposed methodology through simulation and experimental results. The chapter presents the results of a 4x4 Apollonian-shaped fractal MIMO antenna designed with an inter-element spacing of 0.5λ. A prototype of the Apollonian fractal antenna was fabricated and then measured to characterize the diversity performance of the MIMO antenna. Furthermore, a dual-band MIMO antenna was designed using a Vivaldi-shaped structure for wireless communication applications. A decoupling technique was modeled, arranging antenna slots and

tapered slots in specific placements and orientations to enhance isolation.

Chapter 6 presents the proposed MIMO antenna design methodology, which incorporates optimization of performance metrics. The designed antenna aims to achieve a single-element quad-port MIMO antenna suitable for wideband wireless communication applications. The MIMO antenna consists of a symmetrically fed four-feedline microstrip patch antenna with a single radiating element and a frame-shaped partially grounded plane. The chapter also focuses on designing a 2x2 MIMO antenna array for 5G wireless communication applications within the sub-6 GHz frequency range. The antenna array comprises concentrically arranged octagonal-shaped monopole antenna elements. Decoupling approaches such as parasitic elements and slotting are utilized to increase the isolation between the dual antenna ports.

Chapter 7 concludes the thesis by summarizing the main findings and contributions, and providing suggestions for future research directions.

2. MIMO ANTENNA SYSTEMS

MIMO antenna systems have been captivating researchers and developers since the 1990s, with their primary objective being the enhancement of wireless capacity utilization. Over the years, this technology has garnered substantial attention from both the academic and industrial fields, establishing itself as a crucial component within modern mobile communication networks, namely LTE and 5G. MIMO antenna systems take advantage of multiple antennas in both the transmitting and receiving ends, thereby facilitating enhanced performance in terms of data rates, coverage, and reliability. In contrast to the conventional SISO systems, which possess only one antenna at each end, MIMO systems offer a multitude of advantages, encompassing augmented capacity and better resistance to fading. MIMO technology is used not just for network infrastructure, but also in terminal devices, especially antennas. A dedicated researchers and engineers have indeed put in significant effort to design and optimize MIMO antennas, aligning them with the requirements of modern handheld devices. By taking advantage of multiple antennas, MIMO systems create multiple wireless channels, consequently elevating transmission performance and mitigating the deleterious effects of multipath fading [2].

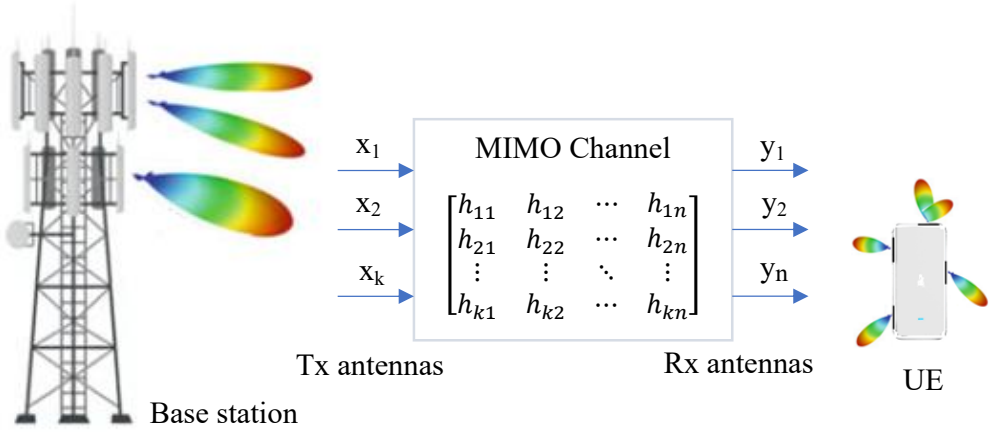

Figure 2.1 : MIMO system for wireless application

The MIMO technique enhances the transmission performance of wireless communication systems based on the channel's robustness and fidelity of the signal. Figure 2.3 presents an illustrated block diagram of the MIMO system. As the name implies, it utilizes multiple transmitting antennas K and receiving antennas N to improve wireless transmission pathways, producing $K \times N$ wireless channels. The MIMO antenna systems are used in mobile terminals for several types of schemes achieved through the following operational technique.

Generally, MIMO antennas have three main advantages: Improved spatial multiplexing is one of the most important benefits of MIMO technology. Through this, several data streams are transmitted through one frequency spectrum and time domain at the same time. Multiplexing in space offers a very high increase in spectral effectiveness, does not need power and bandwidth. In addition, multiple antenna systems provide spatial diversity that improves the reliability and robustness of a wireless communication system. MIMO systems use diverse propagation paths for signals to be received by multiply receiving antennas spaced away. By combining these signals in a constructive way, the BER will be reduced, and hence the effects of multipath fading mitigated. Subsequently, the beamforming technique concentrates the radiated power of the antennas in a particular direction towards the SNR. Beamforming uses many antennas like antenna array for optimizing the transmission path and ultimately boosting the performance of the system. As a result of their superior spectrum efficiency, MIMO antennas have been integrated into a wide range of wireless communication devices, including 4G LTE and 5G networks.

2.1 MIMO Antenna Parameters

Due to the advent of wireless technology, the design of MIMO antennas for user equipment has drawn considerable research interest. However, recent challenges in implementing MIMO antennas in small sizes have prompted the development of techniques that provide better performance criteria than conventional antenna systems. Scattering Parameters (SP), Mutual Coupling (MC), Mean Effective Gain (MEG), Total Active Reflection Coefficient (TARC), and Envelope Correlation Coefficient (ECC) are some of the performance metrics that can be used to evaluate multi-antenna

systems. These metrics can be computed and validated to support the performance of MIMO antennas.

2.1.1 Scattering parameter

The scattering parameter is the proportion of a reflected signal going out of port i to the incoming voltage signal on port j. To prevent reflections, all ports should be terminated with matching loads, except for the nth port in Figure 2.8. MIMO antennas in close proximity can cause interaction between elements, leading to coupling. When an antenna element is excited in proximity space, coupling occurs, causing current to flow in the other elements. As a consequence, an impedance matrix is formed that relies on the reflection coefficient as a parameter of antenna bandwidth, whereas the scattering matrix is determined by the reflection and transmission coefficients. The duple-port network displayed in Figure 2.8.a is used to locate proximity-spaced probes.

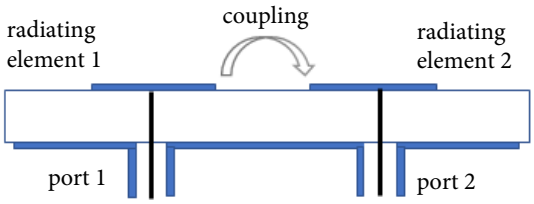

(a) Coupled antenna

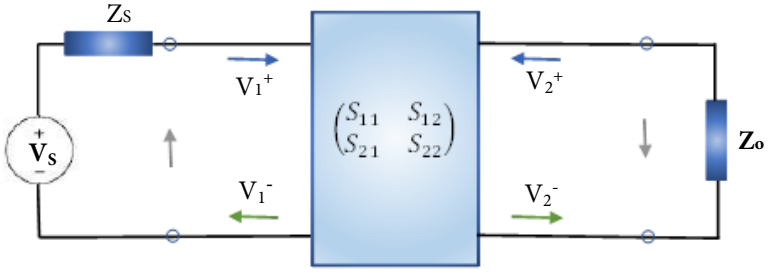

(b) Equivalent circuit

Figure 2.2 : Dual port antenna - coupled antenna and equivalent circuit

$$S_{ij} = \frac{V_i^-}{V_j^+}|_{V_{i\neq j}^+=0} \tag{2.1}$$

Figure 2.8.b displays the equivalent circuit of the dual-port circuit using scattering parameters. Therefore, Sii represents the reflection coefficient at port i when the remaining ports are terminated with matching loads. Similarly, Sij is the transmission

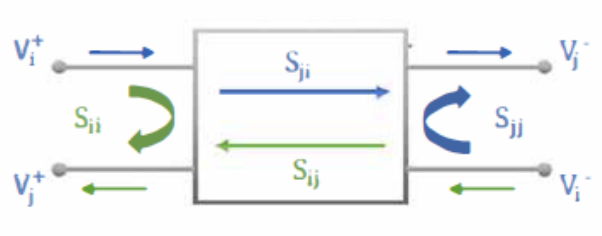

Figure 2.3 : Duple-port network.

coefficient between ports j and i when all other ports are terminated with matching loads, as illustrated in Equation 2.1.

2.1.2 Mutual coupling

Mutual coupling occurs due to the interaction between the proximity of MIMO antenna elements. When a single antenna element is excited, a current is generated in the other element, causing coupling. This coupling is utilized to define a MIMO antenna that can operate in either transmission or reception mode. In Figure 3.1, an active source excites MIMO element n while a 50Ω impedance load terminates MIMO element m. MIMO element n emits electromagnetic waves into open space, and passive element m receives some of the emitted energy, as described in 3. A small amount of energy reflects off the terminal denoted by the number 1, and antenna element n receives some of the re-scattered radiation, as seen by 4, indicating that the total power is not just flowing from the excited element n but also from the passive element m. It is important to inspect mutual coupling to improve performance and conserve energy. The coupling effect can affect passive elements, as they receive undesired radiant energy. Since mutual coupling is symmetrical, reversing the transmitter and receiver antennas will have the same effect.

2.1.3 Envelope correlation coefficient

The ECC is a measurement that indicates the degree of correlation between particular antenna patterns and the signal produced by multiple antenna components. The output parameter is affected by the pattern of several radiating elements. As the inter-antenna coupling increases, the diversity capability of multiple antenna arrays decreases. Whether the multi-element antenna is transmitting or receiving, the entire radiated field in the far-field pattern is calculated, as shown in Figure 2.5.

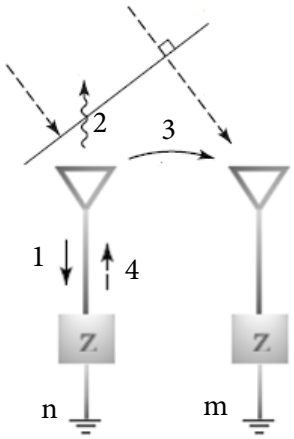

Figure 2.4 : Mutual coupling at receiving

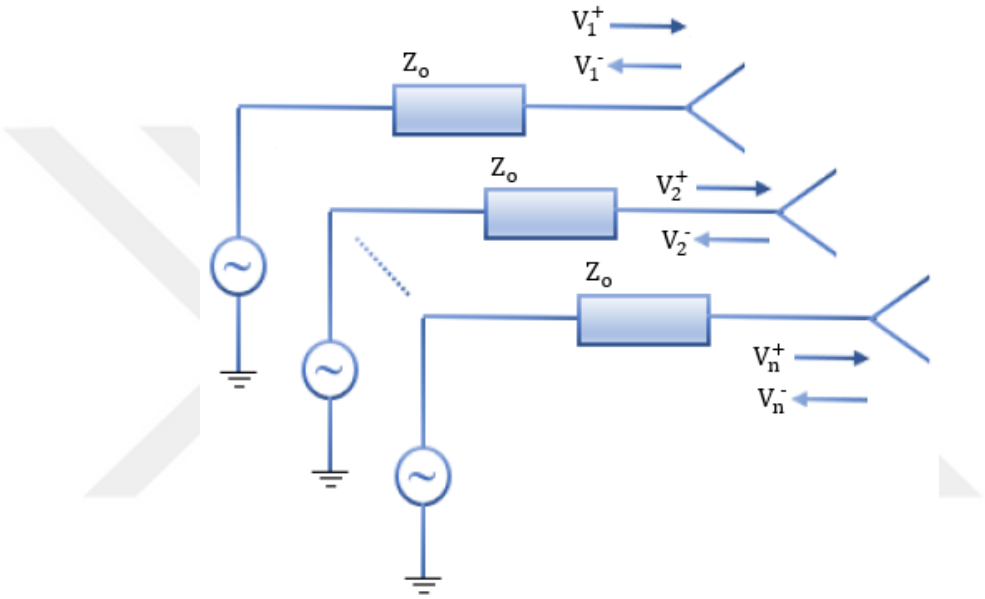

Figure 2.5 : Representation of N-antenna diversity system

The following equations can be used to represent the entire farfield radiated.

$$\vec{E_n} = V_n^+ \sqrt{\frac{\eta}{4\pi}} F_n(\theta,\phi) \frac{e^{-jkR}}{R} \tag{2.2}$$

The voltage V_n^+ at the port's reference plane is supplied to the antenna port n, which generates a field pattern F_n when fed by a matched voltage generator.

The radiated power, however, needs to be proportional to the sum of the power entering the multiple antennas. According to scattering parameter theory, this is:

$$P = V_j^{+\dagger}(I - S^\dagger S)V_j^+ \tag{2.3}$$

$$P = \iint_{4\pi} \frac{|\vec{E}|^2}{2\eta} d\Omega \tag{2.4}$$

Where V_n^+ represents the incoming wave vector of the N element, S is the scattering parameter, and I represents the identity matrix. The overall radiating power from component I can be calculated using the following formula:

$$\iint_{4\pi} F_i.F_i^{\dagger}\, d\Omega = 1 - \sum_{n=1}^{N} S_{i,n}^{\dagger} S_{n,i} \tag{2.5}$$

$$\iint_{4\pi} F_i.F_j^{\dagger}\, d\Omega = - \sum_{n=1}^{N} S_{i,n}^{\dagger} S_{n,j} \tag{2.6}$$

The 3-D patterns of two antennas can be used to determine the coefficient of correlation, that also reflects the degree of independence between the various antennas in a MIMO antenna element:

$$\rho(i,j) = \frac{\iint_{4\pi} F_i.F_j^{\dagger}\, d\Omega}{\sqrt{\iint_{4\pi} F_i.F_i^{\dagger}\, d\Omega \iint_{4\pi} F_j.F_j^{\dagger}\, d\Omega}} \tag{2.7}$$

The ECC is calculated by squaring the correlation coefficient, as shown in Equation 2.10 of [22]. Equation 2.8 was developed to simplify the complex equation and make it easier to calculate the correlation coefficient using scattering parameters.

$$\rho(i,j) = \frac{-\sum_{m=1}^{M} S_{i,m}^{\dagger} S_{m,j}}{\sqrt{\prod_{z=i,j}[1 - \sum_{m=1}^{M} S_{z,m}^{\dagger} S_{m,z}]}} \tag{2.8}$$

The S-parameters technique described in is very quick and simple, but it is only accurate when loss-less antennas are included. As a result, the S-parameter technique has been modified to take the influence of radiation efficiency into consideration. This technique, which is commonly used in the computation of the correlation coefficient, is represented by Equation 2.9

$$\rho(i,j) = \frac{-\sum_{m=1}^{M} S_{i,m}^{\dagger} S_{m,j}}{\sqrt{\prod_{z=i,j}[1 - \sum_{m=1}^{M} S_{z,m}^{\dagger} S_{m,z}]\eta_{radz}}} \tag{2.9}$$

The ECC can be utilized widely in communication systems, which is defined as

$$ECC = |\rho(i,j)|^2 \tag{2.10}$$

2.1.4 Total active reflection coefficient

TARC stands for Total Active Reflection Coefficient, and it is computed as the inverse square root of the total input power divided by the square root of the sum of the reflected power in a multi-antenna system. TARC is expressed in decibels and ranges from zero to one, where values close to zero indicate that all power is radiated and values close to one indicate that all power is reflected. TARC is a powerful tool for studying the impact of various metrics on the performance of MIMO systems, including antenna pattern, gain, and spacing. It can also be used to analyze and optimize antenna designs for specific applications. To compute TARC for dual-port antennas, one can use scattering parameters, as described by [23]. TARC highlights the importance of maintaining resonant frequency consistency, regardless of changes to the phase difference of the antenna components. As shown in Equation 2.11, TARC is obtained by dividing the square root of the total output power by the square root of the total input power.

$$\Gamma_{Tn} = \frac{\sqrt{\sum_{n=1}^{N} |b_n|^2}}{\sqrt{\sum_{n=1}^{N} |a_n|^2}} \tag{2.11}$$

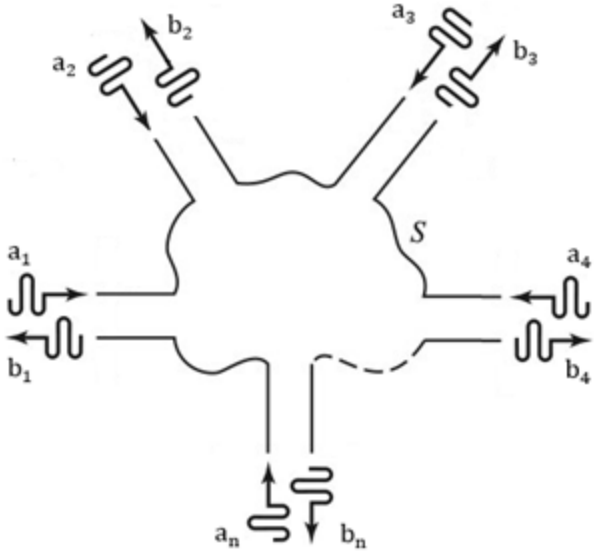

Figure 2.6 : An arbitrary N-port microwave network.

The equation for TARC, which applies to a MIMO system with N antenna ports and utilizes S parameters, has been presented as follows:

$$\begin{bmatrix} b_1 \\ b_2 \\ \vdots \\ b_n \end{bmatrix} = \begin{bmatrix} S_{11} & S_{12} & \cdots & S_{1m} \\ S_{21} & S_{22} & \cdots & S_{2m} \\ \vdots & \vdots & \ddots & \vdots \\ S_{n1} & S_{n2} & \cdots & S_{nm} \end{bmatrix} \begin{bmatrix} a_1 \\ a_2 \\ \vdots \\ a_m \end{bmatrix}$$

$$b_1 = a_1 S_{11} + \sum_{m=2}^{N} a_1 S_{1m} e^{j\theta(m-1)} \tag{2.12}$$

$$b_n = a_n S_{n1} + \sum_{m=2}^{N} a_n S_{\mathrm{nm}} e^{j\theta(m-1)} \tag{2.13}$$

TARC is a crucial metric for describing the frequency bandwidth and radiation performance of MIMO antennas due to their distinct nature [23]. For MIMO antennas with multiple input ports, impedance bandwidth and a constant resonant frequency are necessary, even if the phase of the input signal changes for all input ports. After evaluating the TARC formula in Equation 2.14, an extended TARC equation was developed for multi-port MIMO antennas, which includes scattering features when the antenna is linearly polarized.

$$\Gamma_{Tn} = \frac{\sqrt{\sum_{n=1}^{N} \left| S_{n1} + \sum_{m=2}^{N} S_{\mathrm{nm}} e^{j\theta_{m-1}} \right|^2}}{\sqrt{N}} \tag{2.14}$$

2.1.5 Mean effective gain

The mean effective gain (MEG) is a critical metric for characterizing antennas in fading channels. An analysis of certain primary MEG characteristics is offered, along with their physical implications. It is shown that under certain assumptions, the propagating channel and the antenna are equivalent. This is because the influences of the cross-polarization ratio (XPR) of the channel and the XP discrimination of the antenna are proportional at MEG. Closed integral formulas are provided for MEG in a mixed environment with both stochastic and determinate components. Equation 2.15 can be used to express MEG mathematically.

$$MEG = \int_0^{2\pi} \int_0^{\pi} \left[\frac{\mathrm{XPR}}{XPR+1} G_\theta G_\theta^* P_\theta + \frac{1}{XPR+1} G_\phi G_\phi^* P_\phi \right] d\Omega \tag{2.15}$$

2.1.6 Channel capacity

To evaluate the actual performance of a novel wireless system, a variety of techniques must be utilized, such as channel measurements, simulations, and field trials. However, these approaches can be challenging because the system needs to be tested in multiple propagation environments, which can consume a substantial amount of time and resources. Using channel models that provide essential propagation characteristics and statistics for testing can be an effective approach to addressing the issue. These models are commonly implemented as simulators, enabling the assessment and enhancement of various components of the system in a cost-effective and time-efficient manner.

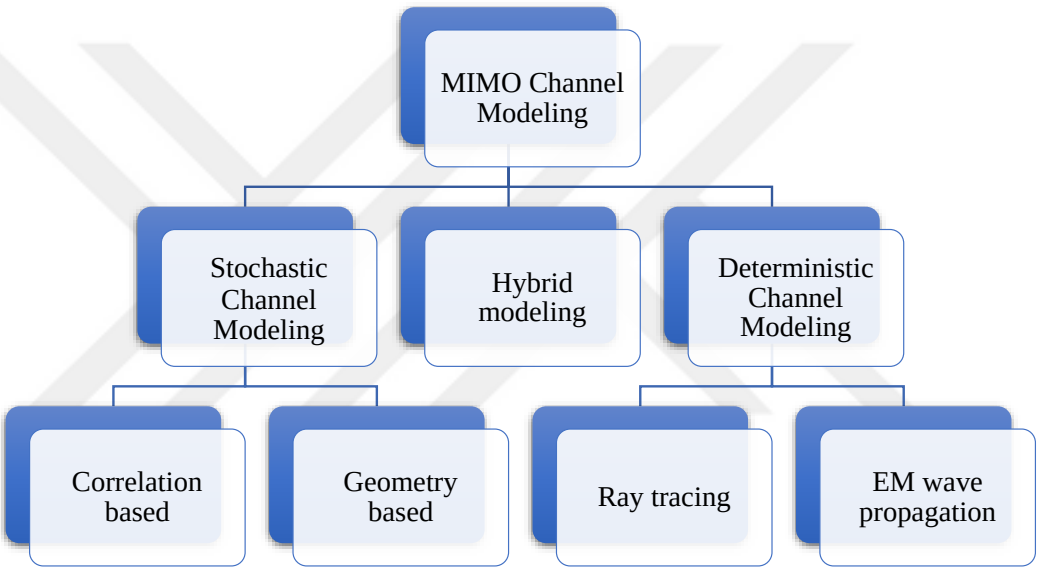

Figure 2.7 : A classification of MIMO channel models

There are three main types of channel modeling approaches: deterministic, stochastic and hybrid. Deterministic models rely on propagation mechanisms in a specific environment, such as electromagnetic wave theory or ray tracing. These models are well-suited for simulating systems in a particular environment due to their site-specific nature. However, they require a physical model that incorporates precise geographical and morphological data related to the environment. The complexity of this model may vary depending on both the environment and the intended level of modeling accuracy. Moreover, deterministic channel models are inadequate for accurately representing real-world channels due to their lack of randomness and variability.

To validate results, it is important to use measurements or simulations based on statistical channel models. Stochastic models are designed to statistically replicate the essential characteristics of a channel's behavior. Rather than attempting to predict propagation in a specific environment, these models represent the statistical behavior of key propagation properties. Stochastic channel models, such as the Rayleigh fading model and the Rician fading model, are commonly used to characterize the effects of signal attenuation and multipath propagation on wireless communication channels. Correlation-based modeling aims to capture the correlation properties between antenna elements at the transmitter and/or receiver, assuming that antenna correlation is the primary factor affecting MIMO system performance. In contrast, geometry-based modeling considers the physical placement of antennas and the communication environment, with the goal of capturing the channel's spatial characteristics, including path loss, shadowing, and scattering effects.

The Rayleigh channel model is a stochastic model used to define the behavior of wireless channels, in which signals are affected by multipath fading. The Rayleigh model is commonly used in designing and analyzing wireless communication systems, particularly in the development of diversity techniques that help mitigate the effects of fading. It is also used to simulate wireless communication systems and predict their performance under different conditions. The Rayleigh channel model is particularly useful in wireless communication systems that operate in urban or indoor environments where numerous obstacles cause multipath propagation. The Rayleigh channel model can be represented mathematically by a complex Gaussian random variable with a mean of zero and a variance that scales with the distance between the transmitter and receiver. The Rician channel model is a stochastic model characterized by a dominant line-of-sight signal (LOS), in addition to scattered signals that undergo Rayleigh fading. The κ-factor is a parameter that determines the strength of the LOS signal relative to the scattered signals.

$$H = \sqrt{\frac{\kappa}{1+\kappa}} H_{LOS} + \sqrt{\frac{1}{1+\kappa}} H_{Rayleigh} \tag{2.16}$$

where the κ-factor are utilized to indicate the strength LOS dominant signal. When the κ-factor is high, the LOS signal dominates the received signal, resulting in a

more deterministic model. Conversely, a low κ-factor indicates that the scattered component dominates the received signal, making the model more similar to the Rayleigh fading channel model. The Rician channel model is commonly used in wireless communication systems that operate in environments with a clear LOS path between the transmitter and the receiver, such as outdoor or rural areas.

A MIMO channel model revolutionizes traditional SISO systems by enhancing capacity without requiring extra transmit power or frequency spectrum. A communication channel can transmit reliable information at a maximum rate based on Shannon capacity, also known as channel capacity. The Shannon-Hartley theorem was developed by Claude Shannon in 1948 and uses a mathematical formula to calculate this capacity. As a crucial parameter for design and optimization of communication systems, it determines the upper limit of achievable data rates while taking noise and interference into account.

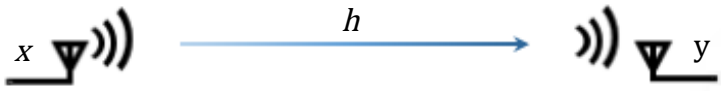

Figure 2.8 : SISO System

The received power y is expressed in terms of the channel matrix h, the input power x and noise power n as

$$y = hx + n \tag{2.17}$$

In SISO systems, the capacity in bits/sec can be calculated as follows:

$$C = B\log_2 det(I + \frac{P}{\sigma^2}) \tag{2.18}$$

where B denotes the channel bandwidth in Hz, P is the transmit power, and σ^2 represents the noise power at the receiver.

In comparison with single-input, single-output (SISO) systems, MIMO antenna systems have improved channel capacity in multipath propagation environments.

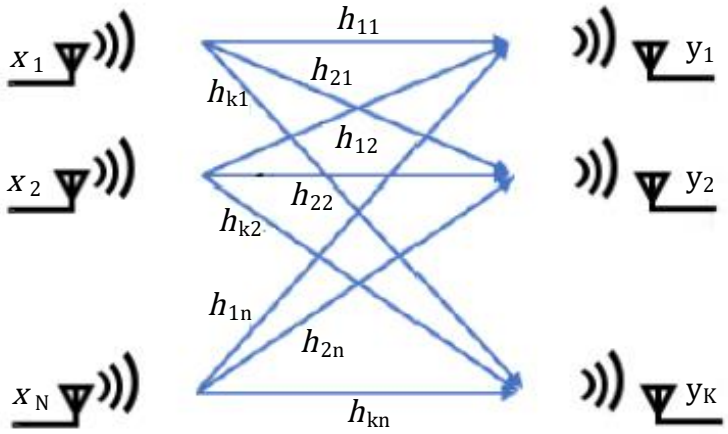

Figure 2.9 : MIMO channel model

$$y_k = \sum_{n=1}^{N_t} h_{kn} x_n + n_k \tag{2.19}$$

where y indicates the received signal, x denotes the transmitted signal, n is the noise, and the channel is represented by the complex matrix h_{kn}.

$$C = B \log_2 \left[det(I_k + \frac{P}{\sigma_n^2 N_n} HH^{\dagger}) \right] \tag{2.20}$$

where C represents the capacity of Rayleigh channel, and the estimation formula can be determined in terms of higher SNR. R represents the reception matrix that affects the desired multi-antenna channel capacity.

$$C = \mathbb{E} \left\{ \log_2 \left[det(I_k + \frac{P}{\sigma_n^2 N_n} HH^{\dagger}) \right] \right\} \tag{2.21}$$

where C refers to the ergodic capacity, $\mathbb{E}$ represents the expectation operator, $\frac{P}{\sigma_n^2}$ is the signal-to-noise ratio, H indicates the channel matrix, and $H^{\dagger}$ indicates the conjugate transpose of H.

$$H = R^{\frac{1}{2}} H_w \tag{2.22}$$

$$R = \left(\sqrt{\eta} \sqrt{\eta}^T \right) \odot \Psi \tag{2.23}$$

where $\odot$ denotes the hadamard product, and η is the column vector of the total efficiency including the radiation and mismatch efficiencies that can be computed through Equation 6.3, η is given as:

$$\eta = \begin{bmatrix} \eta_1 & \eta_2 & \cdots & \eta_k \end{bmatrix}^T$$

$$\Psi = \begin{bmatrix} 1 & \rho_{1,2} & \cdots & \rho_{1,n} \\ \rho_{1,2}^{\dagger} & 1 & \cdots & \rho_{2,n} \\ \vdots & \vdots & \ddots & \vdots \\ \rho_{1,n}^{\dagger} & \rho_{2,n}^{\dagger} & \cdots & 1 \end{bmatrix}$$

The interrelationship between channel capacity and multi-antenna characteristics is not as intuitive as in a solitary antenna system. This is because multiple factors can affect the capacity of such systems simultaneously. Therefore, researchers have conducted several studies to address this issue [36]-[39]. One way to characterize the multiplex efficiency (MUX) of a multi-antenna system is by measuring the loss in power efficiency required to achieve the same channel capacity as a reference multi-antenna system in a similar propagation environment. If the transmitter has no channel information, the channel matrix k x n can be expressed as:

$$\eta_{MUX} = \sqrt[N]{\prod_{n=1}^{N} \eta_n (1 - |\rho_{ij}|^2)} \tag{2.24}$$

η denotes the overall efficiency of the ith port of a multi-antenna, which includes mismatch, dielectric, conductive, and coupling losses. The overall efficiency of the antenna is determined as follows:

$$\eta_i = \eta_{i,rad}(1 - |S_{ii}|^2 - \sum_{i \neq j} |S_{ij}|^2) \tag{2.25}$$

Where $\eta_{i,rad}$ is the radiating efficiency of the nth port, which is computed as the ratio of the transmitted power to the received power.

2.2 Proposed Antenna Design Methodology

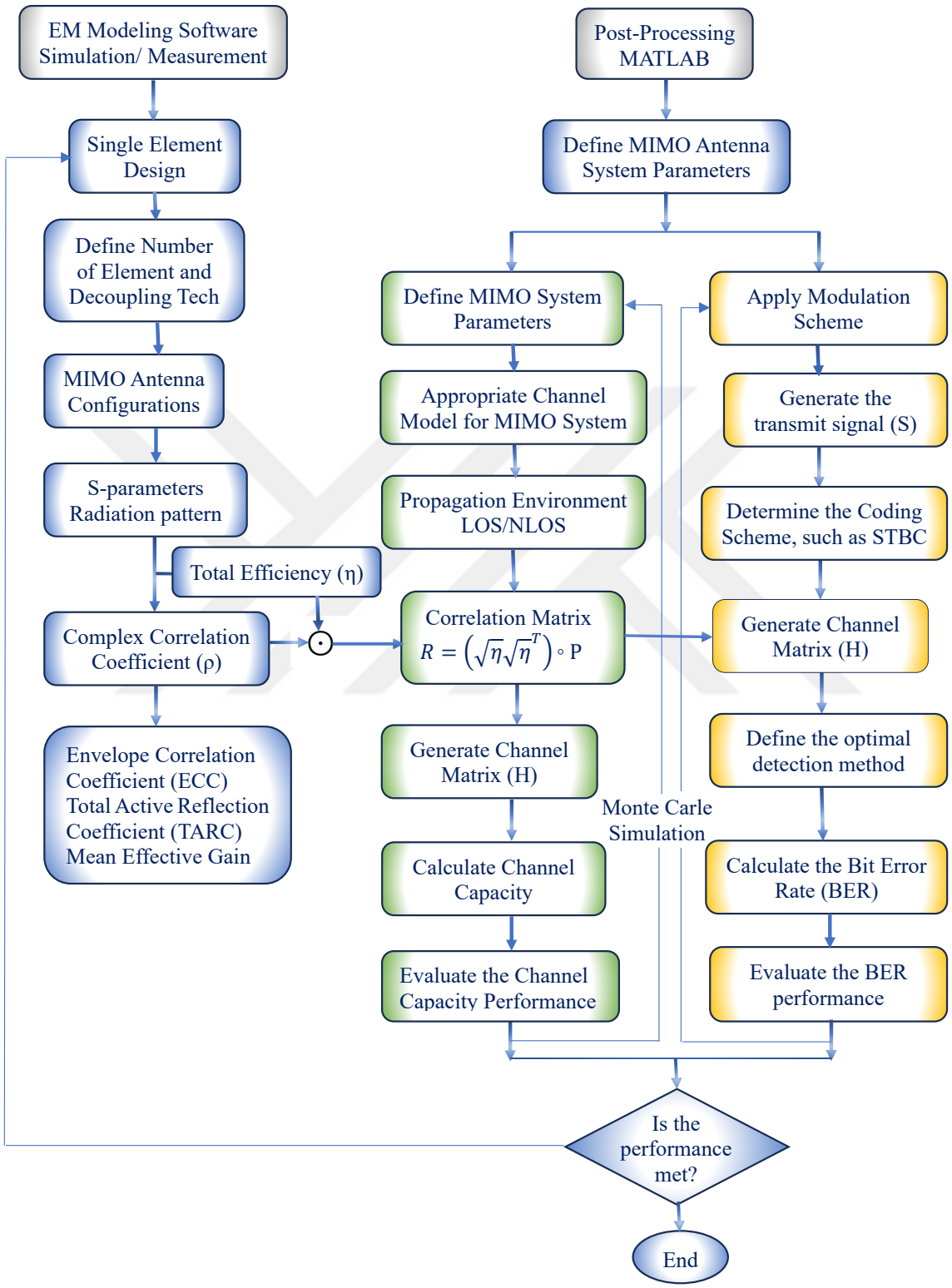

Figure 2.10 : Design methodology flow chart.

3. ISOLATION ENHANCEMENT TECHNIQUES IN MIMO SYSTEMS

3.1 Mutual Coupling

Mutual coupling occurs due to the interaction between the proximity of MIMO antenna elements. When a single antenna element is excited, a current is generated in the other element, causing coupling. This coupling is utilized to define a MIMO antenna that can operate in either transmission or reception mode. In Figure 3.1, an active source excites MIMO element n while a 50Ω impedance load terminates MIMO element m. MIMO element n emits electromagnetic waves into open space, and passive element m receives some of the emitted energy, as described in 3. A small amount of energy reflects off the terminal denoted by the number 1, and antenna element n receives some of the re-scattered radiation, as seen by 4, indicating that the total power is not just flowing from the excited element n but also from the passive element m. It is important to inspect mutual coupling to improve performance and conserve energy. The coupling effect can affect passive elements, as they receive undesired radiant energy. Since mutual coupling is symmetrical, reversing the transmitter and receiver antennas will have the same effect.

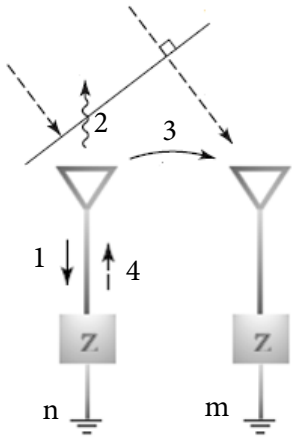

Figure 3.1 : Mutual coupling at receiving

3.2 Isolation Techniques

This section presents several techniques for enhancing isolation in MIMO antenna systems. The techniques aim to minimize mutual coupling and achieve a compact footprint in the antenna design.

3.2.1 Decoupling networks

Decoupling networks are used to reduce mutual coupling among antenna components by generating the appropriate interference against initial antenna coupling. The decoupling network consists of parasitic elements, reactance loads, and transmission lines. A network model is designed to compute the dimensions of the transmission line and load reactance to meet the high isolation requirements determined by the antenna impedance. Figure 3.2.a shows an inverted F antenna (IFA) with a shorting pin connecting the grounding arm to ground. Decoupling between antenna elements is achieved using a T-shaped element. When a parasitic decoupling network is used, the isolation increases by 15 dB. Figure 3.2.b shows the decoupling network for three aligned monopole antennas [13]. It is connected to each of the three antenna radiators to form a coupling path in addition to the conventional antenna, which improves isolation.

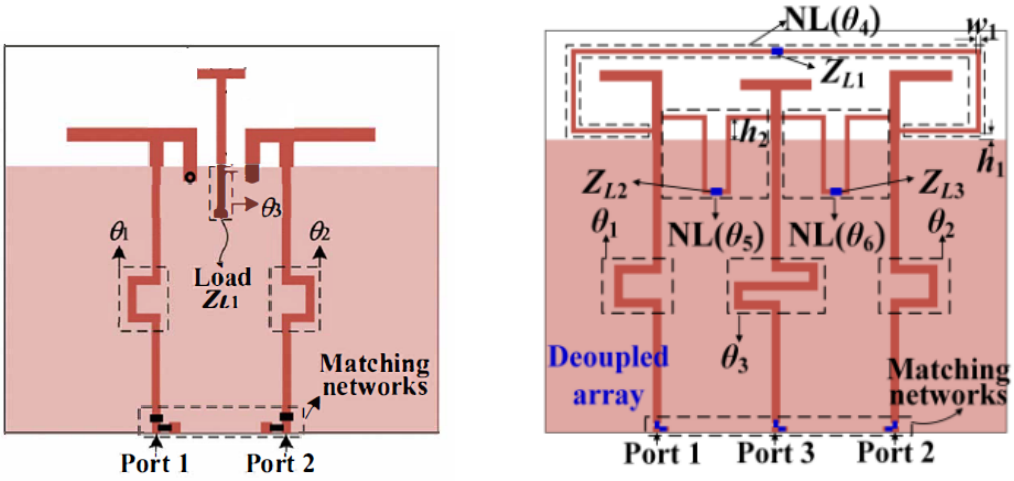

(a) The IFA array [15]

(b) The monopole array [13]

Figure 3.2 : The IFA and monopole array use decoupling networks

3.2.2 Parasitic elements

Parasitic elements are used as reflectors or resonators in MIMO systems to reduce the mutual coupling (MC) between resonating antennas. The parasitic element establishes an additional coupling link between the radiating elements, canceling the previous coupling. This process is identical to neutralizing conduction, although there is no physical connection between the radiating components. Parasitic elements have no intrinsic current excitation, but radiation from a nearby source could induce a significant current. In [24], as illustrated in Figure 3.3.a, the square structure is loaded with nearby patch elements. Two square parasitic elements are inserted next to each patch element. When parasitic elements are inserted, the induced current of the excited patch couples preferentially to the parasitic elements rather than to the unexcited patch. These parasitic elements act as a resonator, affecting the distribution of the radiation field and thus reducing mutual coupling. Figure 3.3.b shows the decoupling approach consisting of metallized via walls and neutralized networks with short-circuited step impedances used to minimize MC [25].

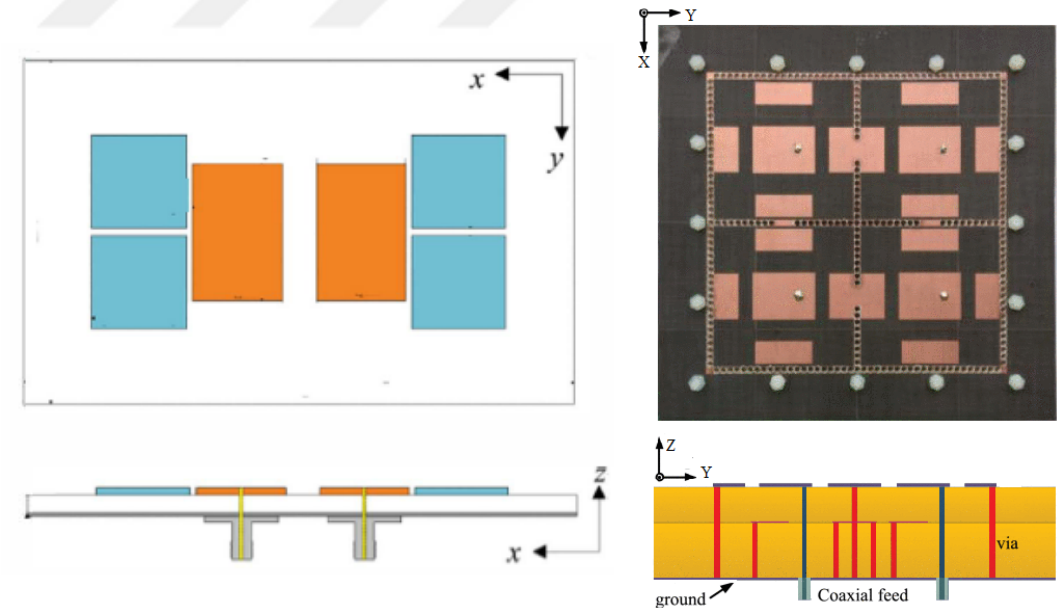

(a) The quadruple Parasitic Elements [24] (b) The multiple parasitic patches [25]

Figure 3.3 : The quad and multiple patches are based on parasitic elements.

3.2.3 Defected ground method

The defected ground method (DG) is utilized to increase operating bandwidth and gain, minimize mutual coupling between elements and unwanted cross-polarization, and create a notched band that prevents band interference. Each DG structure has unique properties that impact the antenna performance based on its design and size. A fractal unit cell is used in Figure 3.4.a to create the DG structure. Two lateral line segments are joined by a vertical line to form this unit cell. Fractal DG unit cells are the third iteration of a fractal structure arranged horizontally to improve isolation [26]. The Fractal DG method with bandgap filtering properties is used to lessen the mutual interaction between the components of a patch antenna. In this scenario, the Fractal DG method is used to lower the mutual coupling between two patch antenna components by more than 30 dB. As shown in Figure 3.4.b, a periodic S-shaped DGS is developed to minimize the mutual coupling between the antenna elements [27]. It distorts the fields and allows currents to flow between the microstrip antenna terminals to relieve them from mutual coupling.

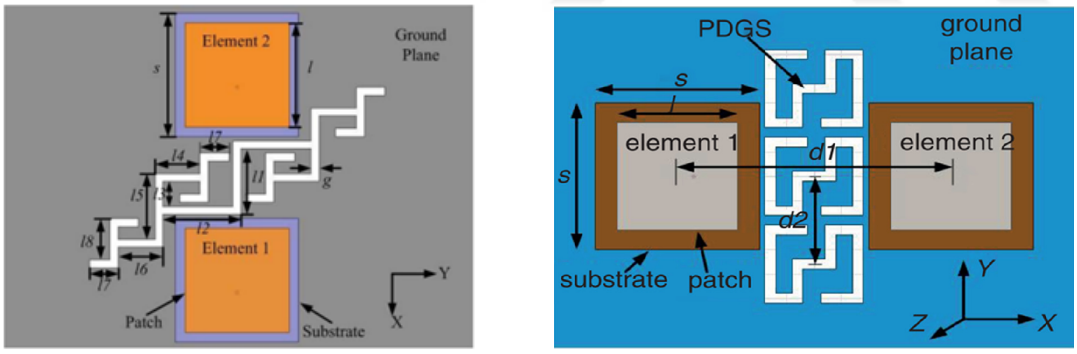

(a) FDGS technique [26]

(b) PDGS technique [27]

Figure 3.4 : The MIMO antennas utilize the FDGS and PDGS methods.

3.2.4 Neutralization lines

The neutralization technique allows for port decoupling by utilizing side-by-side copper strip lines that attenuate reactive coupling between antennas. The neutralization line (NL) induces phase-reversal currents that suppress unwanted currents in the radiator's structure. A neutralization line connects the dual symmetrical antennas, enhancing isolation between the dual proximity ports. A NL-based UWB MIMO antenna is composed of two thin strips joined by closely spaced monopoles and is linked with a rectangular metal plate in the midst of the antenna model. The UWB MIMO antenna is designed to operate between 3.51 and 9.89 GHz with a 10 dB impedance bandwidth. The NL is located between two monopole elements [28], inducing a current on the NL and generating an additional radiation field, which reduces mutual coupling. Port decoupling is achieved by adjacent metal strips acting as neutralizers for the reactive coupling of the antennas. Figure 3.5.a shows that a planar MIMO antenna consists of two symmetrically radiating parts connected by a neutralizing line [29]. This line cancels the reactive coupling and reduces MC. Figure 3.5.b illustrates the insertion of a Hilbert fractal form of the second phase based on the neutralizing line [30]. Additionally, the antenna has a truncated Minkowski fractal structure on the upper edges and defective ground, which improves MIMO system isolation.

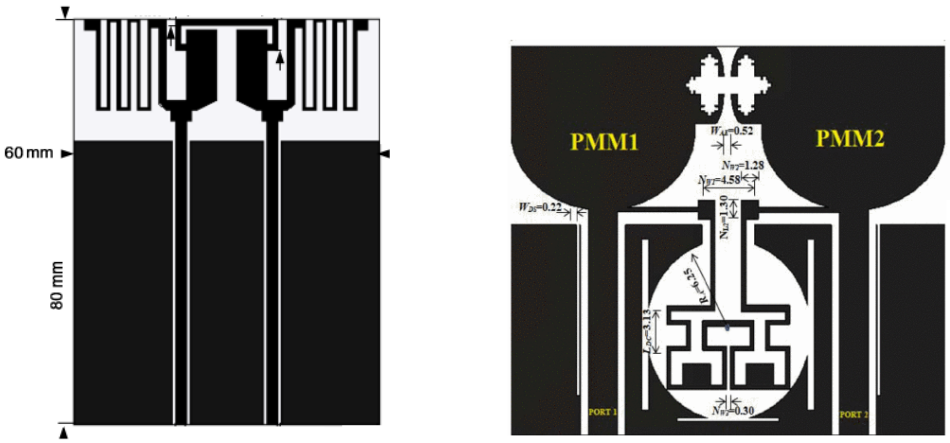

(a) Folded monopole [29] (b) Hilbert Fractal based [30]

Figure 3.5 : MIMO antenna based on NL.

3.2.5 Metamaterials

A metamaterial (MTM) is a material that has been artificially structured to display exceptional electromagnetic characteristics that are not abundant in nature. There are two main groups in which metamaterials can be classified: the first group includes single and double negatives, while the second category includes photonic bandgap materials. The metamaterial structure can create an electromagnetic bandgap that can be used as a stopband and bandpass filter in a specific frequency band. Using a metamaterial within the surrounding antenna elements enhances the isolation between these elements. In [1], an array of MTM absorbers is set between two patch antenna elements, as shown in Figure 3.6, to reduce mutual coupling and decrease the scale of the array. The antenna element with the excitation port induces current into the MTM absorber array, which generates its own flux to counteract the incident field. Due to the magnetic response being lessened, current flowing between antenna elements is reduced. By employing the metamaterial surface to produce surface wave suppression [10], a method to boost an antenna's gain is presented. The phase reflectance and matching impedance characteristics of the MTM surface make it a suitable reflector.

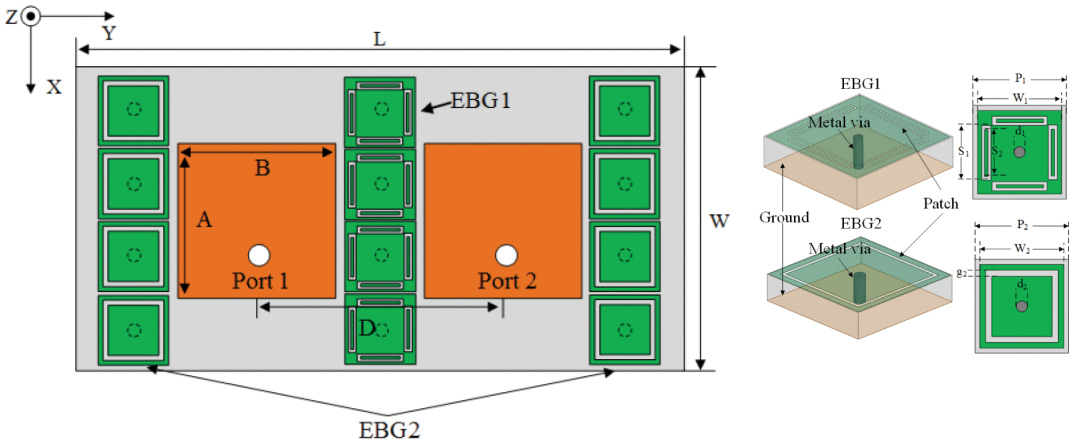

(a) Top layer (b) Unit cell of the two EBG

Figure 3.6 : The MIM antenna utilizes an EM bandgap [1].

Table 3.1 : A comparison of the designed and previously reported MIMO antennas.

Technique	Benefits	Drawbacks
Decoupling Networks	Provides flexibility in controlling the coupling Reducing mutual coupling	Requires Extra space Requires precise design and tuning
Parasitic Elements	Good diversity gain High isolation	Detuning due to parasitic effect
Defected Ground Method (DGS)	Effective in reducing mutual coupling Relatively simple design Cost-effective solution	Limited bandwidth and frequency range Require precise design and optimization
Neutralization Lines (NL)	Provides flexibility in controlling the coupling Effective in reducing mutual coupling	Requires careful placement and tuning of NL low frequencies
Metamaterials	Precise control of wave propagation Can achieve high levels of isolation	Expensive Fabrication complexity
Frequency Selective Surfaces (FSS)	Effective for multiband applications	Can be bulky and require complex design

3.3 Limitations of Current Approaches

While existing isolation enhancement techniques have proven to be effective in reducing mutual coupling, they often face certain limitations such as limited bandwidth effectiveness, increased complexity and cost of implementation. For instance, parasitic elements and metamaterials may only be effective over a narrow bandwidth, while decoupling networks and neutralization lines can add complexity to the antenna design and fabrication process. Additionally, the use of metamaterials and some decoupling networks can be expensive due to the specialized materials and manufacturing processes required. Given these limitations, it is crucial to carefully consider these factors when selecting a technique for a specific application, as it may be necessary to trade off between cost, complexity, and bandwidth to find the best solution.

4. COMPACT QUAD-ELEMENT MIMO ANTENNA FOR LTE/5G BANDS

The requirement for improved data transmission rates and channel capacities in wireless communication systems operating in environments with significant scattering has increased due to advancements in wireless technology. Fortunately, MIMO antennas have been verified to be effective in enhancing network ability and information costs without having extra transmission power. MIMO systems use multiple antennas at both the transmitting and receiving ends of wireless devices, leading to remarkable progress in wireless communication research [31].

The effectiveness of MIMO antennas greatly relies upon their ability to lower the correlation coefficient caused by electromagnetic wave couplings between nearby radiating components. Therefore, isolation techniques can enhance antenna performance while reducing correlation in the proximity region for MIMO antenna systems [32]. Although several approaches have been proposed in the literature to enhance MIMO antenna isolation throughout an operating frequency range, a hybrid approach has not yet been effectively utilized to enhance the isolation over a broad range of operating frequencies for LTE/Wi-Fi and sub-6 applications.

This study recommends a compact four-element tapered radiator antenna for MIMO applications. The antenna element with dual-elliptical tapering gives improved impedance matching throughout the frequency variety, a symmetrical radiation pattern, and ease of construction. The developed MIMO antenna can be used in portable devices supporting LTE/Wi-Fi/5G NR.

To reduce mutual coupling in between the four radiators, a decoupling technique utilizes parasitic stubs, positioning and orientation, including a cross-shaped stub in between the orthogonal symmetries of the radiators and ring-shaped red stripes in between the partial ground planes. The created MIMO system is compact, has a reduced envelope correlation coefficient, and provides high isolation between elements. The proposed style technique is verified through simulated and measured results.

4.1 Configuration of a Single Antenna

The configuration of the tapered elliptical radiating antenna is illustrated in Figure 4.1. This antenna consists of three 3 elements: a tapered radiating component, a partially grounded part, and a microstrip transmission line. The tapered radiating element is excited by a 50 Ω feed from the microstrip transmission line. The antenna is constructed using an FR4 substrate with a relative permittivity of 4.3 and a loss tangent of 0.035. The copper layer attached to the substrate is 0.025 mm in thickness, and the overall dimensions of the antenna are $30.75 \times 35.25 mm^2$. The layout and simulation of the antenna were accomplished utilizing CST software. The optimal dimensions for the tapered elliptical patch antenna exist in Table 4.1.

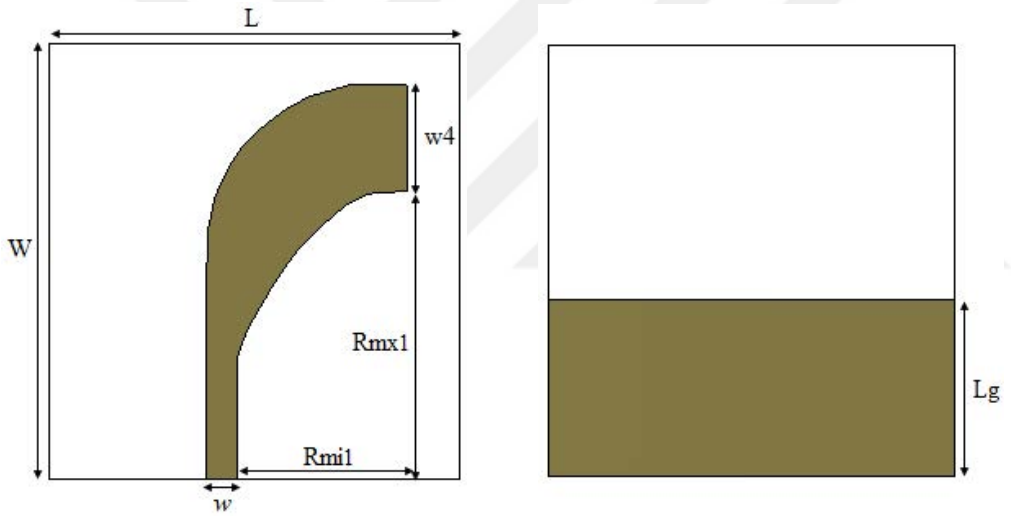

(a) Top layer. (b) Bottom layer.

Figure 4.1 : The dual-elliptically tapered antenna's geometry..

Table 4.1 : Optimum dimensions of the dual-elliptically tapered antenna.

Parameter	Value (mm)	Parameter	Value (mm)
W	35.25	Rmx1	19.75
L	30.75	Rmi1	15.15
w	2.85	w4	9.5
Lg	10	Wg	30.75

4.2 Parametric Study of Impedance Characteristics

A parametric study was conducted using simulations to investigate the impedance bandwidth and dimensional reduction of a dual elliptically tapered antenna. The researchers focused on varying the length of the tapered slots (Rmx1) and measuring the return loss of the antenna, as shown in Figure 6.2. The results indicated that changes in the shorter length of Rmx1 had a minimal impact on the impedance bandwidth. Therefore, to achieve a smaller dual elliptically tapered antenna, adjustments to the size of the microstrip line would be necessary.

Furthermore, the researchers examined the effect of changing the width (w4) of the tapered radiating slot on the impedance bandwidth, as illustrated in Figure 6.3. It was observed that the width of w4 had a significant influence on the impedance characteristics of the antenna. A larger w4 improved impedance matching at lower frequencies, while a smaller w4 caused the radiating taper to become too thin, resulting in poor impedance characteristics at lower frequencies.

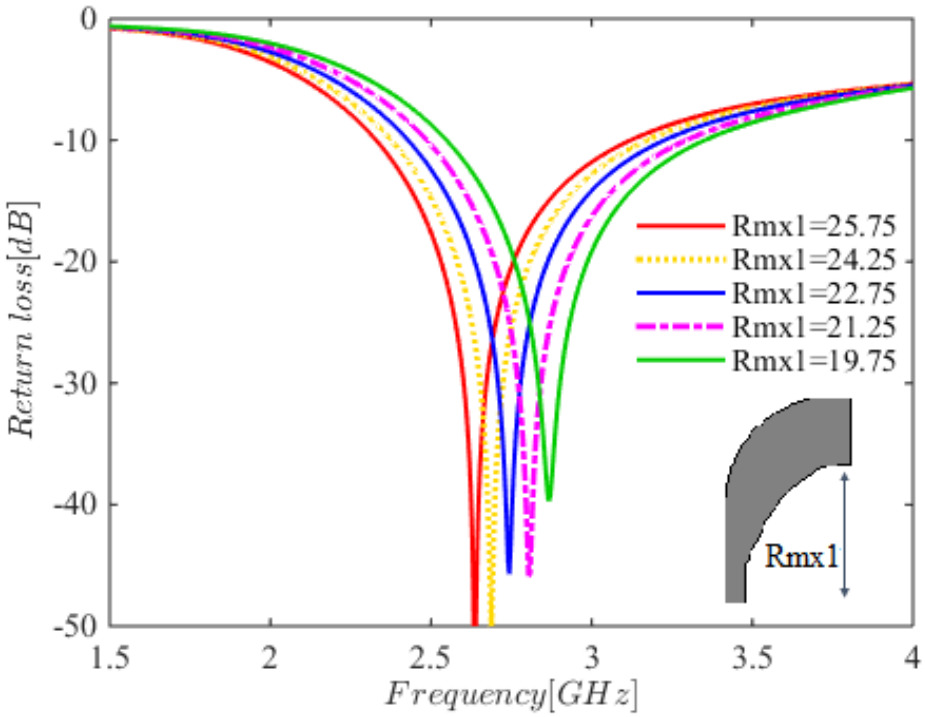

Figure 4.2 : S_{11} plotted against the various lengths of Rmx1 of the tapered slot.

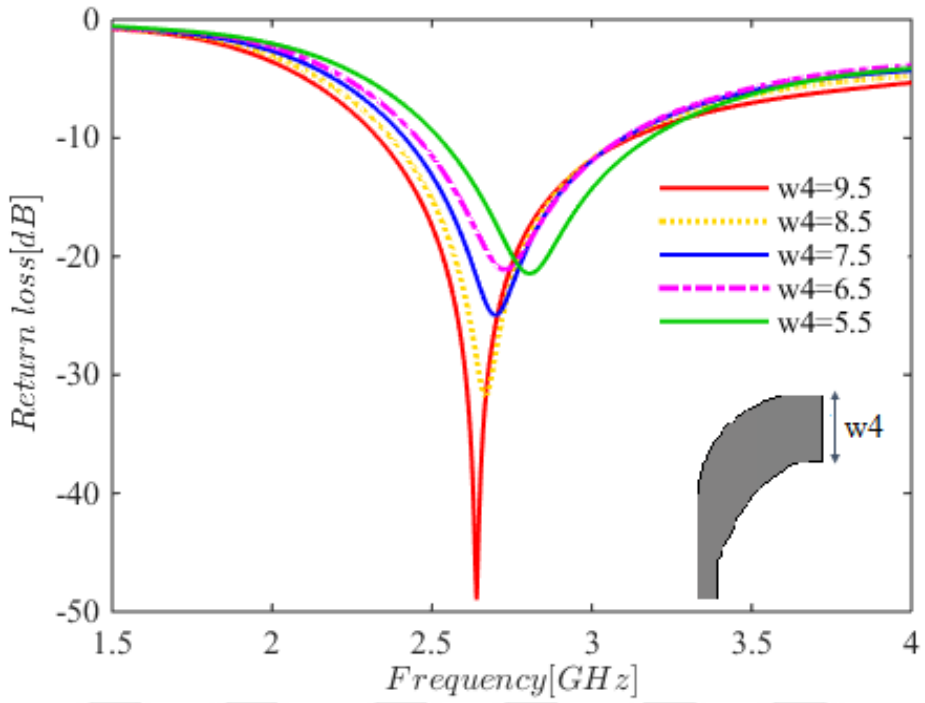

Figure 4.3 : S_{11} for the tapered slot's variable width, w4.

4.3 Design of a MIMO Antenna Configuration

Figure 6.4 displays the quad-element MIMO antenna, which features a bifold elliptically tapered slot radiator.The paired elliptically tapered antennas provide improved impedance matching over the required frequency range, as well as symmetrical radiated patterns. The MIMO antenna was constructed using an FR4 substrate with a relative dielectric constant of 4.4, a thickness of 1.6 mm, and a loss tangent of 0.035, resulting in an overall size of $66 \times 66 mm^2$. A tapered antenna with a microstrip feed was fabricated and excited with a characteristic impedance of 50Ω. The radiating antenna element's dimensions were optimized parametrically using computer simulation tools (CST) to operate in the LTE (2.3-2.4 GHz, 2.496-2.69 GHz), Wi-Fi (2.4 GHz) and NR (2.3-2.4 GHz, 2496 – 2690 GHz) frequency bands. The key physical dimensions of the MIMO antenna are presented in Table 6.2.

Table 4.2 : Optimum dimension of the designed MIMO Antenna.

Parameter	Value (mm)	Parameter	Value (mm)	Parameter	Value (mm)	Parameter	Value (mm)
L	66	Rx	29.25	w1	3	w3	10
W	66	Ri	18	w2	3	l1	4.75
R	1.5	l2	14	l3	30.75	S	5.3
w	2.85	arc1	5	w5	8	-	-

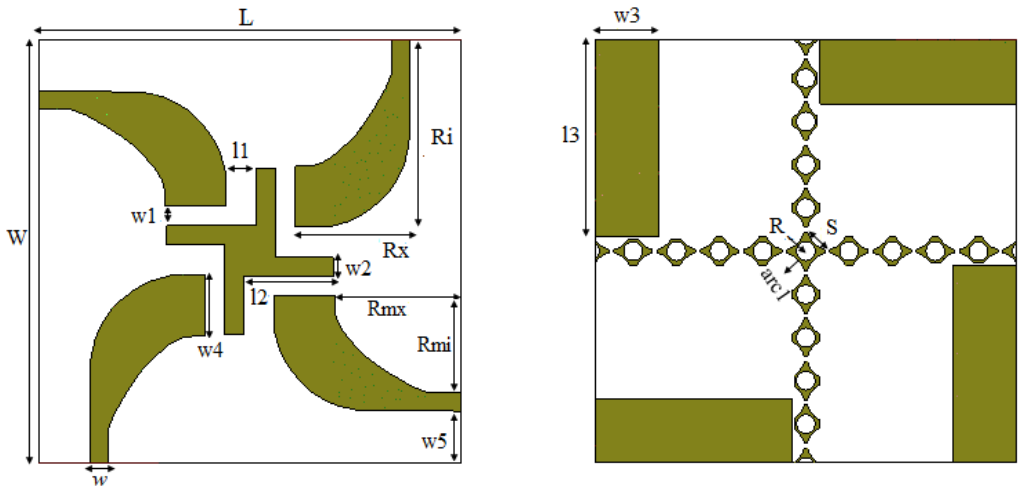

(a) Top layer. (b) Bottom layer.

Figure 4.4 : Dual-elliptically tapered MIMO antenna design geometry

4.4 Analysis of quad-element MIMO antenna

The impact of isolation techniques on MIMO antenna performance was investigated through a parametric study conducted using CST Microwave Studio. Various techniques, such as cross-shaped stubs, complementary spiral ring resonators (CSRs), and annular strips, were employed to enhance the reflection coefficient frequency range and reduce mutual coupling. Figure 6.5 depicts a dual elliptically tapered MIMO antenna, illustrating the presence and absence of cross stubs between elements. The inclusion of a cross stub effectively reduces mutual coupling and improves impedance matching across the frequency range.

In Figure 6.6, S-parameter simulation results for a quad elliptically tapered slot MIMO antenna are presented, showcasing the antenna's performance with and without a cross stub between elements. The MIMO antenna incorporating the cross-shaped stub exhibits a frequency range of 2.3 to 2.8 GHz. Within this range, the mutual coupling between diagonally arranged elements (S31) and adjacent elements (S21) remains below -20 dB, indicating minimal interference. However, at the center frequency of 2.45 GHz, the mutual coupling between diagonally arranged elements (S31) experiences an increase of approximately -10 dB compared to the results without the cross-shaped stub.

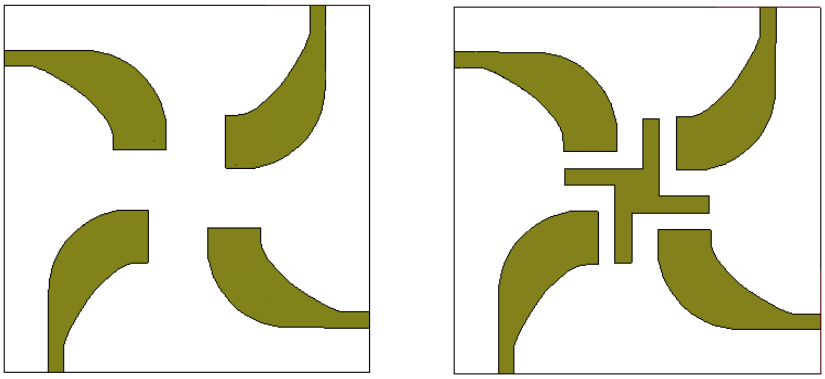

(a) without cross-shaped stub (b) with cross-shaped stub.

Figure 4.5 : MIMO antenna design with and without cross-stub.

Figure 6.5 and 6.6 visually represent the simulation outcomes for the two MIMO antennas, providing valuable insights into the effectiveness of the isolation techniques employed. The antenna shown in Figure 6.8 is a quadruple dual antenna with an

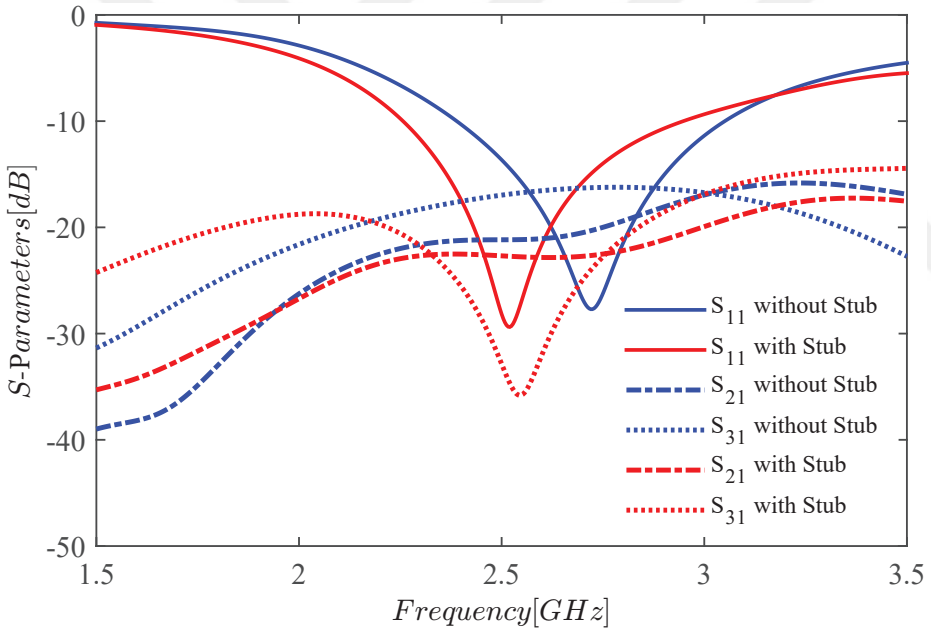

Figure 4.6 : S-parameters of MIMO antenna without and with stub.

elliptically tapered slot, designed for MIMO applications. It is supported by annular and complementary spiral ring resonators, as well as a matching circuit consisting of capacitances (determined by the space between the ring-shaped strips) and inductances (determined by the width of the strips). The ring-shaped strips were included in the resonator's ring shape to lower the resonant frequencies. The S-parameters obtained with both complementary spiral ring resonators (RSRs) and conventional spiral ring resonators (CSRs) are presented in Figure 6.9. As a result of using RSRs, the mutual

coupling (S21) between the antenna components and the resonators is slightly reduced over the target frequency range.

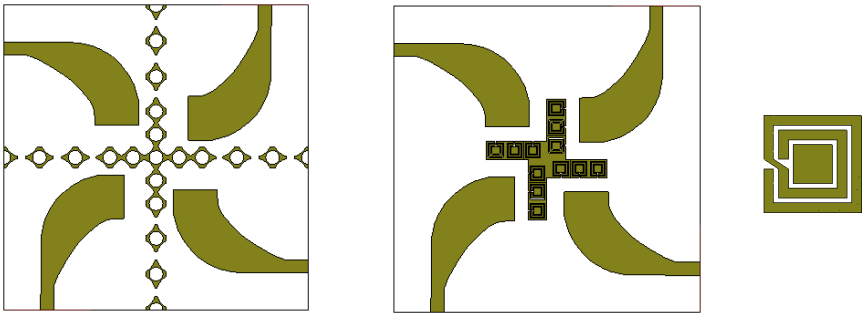

(a) with ring-Shaped. (b) with CSRs. (c) Unit cell CSR.

Figure 4.7 : The quad element MIMO antenna with annular and CSRs

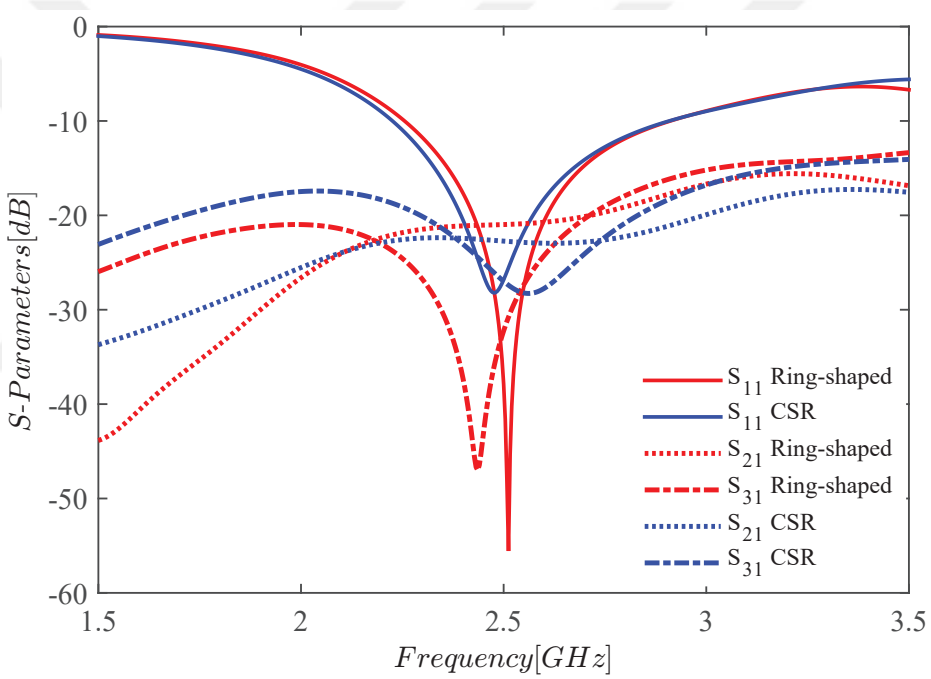

Figure 4.8 : The MIMO antenna S-parameters with annular and CSRs.

The image in Figure 6.10 shows four MIMO antennas with a dual-elliptical tapered shape and annular stripes between their partial ground planes. To compare performance, Figure 6.11 plots the S-parameters of the quadruple elliptical tapered slot MIMO antennas with and without annular stripes. The MIMO antenna with annular stripes has a 500 MHz bandwidth for $S11 < -10\ dB$ in Figure 6.11. Mutual coupling between diagonally placed (S31) and adjacent (S21) elements remains below $-20\ dB$ from 2.2 to 2.7 GHz, ensuring minimal coupling between antenna elements across the frequency range.

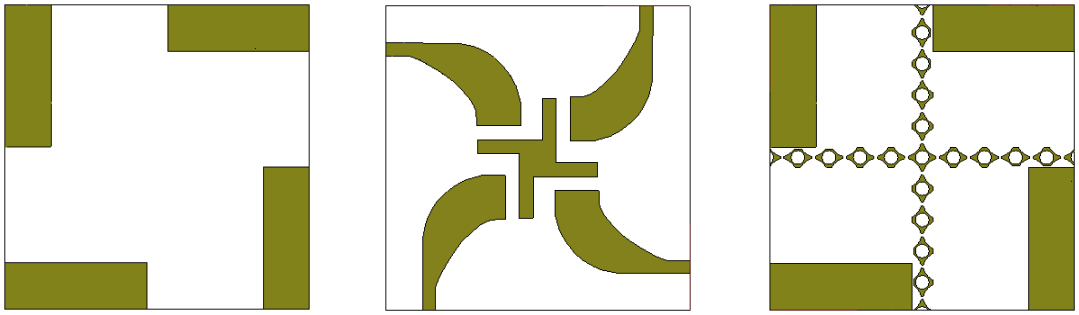

(a) without annular-stripes. (b) Top layer. (c) Annular-stripes.

Figure 4.9 : Designed quad-element MIMO antenna.

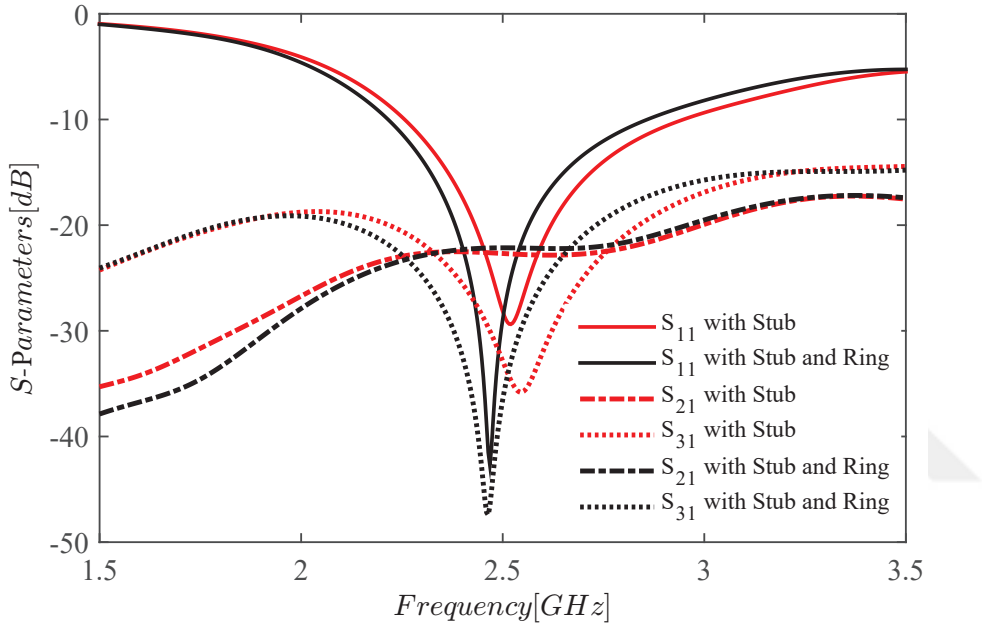

Figure 4.10 : S-parameters of MIMO antenna with stub vs with stub and ring stripes.

4.5 Current Density

To explore the mutual coupling effects of the proposed MIMO antenna, a surface current distribution can be utilized at a frequency of 2.45 GHz. The surface current distribution of a quad-element MIMO antenna is illustrated in Figure 4.11, which highlights the influence of a cross-shaped stub and annular strips on mutual coupling. By inducing surface currents that weaken the initial coupling between radiating antenna elements, the cross-shaped stub and annular strips effectively decrease mutual coupling. Consequently, incorporating both cross-shaped stubs and annular strips is critical for reducing mutual coupling.

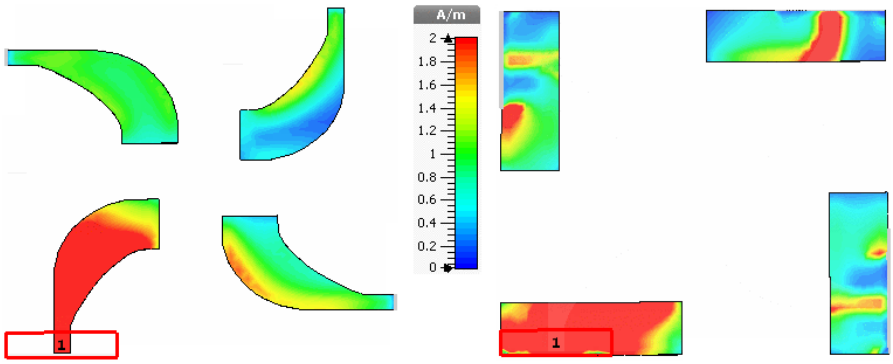

(a) Without stub top and bottom layer.

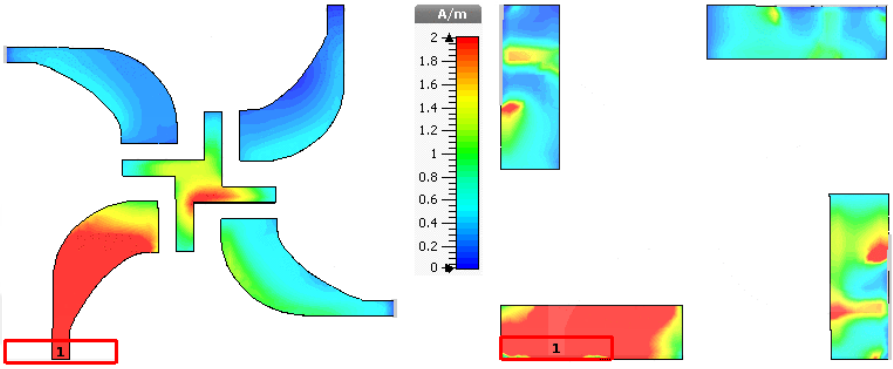

(b) With stub top and bottom layer.

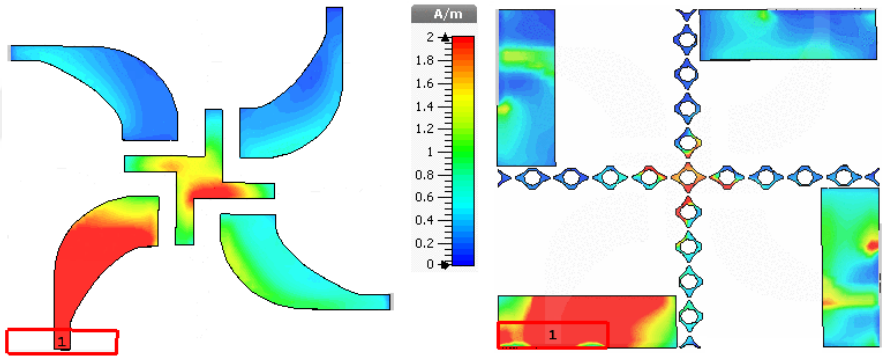

(c) With stub top and ring bottom layer.

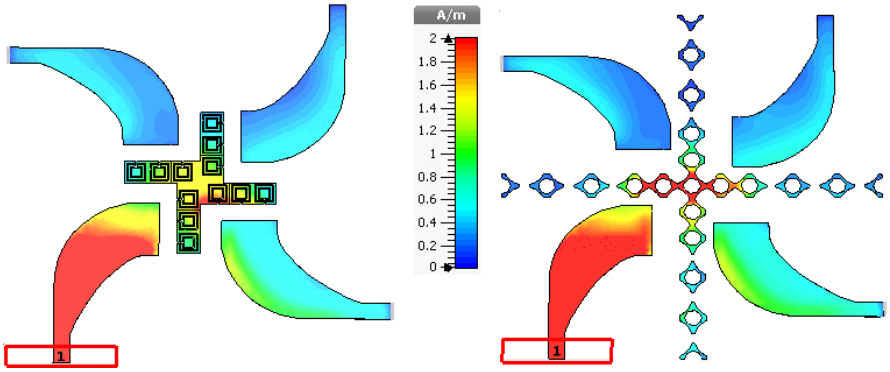

(d) With ring and CSRs between elements.

Figure 4.11 : The current distributions at 2.45 GHz when port 1 is excited.

Furthermore, Figure 4.11 illustrates the current distribution of a small quad-element MIMO antenna that operates at 2.45 GHz and employs annular strips and complementary spiral ring resonators (CSRs). The figure reveals that integrating CSRs into MIMO antennas can impede radiated energy and reduce transmitted power between neighboring elements by inducing a current flow through both the metallic stub and the CSRs. This results in a slight improvement in mutual coupling (S21) between adjacent antenna elements.

4.6 The Proposed Antenna: Results and Evaluation

To validate the proposed antenna design, we fabricated a prototype, which is shown in Figure 4.12. The prototype was tested by measuring its S-parameters using a Rohde & Schwarz spectrum analyzer. During the testing process, we excited two of the four antenna ports, while terminating the remaining two with 50Ω loads.

(a) Top layer. (b) Bottom layer.

Figure 4.12 : Prototype of the designed dual-elliptically tapered MIMO antenna.

The MIMO antenna used in this study was evaluated for both simulated and measured reflection coefficients. The results are presented in Figure 4.12. The graph in Figure 4.12 demonstrates a significant similarity between the simulated and experimental data for the reflection coefficient. Furthermore, the proposed quad-element MIMO antenna proves to be effective in the frequency range of 2.3 GHz to 2.7 GHz, with a reflection coefficient of less than -10 dB, as shown in Figure 4.12. The radiating antenna elements

exhibit excellent resonance at a central frequency of 2.46 GHz in both the simulations and measurements.

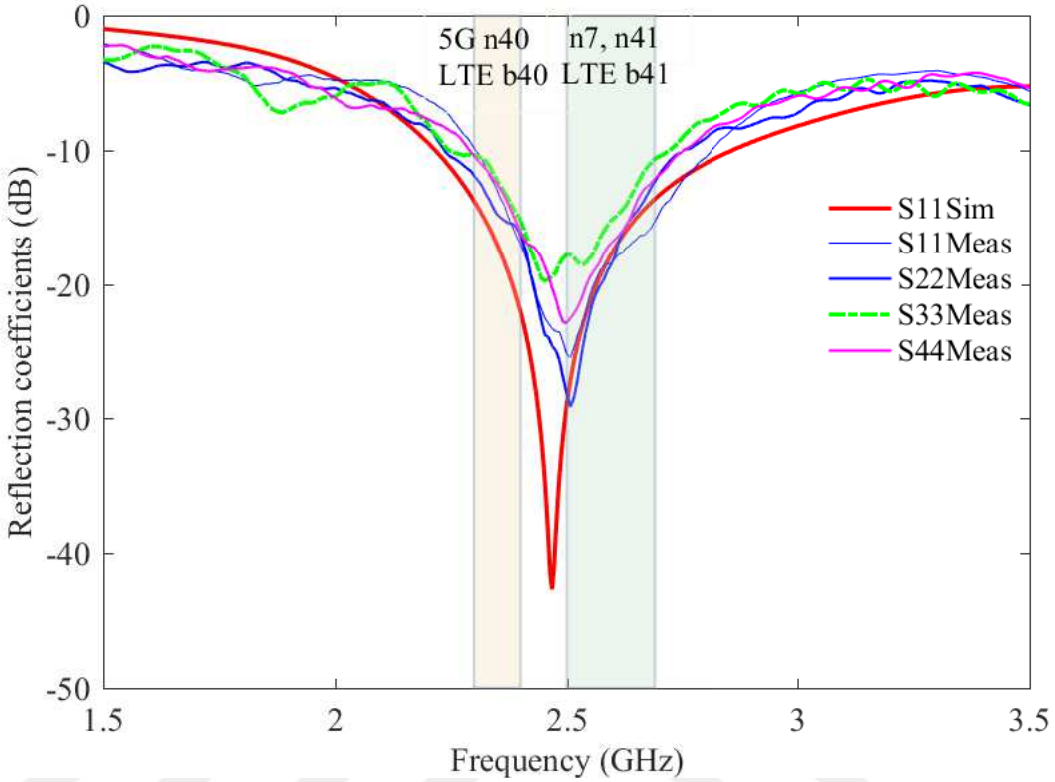

Figure 4.13 : Reflection coefficients of dual-elliptically tapered MIMO antenna.

Based on the preliminary simulation results, the final version of the planned antenna was selected as it demonstrated minimal mutual coupling and excellent impedance matching. As shown in Figure 4.12, neighboring components (S21, S14, S43, S32) exhibited mutual coupling of more than 17 dB, and diagonal paired components (S31, S24) exhibited mutual coupling of more than 21 dB across the desired frequency range. However, both experimental and simulation-based isolation measurements were less than -17 dB, indicating a reduction in mutual coupling for components S21, S14, S43, and S32. The graph indicates that the results from both testing and simulation are in reasonable agreement, although the use of lossy materials, soldering errors, and manufacturing imperfections are the primary reasons for slight discrepancies between simulated and measured findings.

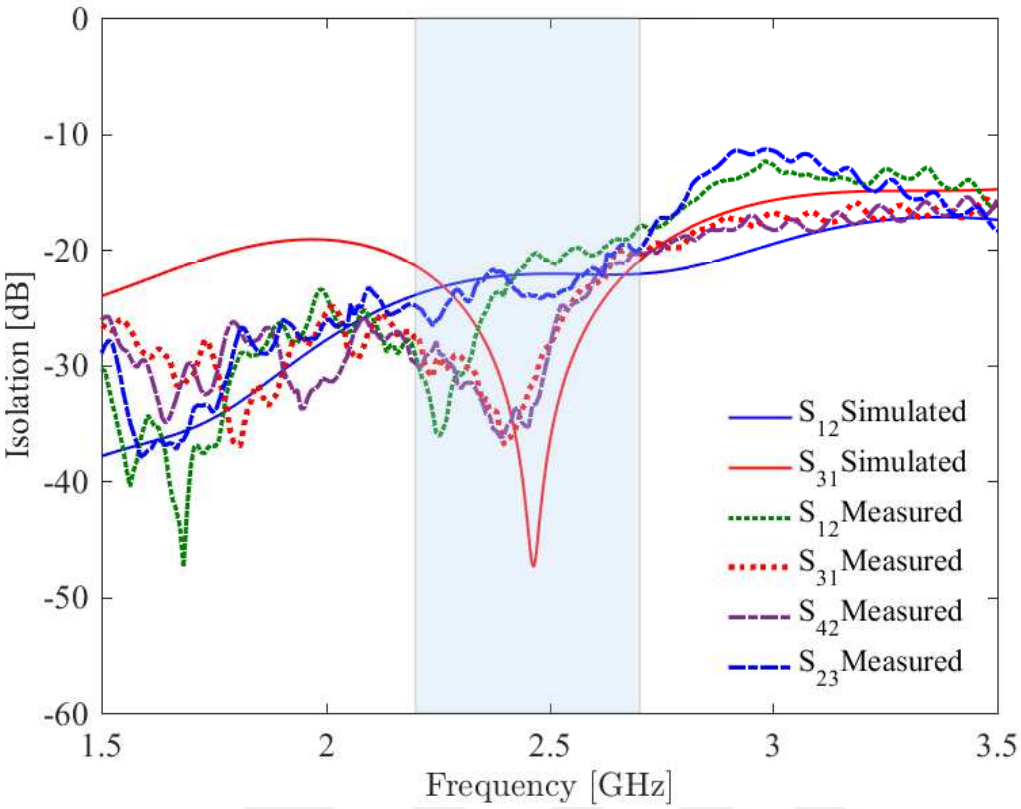

Figure 4.14 : Isolation dual-elliptically tapered MIMO antenna.

4.6.1 Radiation patterns

The diagram depicted in Figure 4.15 showcases the computer-generated radiation patterns of specific antenna components equipped with quad ports that operate at a frequency of 2.45 GHz. The radiation patterns observed in both the E-plane (co-pole and cross-pole) and H-plane (co-pole and cross-pole) of the antenna for all four modes indicate that the microstrip feed ports 1, 2, and 4 have mutually perpendicular polarization planes. This configuration can produce a range of radiation patterns. The antenna elements have linear polarization, which yields a solid performance for cross-polarization at 2.45 GHz, with an E-plane of approximately 15 dB. Additionally, Figures 4.16 and 4.17 illustrate the simulated radiation patterns of the four-beam antenna elements for the E-plane (co-pole and cross-pole) and the H-plane (co-pole and cross-pole) at 2.3 GHz and 2.6 GHz, respectively. The symmetrically arranged double tapered radiation slots of the proposed MIMO antenna generate diverse radiation patterns.

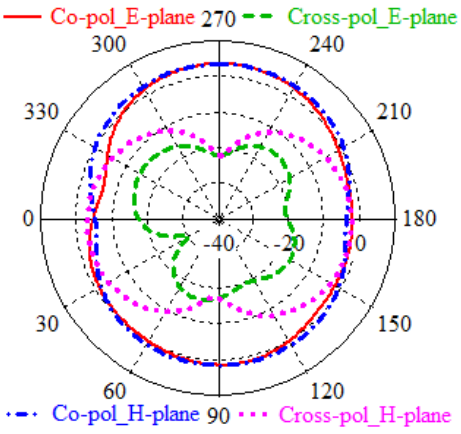

(a) port 1.

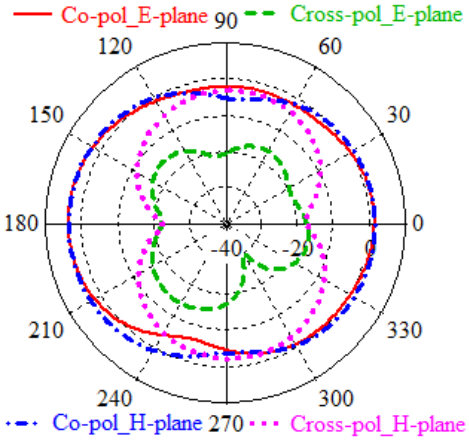

(b) port 2.

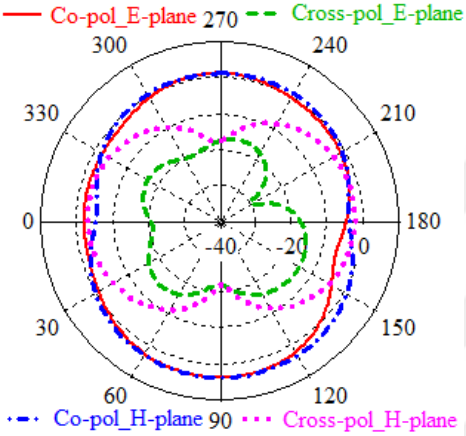

(c) port 3.

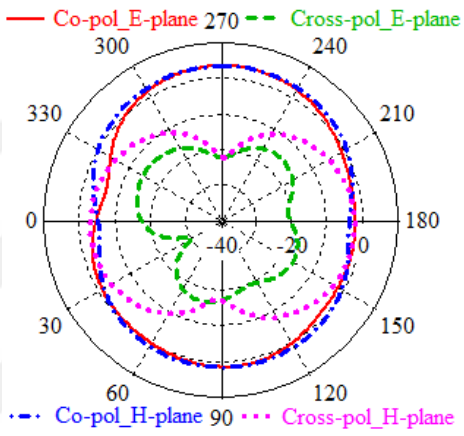

(d) port 4.

Figure 4.15 : Radiation patterns at 2.45 GHz in two principal planes

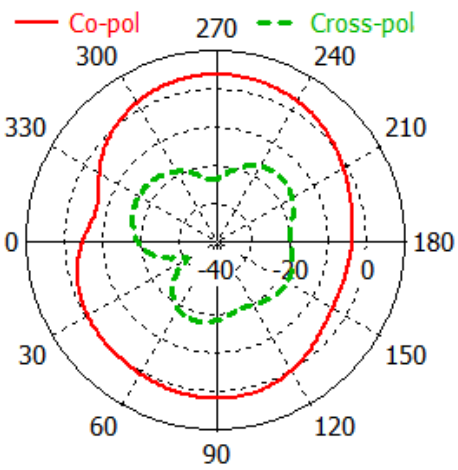

(a) E-plane.

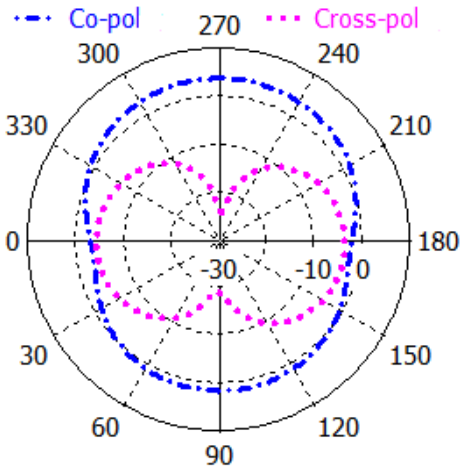

(b) H-plane.

Figure 4.16 : Radiation patterns at 2.30 GHz in two principal planes.

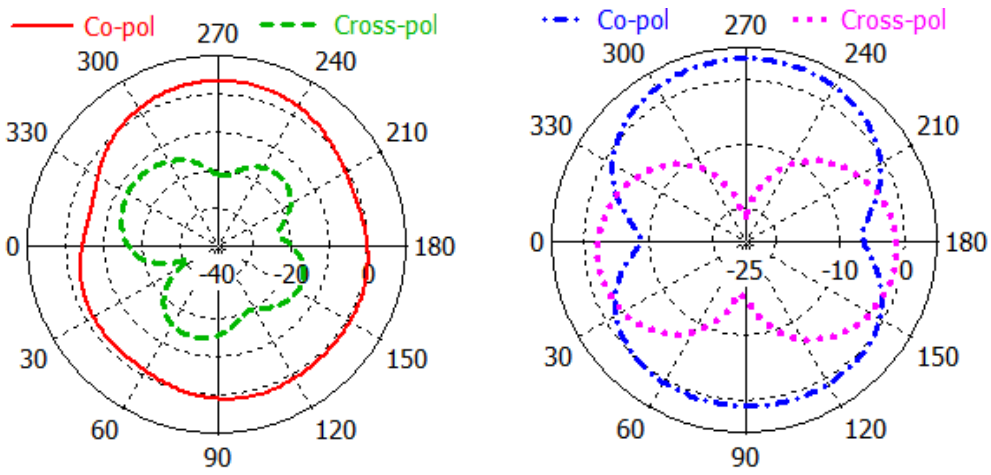

(a) E-plane. (b) H-plane.

Figure 4.17 : Radiation patterns at 2.60 GHz in two principal planes

4.6.2 Diversity Performance of the Designed Antenna

Diversity performance of the designed quadruple radiating element MIMO antenna can be evaluated using metrics such as ECC, capacity loss, channel capacity, and total active reflection coefficient. By optimizing the antenna design and carefully considering the antenna placement, orientation, parasitic element and annular stripes, the diversity performance of the MIMO antenna system can be improved, resulting in improved signal quality and reliability of the wireless link.

The Envelope Correlation Coefficient (ECC) is used to measure the degree of coupling between adjacent and diagonal MIMO antenna components, with a lower value indicating better antenna diversity performance. The calculation of the coefficient of correlation between antenna elements involves the use of scattering parameters, which are described in [22], [33], and [34].

The measured envelope correlation coefficients (ECC) agree closely with the simulated values in the model, as shown clearly in Figure 1. Specifically, the results for both adjacent and diagonal elements are below 0.04 and 0.03 respectively, demonstrating the accuracy and precision of the measurements. These findings indicate good diversity performance of the quadruple radiating element MIMO antenna, an essential factor for reliable wireless communication in practice. The results thus imply promise for designing future MIMO antenna systems, as high diversity is critical for robust wireless transmission. Achieving good isolation between elements through proper

design is key to minimizing correlation and maximizing diversity gain. The results imply that optimizing these types of MIMO antennas through careful adjustment of such design parameters could deliver significant increases in spatial multiplexing for wireless systems. The performance demonstrated here provides motivation to further research optimizing these antennas to realize their full benefits.

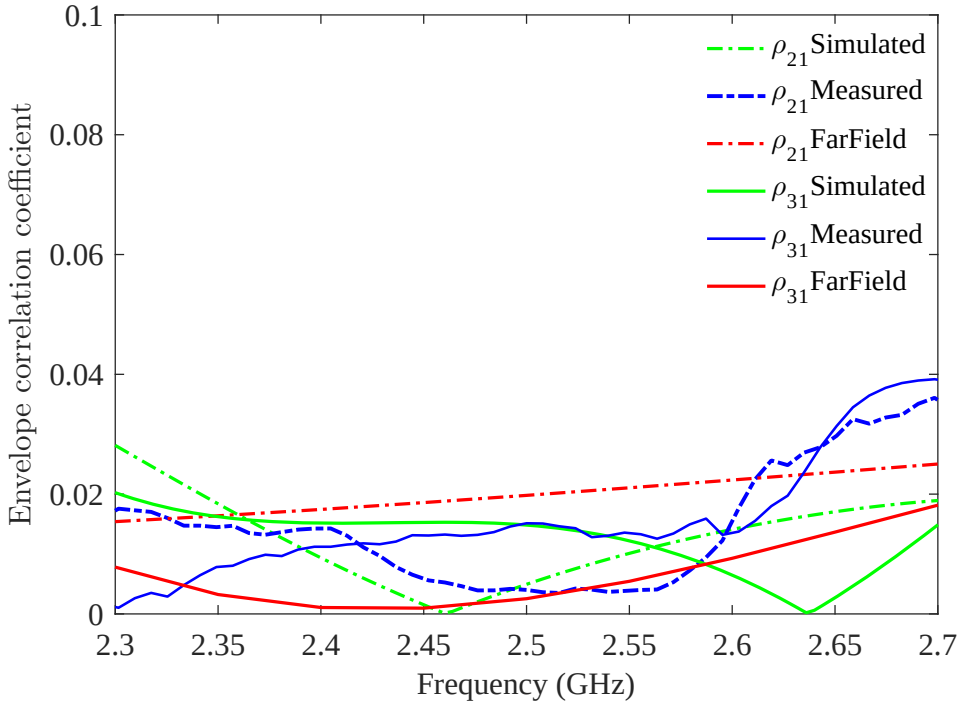

Figure 4.18 : Envelop correlation of the designed MIMO antenna.

Channel capacity loss represents the maximum reduction in achievable data transmission rate at an acceptable error rate. It is a crucial metric for assessing the performance of an N x N MIMO (multiple-input multiple-output) antenna system. Channel capacity refers to the maximum rate at which data can be sent through a communication channel with an acceptably low error rate. This key performance metric for MIMO antenna systems has been examined in previous studies such as [35] and [36]. The channel capacity loss formula can be applied to compute the capacity loss for MIMO configurations.

$$C_{loss} = -\log_2 det(\psi)^R \tag{4.1}$$

where ψ^R is the receiving antenna correlation matrix.

$$\psi^R = \begin{bmatrix} \delta_{11} & \delta_{12} & \dots & \delta_{1j} \\ \delta_{21} & \delta_{22} & \dots & \delta_{13} \\ \vdots & \vdots & \ddots & \vdots \\ \delta_{i1} & \delta_{i2} & \dots & \delta_{ij} \end{bmatrix} \tag{4.2}$$

where i=j $\delta_{ij} = 1 - \sum_{n=1}^{N} S_{i,n}^{*} S_{n,j}$ and $i \neq j$ $\delta_{ij} = -\sum_{n=1}^{N} S_{i,n}^{*} S_{n,j}$

To assess the channel capacity loss of a MIMO antenna, the process involves utilizing scattering parameters through measurements and simulations, as mentioned in Equation 4.1. The results displayed in Figure 4.19 indicate that the average channel capacity loss across the entire frequency range of operation is less than 0.6 b/s/Hz, a value considered acceptable for practical MIMO systems. However, the results also illustrate minor variations, which may be attributed to factors such as fabrication precision, soldering, and feed cable effects. These elements have the potential to cause deviations in the performance of the MIMO antenna, and their impact should, therefore, be considered when evaluating the antenna's channel capacity loss.

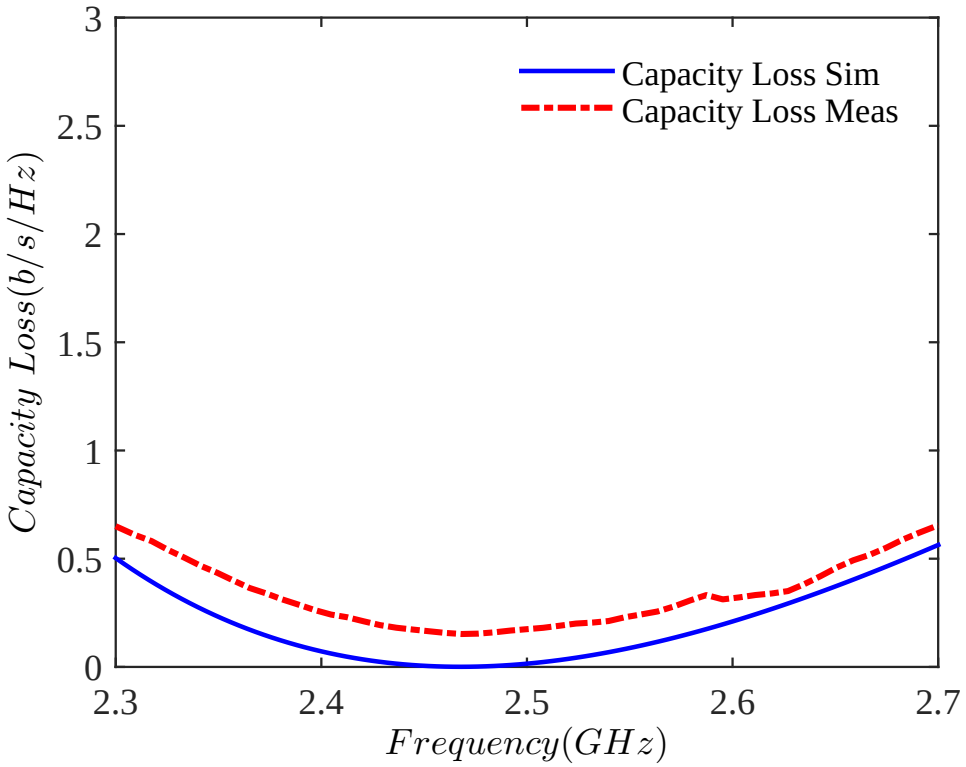

Figure 4.19 : Capacity loss of the designed MIMO antenna.

Multiple-input multiple-output (MIMO) antennas are widely used in wireless communication systems due to their ability to improve data rates and reduce errors. The Total Active Reflection Coefficient (TARC) is an important parameter for analyzing the characteristics of MIMO antenna configurations. As described in [23], TARC helps assess the operating frequency range and radiation performance of MIMO systems by calculating the square root of the total reflected power divided by the total incident power for an N-port antenna array. TARC highlights the importance of maintaining resonance, independent of phase shift fluctuations among antenna components. For lossless dielectric MIMO antennas, the scattering matrix can be utilized to derive TARC through the following equation. This metric provides crucial insights into the frequency and radiation behaviors of MIMO antenna designs.

Figure 4.20 presents the calculated and measured TARC values for the proposed antenna design. The TARC results were produced using Equation 2.14 across a phase range of 0° to 90° in 30° increments. The figure distinctly exhibits the two operating frequency bands of the antenna, where the TARC remains below -10 dB. This demonstrates the stable resonance performance across the intended bands, validating the design through close agreement between the simulated and measured TARC values.

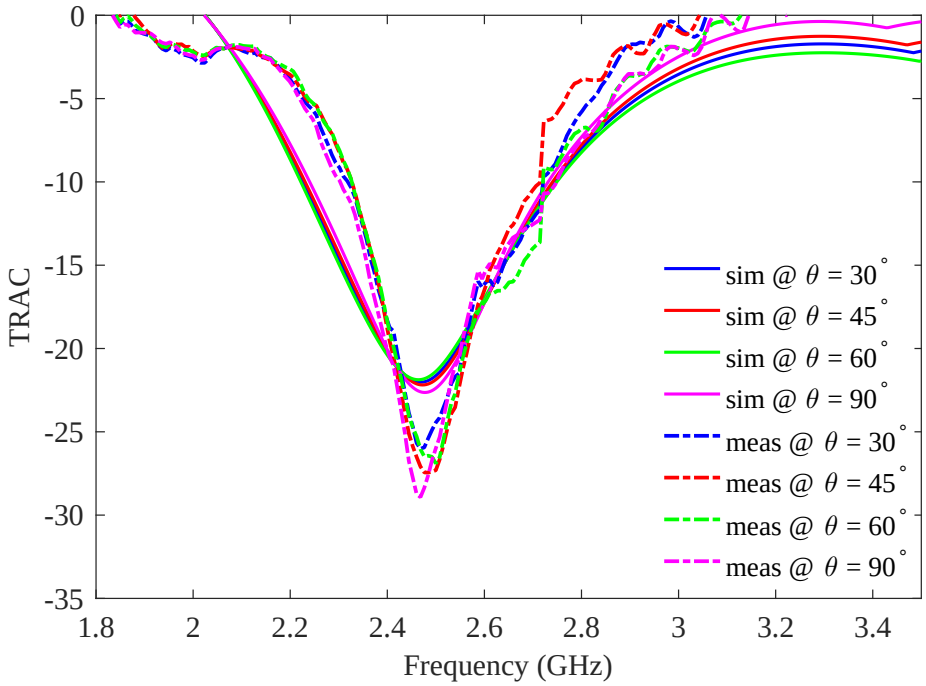

Figure 4.20 : TARC with various phases.

Channel capacity refers to the maximum achievable data rate through a MIMO system with minimal errors. The relationship between channel capacity and MIMO antenna characteristics is not as intuitive as in a single antenna system because various factors can simultaneously affect capacity in MIMO antenna networks, as investigated in studies like [1]-[4]. One method to characterize the multiplexing efficiency of a MIMO array is to compute the reduction in power efficiency needed to attain the same channel capacity as a reference multi-antenna system under similar channel conditions. If the transmitter has no channel information, the M x K channel matrix can be expressed using Equation 2.21.

To evaluate the channel capacity of a MIMO system, generate multiple channel realizations for the 4x4 MIMO system using an appropriate channel model. This could involve modeling the propagation environment, antenna array characteristics, and other relevant factors. Incorporate the impact of antenna efficiency and correlation into the channel model. Antenna efficiency affects the received signal power, while antenna correlation impacts the independence of the MIMO subchannels.

Analyze the resulting ergodic capacity values to determine the impact of antenna efficiency and correlation. This could involve comparing the capacity distributions, mean values, or other statistical measures under different antenna efficiency and correlation conditions.

The ergodic channel capacity of the proposed 4x4 antenna element MIMO system was evaluated through channel realizations. The results indicate that the capacity of the correlated MIMO channels is higher than the capacity of the 4x4 channels with unknown channel state information (CSI) at the transmitter. This evaluation took into consideration both antenna efficiency and correlation, as depicted in Figure 6.17. The simulated channel capacities of the proposed 4x4 MIMO system are 21 bps/Hz with correlation and 20.5 bps/Hz with both efficiency and correlation. In comparison, the simulated channel capacity with independent and identically distributed (i.i.d) channels reaches 22 bps/Hz.

Furthermore, the measured channel capacities of the proposed MIMO system were found to be 19.5 bps/Hz for both correlation and efficiency, at a signal-to-noise ratio (SNR) of 20 dB. These findings highlight the impact of correlation and efficiency on the overall channel capacity of the 4x4 MIMO system.

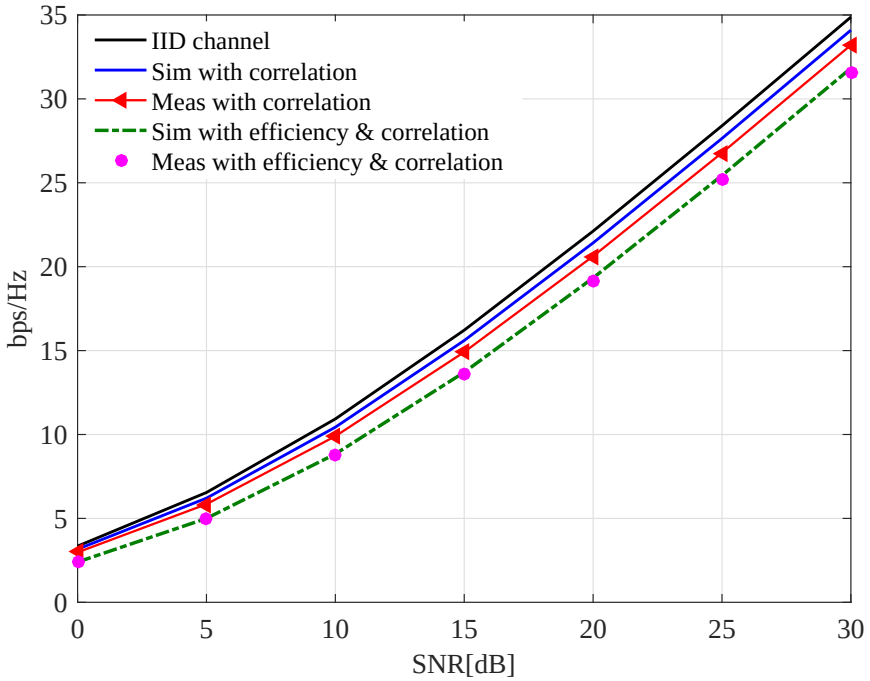

Figure 4.21 : Capacity of the MIMO system over Rayleigh fading channel.

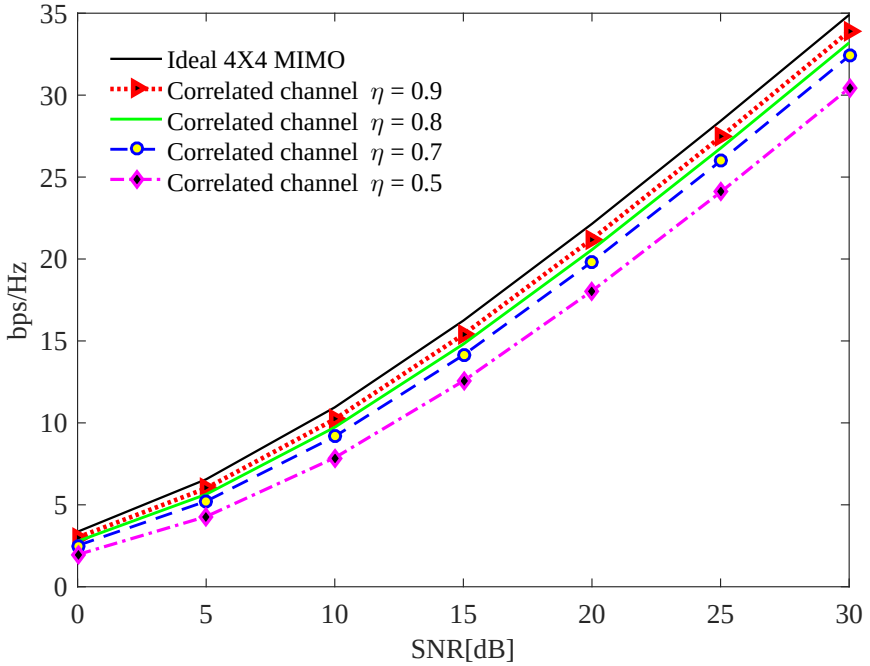

Figure 4.22 : Comparison of capacity versus efficiency.

As shown in this Figure 4.22, when the efficiency (η) increases, the channel capacity increases. Figure 4.22 shows the channel capacities of the proposed array when changing efficiency from 0.5 to 0.9. Where, increasing efficiency at 0.5, 0.7, 0.8 and 0.9 results in a capacity enhancement of 3% incremental increases as shown by 18.1454, 19.8928, 20.6322, and 21.2811 bps/Hz respectively.

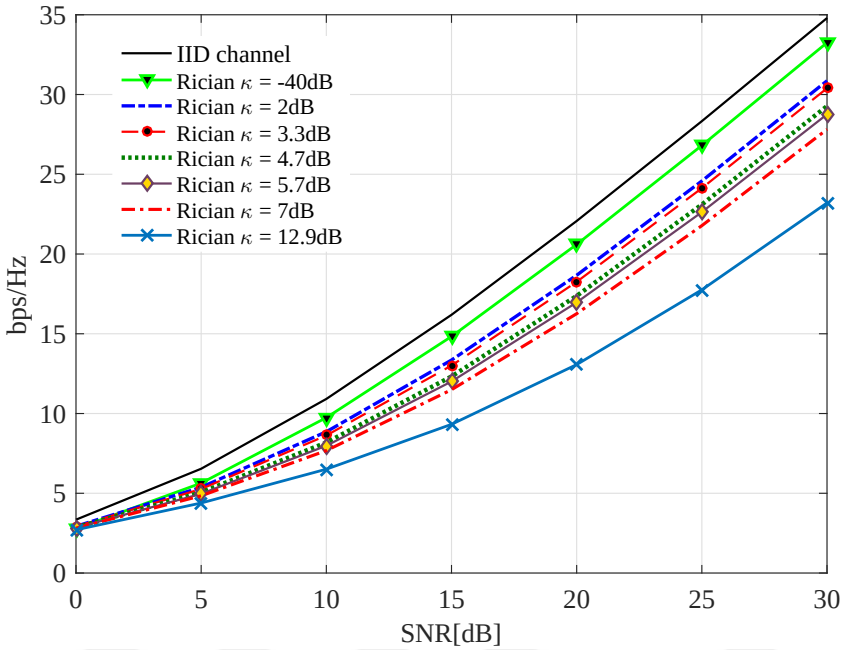

Figure 4.23 : Capacity of the MIMO system over Rician fading channel.

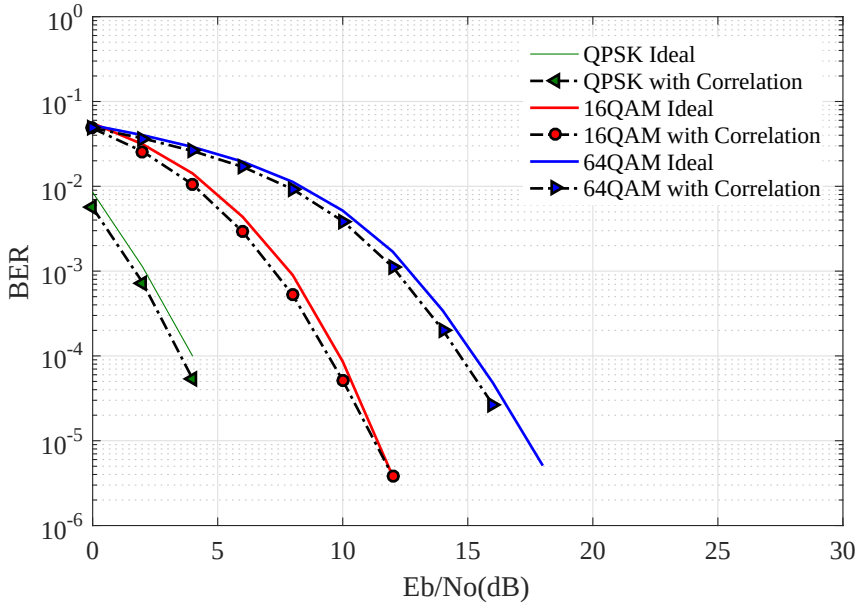

Figure 4.24 : BER of the MIMO system.

In Figure 4.23, the ergodic capacity of a wireless communication system decreases as the Rician K-factor increases. This is because as the K-factor increases, the

line-of-sight (LOS) component of the signal strengthens relative to the scattered signal components. However, the impact of the K-factor depends on the specific application and environment. In some cases, a higher K-factor may actually be beneficial. For instance, in LOS environments, a high K-factor can lead to a stronger and more reliable line-of-sight signal. Figure 4.24 demonstrates that the bit error rate (BER) relies on both the modulation technique and the SNR. Higher modulation orders, such as 64-QAM, may transmit more bits per symbol but they need a higher SNR to achieve the same BER as lesser modulation orders like QPSK or 16-QAM. In order to attain a desired BER, greater modulation orders require an elevated SNR. For example, 64-QAM may need an SNR of 15 dB to obtain a BER of 10-4, but QPSK only requires 4 dB SNR and 16-QAM requires roughly 10 dB SNR for the same BER. This is because when there are more constellation points packed closer together, noise has a greater likelihood of causing errors.

The data presented in Table 6.3 compare the MIMO antenna developed in this study with previously researched four-element MIMO antennas, focusing on isolation, gain, and bandwidth. The designed antenna is more compact but still achieves an acceptable degree of isolation exceeding 17 dB through a frequency range of 2.3-2.7 GHz. In contrast, the antennas described in [37] and [38] have larger dimensions, providing higher gain but not matching the level of isolation achieved by the proposed antenna. Notably, the proposed MIMO antenna has the smallest dimensions of all the antennas reviewed.

Table 4.3 : A comparison of the designed and previously reported MIMO antennas.

Ref.	Size (mm)	BW GHz	Isolation dB	Peak Gain dBi	Material
[37]	$70X70$	2.37-2.69	> 17	3.98	$FR4$
[38]	$100X50$	2.40-2.80	> 12	not	$FR4$
[39]	$85X85$	2.32-2.95	> 17	3-5.5	$Ro4003C$
[40]	$45X90$	2.23-2.64	> 13	2.7	$FR4$
Proposed Antenna	$66X66$	2.30-2.70	> 17	3.67	$FR4$

5. MIMO ANTENNA SOLUTION FOR 5G SUB-6 USER EQUIPMENT

The growth of wireless technology has given rise to the development of MIMO antennas that can accommodate UE communication systems operating across various single to multi-frequency bands [41]. 5G spectrum allocation is classified into sub-6 GHz low to mid-band and high-band mm-Wave spectrum. Typically, the sub-6 band is used to achieve wider coverage and enhanced penetration through obstacles like walls, while the high-band mm-Wave has the potential to provide faster data speeds but with reduced range and higher susceptibility to obstructions. Currently, the n78 band range (3.3 - 3.8 GHz) and the n79 band range (4.4 - 5.0 GHz) are the most commonly utilized bandwidths for 5G communication systems [42]. However, to meet the technical specifications and data rate requirements of 5G, the Federal Communications Commission (FCC) mandates that at least 100 MHz of bandwidth be allocated to the sub-6 spectrum [43].

In this chapter, two novel antennas have been designed to support both n78 and n79 bands operating with single- and dual-band frequency spectrum respectively. The designed antennas exhibit good impedance matching, cost-effectiveness, and compactness. The configurations utilize either the Apollonian fractal or the tapered slot concept to create MIMO antennas. The two novel configurations are capable of enhancing isolation by utilizing placement and orientation mechanisms, leading to outstanding diversity performance with minimal ECC. The first design uses a single-band monopole and a wideband quad-element Apollonian fractal MIMO antenna system to enable 5G Sub-6 operation on the n78 band. Meanwhile, the second design incorporates a single element with four tapered slots and defective radiating slots, designed to improve isolation in a dual- and wide-band MIMO antenna system operating on both the n78 and n79 sub-6 GHz bands.

5.1 Quadruplet Apollony Radiating Antenna Elements for Sub-6 5G Apps

Over the last few years, several works of literature have proposed using fractal shapes to build multi-antenna systems. Fractal geometry has helped miniaturize antennas and widen their bandwidth in limited space due to fractals' characteristic features, such as self-similarity and space-filling properties. Gurjar et al. [44] demonstrated a two-element MIMO antenna with an 8-shaped fractal structure and a T-shaped ground plane. The isolation of this antenna is approximately 15 dB across a bandwidth of 3.18 to 11.5 GHz. Bhattacharya et al. [45] proposed a twin monopole slotted antenna using a Koch snowflake shape. The minimum isolation level achieved in this study was greater than 22 dB in a range of 3.0 to 11.1 GHz. Das et al. [46] presented a hexagonal wide slot antenna using fractal geometry. Isolation in this design was greater than 18 dB over a bandwidth of 2.88 to 11 GHz. Tripathi et al. [47] suggested using the outer edges of two octagonal geometries combined with Koch's fractal geometry to obtain the working band of the UWB MIMO fractal antenna, which was in the range of 3.18 to 11.5 GHz.

Previous works have designed MIMO antennas using fractal geometries such as Sierpinski's triangle and Koch's snowflake [citations]. However, this study proposes a new fractal-shaped MIMO antenna based on the Apollonian structure. Specifically, we propose a four-element antenna for MIMO applications utilizing placement and orientation isolation techniques to take advantage of antenna diversity. The radiator is loaded with a microstrip line employing a quarter-wave transform to improve impedance matching. The Apollonian-shaped design offers miniaturization, low inter-element coupling, and low ECC. We simulate the antenna in CST and fabricate prototypes to verify the design. Thus, the proposed Apollonian fractal MIMO antenna is suitable for 5G user devices, providing miniaturization, isolation, and diversity gain.

5.1.1 Single Apollony-Shaped Antenna

Figure 5.1 illustrates the planar fractal antenna with an Apollonian shape. This antenna is composed of two layers, with the ground plane situated at the bottom and the Apollonian fractal antenna on the front layer. The microstrip, which has a characteristic impedance of 50 ohms, incorporates an Apollonian fractal antenna that employs a quarter-wave transformation. This design results in a circular patch that resonates at a frequency of 3.5 GHz in the initial implementation [48]. The proposed antenna has a height of 1.6 mm, a relative dielectric constant of 4.3, and a tangent loss of 0.025 based on the FR-4 PCB. The dimensions of the antenna are $40 \times 40 mm^2$. The optimal dimensions of the Apollonian-shaped monopole antenna are presented in Table 5.1.

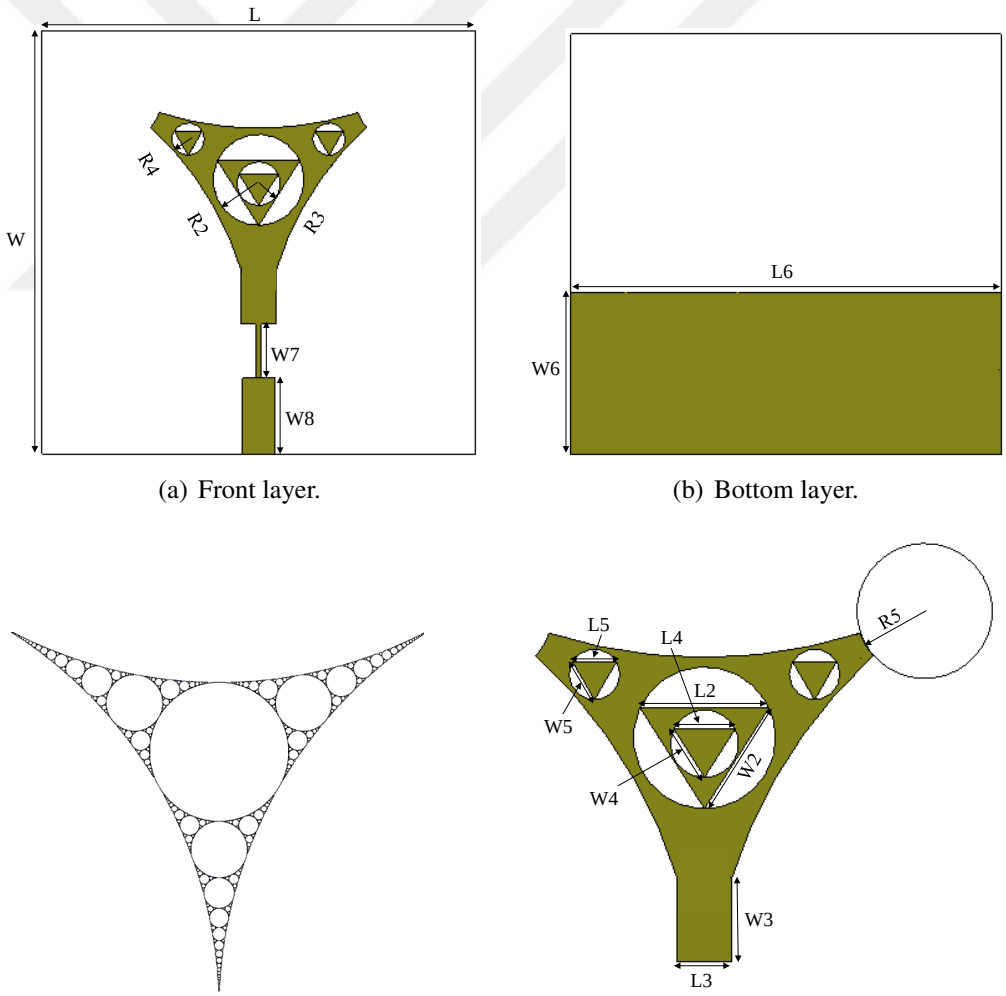

(a) Front layer. (b) Bottom layer.

(c) Apollony structure [49]. (d) Magnified section.

Figure 5.1 : The Apollony-shaped fractal antenna layout.

Table 5.1 : The designed MIMO antenna's dimensions.

Parameters	Value (mm)	Parameters	Value (mm)	Parameters	Value (mm)
L	40	L2	7.6	L3	3.2
W	40	W2	7.05	W3	4.9
L4	3.6	L5	2.6	L6	40
W4	3.37	W5	2.6	W6	17
R2	4.2	R3	2	R4	1.5
W7	5	W8	7	R5	2.84

5.1.2 Design Evaluation of Apollony-Shaped Antenna

Figure 5.2 shows a four-step design evaluation of an Apollonian fractal monopole antenna, which was used to verify the design. Adjusting the frequency response (using the n78 antenna topology) is crucial to achieve wideband functioning. Initially, the Apollonian shape was formed by constructing three circles with the same radius of 30 mm, which are mutually tangent to each other, as illustrated in Figure 5.1c. The region between the three circles is called a solid Apollonian shape, as displayed in Figure 5.2a with a microstrip feed. In the second stage, the Apollonian-shaped antenna was matched to the feed line (50 Ω) using a quarter-wavelength transmission line, as exhibited in Figure 5.2b. The goal is to increase the antenna's impedance bandwidth during phase 1.

In the next design stage, circles with radii of 4.2 mm and 1.5 mm were added in the center and two corners of the solid Apollonian shape, as displayed in Figure 5.2c. The Smith chart in Figure 5.3 shows that the slots provide capacitive loading to the radiating components in phase 3 by exploring the impact of modifying the fractal geometry on the monopole antenna's input impedance. The Smith chart in Figure 5.3 also exhibits that parasitic components provide inductive loading to the Apollonian fractal antenna. Therefore, when the triangular parasitic elements are inserted into the Apollonian radiating element, the capacitive loading reduces, and the plot switches to inductive at phase 4. The optimum dimensions for achieving the best impedance matching over the n78 band (3.3 - 3.8 GHz) were determined. The fractal planar antenna with an Apollonian shape was created for 5G applications, utilizing a microstrip feed line and modifying the quarter wavelength to improve its bandwidth. The simulated S11 for each of the four antenna stages is described in Figure 5.4. The plot shows how the

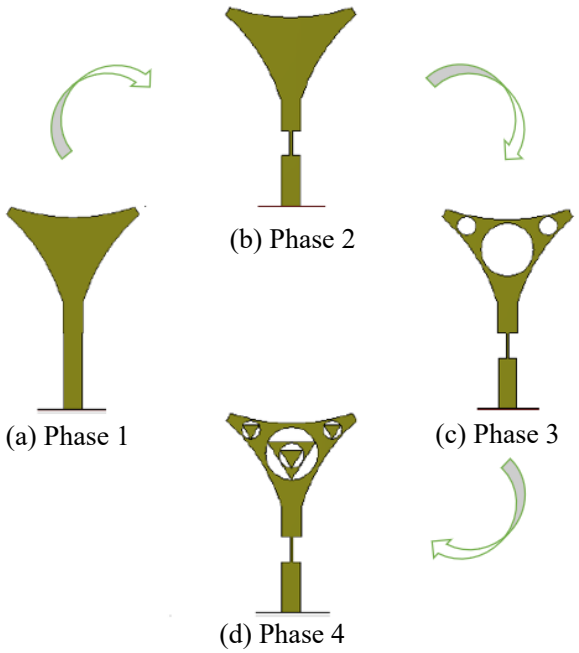

Figure 5.2 : Apollony fractal antenna design evolution.

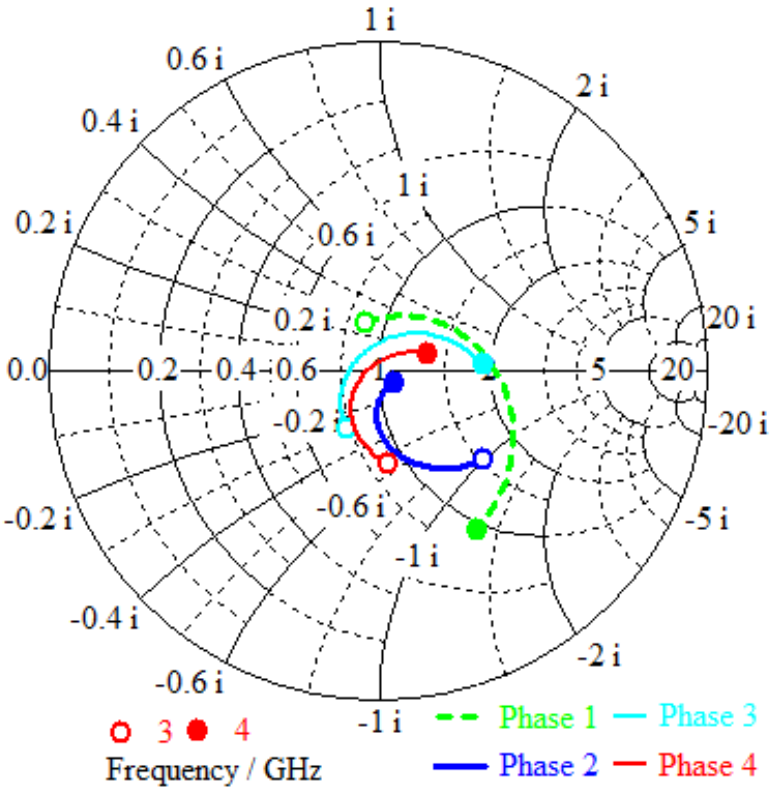

Figure 5.3 : Smith chart analysis of the impedance of the proposed antenna..

design of the antenna evolved to achieve operational frequencies in the n78 band, as depicted by the scattering parameters. Figure 5.5 depicts the input impedance of the antenna for the Apollony design evolution.

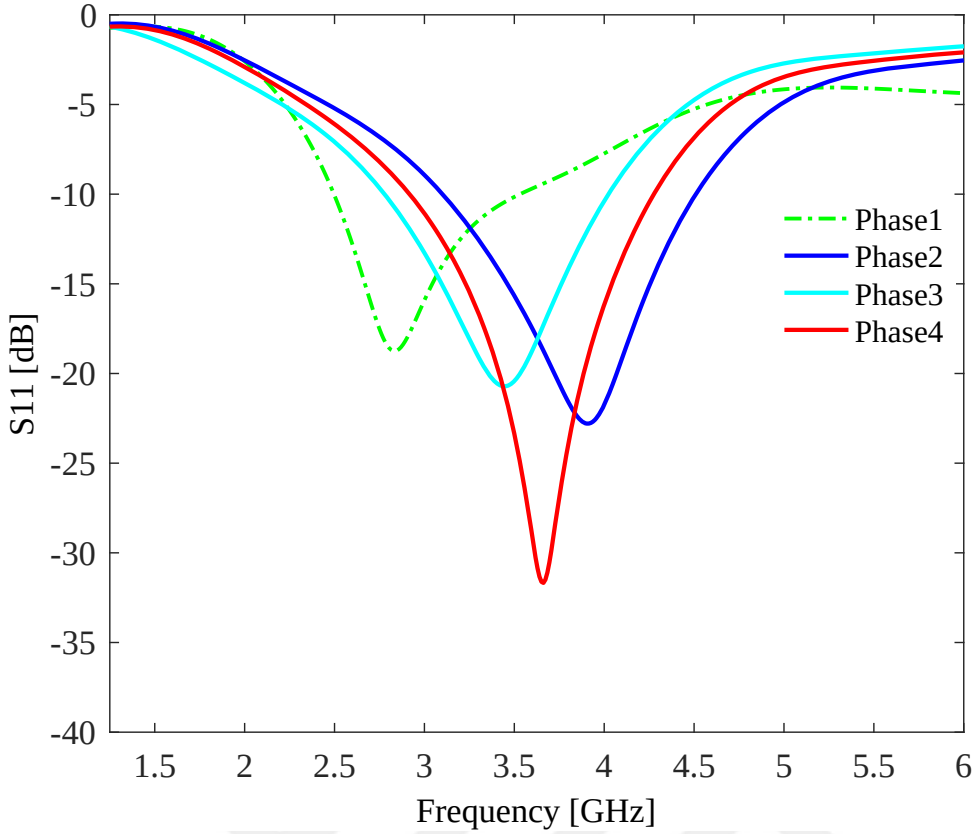

Figure 5.4 : Evolution of S11 for the Apollonian-shaped fractal antenna design.

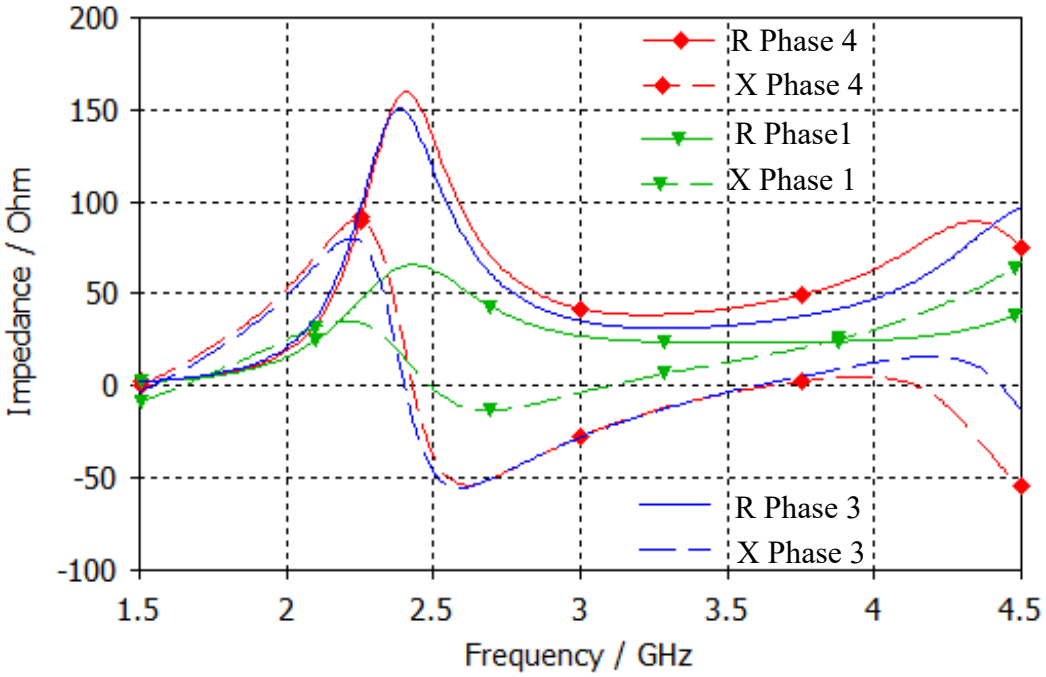

Figure 5.5 : Input impedance of the Apollony fractal antenna.

5.1.3 Design and Prototype of MIMO Antennas

Figure 5.6 shows an Apollonian-shaped fractal MIMO antenna designed for 5G applications. The antenna is a fractal monopole with a quarter-wave microstrip feedline and partial ground on the bottom layer. Two symmetrical monopoles are positioned perpendicular to each other to use diversity in the antenna. The antenna is modeled using the Finite Element Method (FEM) with the commercial simulator CST. Prior to PCB fabrication, the antenna is designed through computer simulation with specific parameters, including dimensions of 80 mm x 80 mm (length x width), a dielectric constant of 4.3, and a thickness of 1.6 mm. The feedline's thickness of 2.95 mm allows for operation with a 50 Ω characteristic impedance. The quad-ports MIMO antenna is designed to support the NR Band 78, a frequency band used for 5G applications.

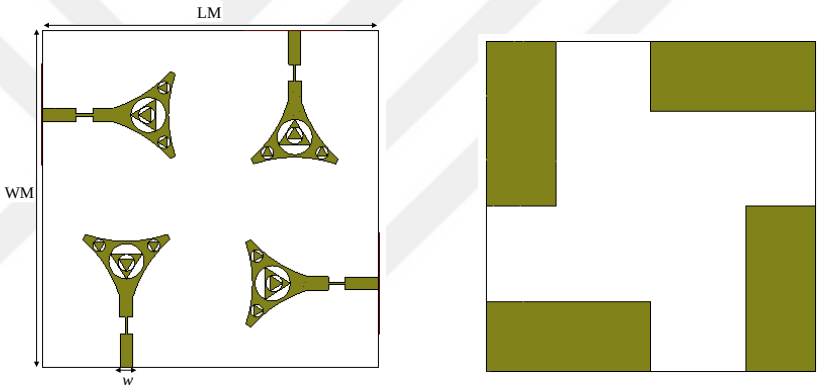

(a) Front layer (b) Back layer

Figure 5.6 : Layout of the Apollonian-shaped fractal MIMO antenna.

(a) Front view (b) Back view

Figure 5.7 : Prototype of the Apollonian-shaped antenna after fabrication.

5.1.4 Result and Discussion of Apollony-Shaped antenna

The Apollonian-shaped fractal MIMO antenna was fabricated, as shown in Figure 5.7, and tested experimentally for MIMO applications using the 5G n78 spectrum. The scattering parameter values were measured, and the signal behavior was analyzed using a Spectrum Analyzer (R&S FSH3). During the experiment, the two ports of the MIMO antenna were excited, while the other ports were terminated with a 50-ohm load. The simulated and experimental reflection coefficients of the fractal MIMO antenna with the Apollonian shape are shown in Figure 5.8. The proposed quadruple radiating antenna operates in the impedance range of 3 to 3.8 GHz and has a reflection coefficient of less than -10dB. These findings reveal that the simulation and experimental results for the reflection coefficient are quite similar to each other.

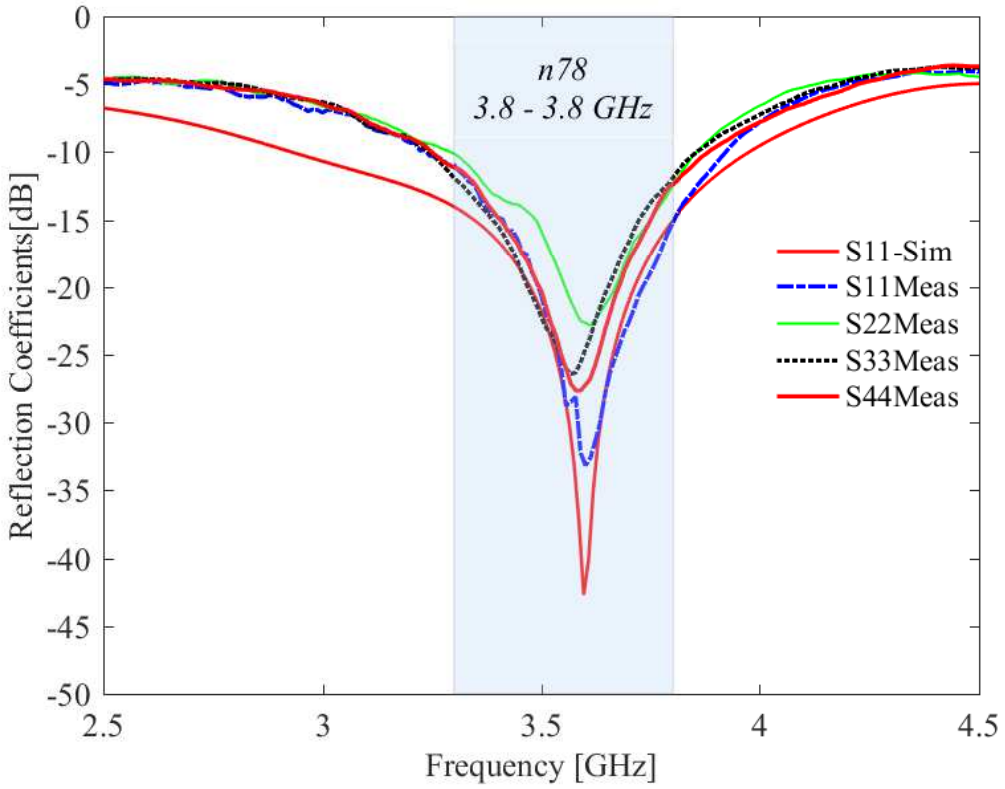

Figure 5.8 : Reflection coefficients of the Apollonian fractal antenna.

According to the experimental and simulation-based findings presented in Figure 5.9, it is evident that effective isolation between nearby elements (S21, S14, S43, and S32) was achieved, with values consistently less than -20dB. Additionally, mutual coupling

between the diagonal elements (S31, S24) was consistently below -25dB within the operational frequency spectrum. These results indicate that a reasonable comparison can be made between the experimental and simulation results in terms of isolation measurement. However, due to manufacturing imperfections, welding, and the use of lossy dielectric material, there is a slight impact on the measurement findings, causing some variation between the experimental and simulation results.

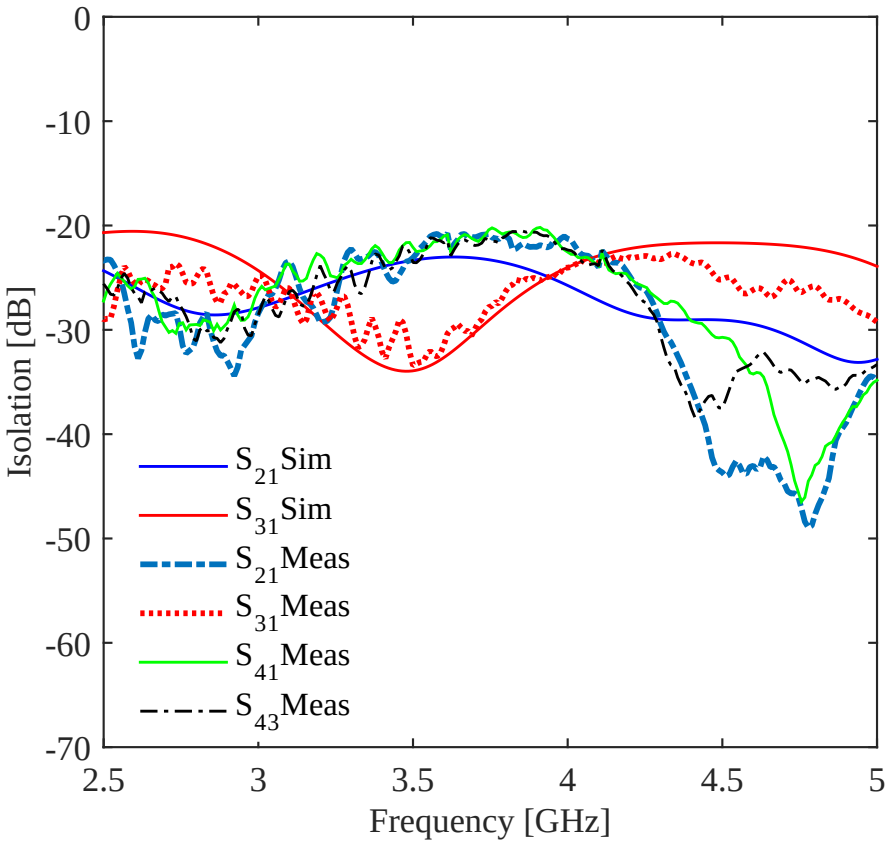

Figure 5.9 : Isolation performance of the Apollonian-shaped fractal antenna.

Figure 5.10 demonstrates that utilizing placement and orientation mechanisms results in a reduction of surface currents induced in both the opposite and adjacent antenna elements, aiming to mitigate mutual coupling between the quadruple feeding ports. The graph presented in Figure 5.11 displays the realized gain and radiation efficiency of the Apollonian fractal MIMO antenna. The ability of the Apollonian MIMO antenna to maintain a gain of 5 to 5.5 dB across the operational frequency range underscores its reliable performance. Moreover, the simulated radiation efficiency of the antenna is a critical aspect of its functionality. The results demonstrate that the Apollonian MIMO antenna can maintain a minimum efficiency of 77 % within the operating bandwidth,

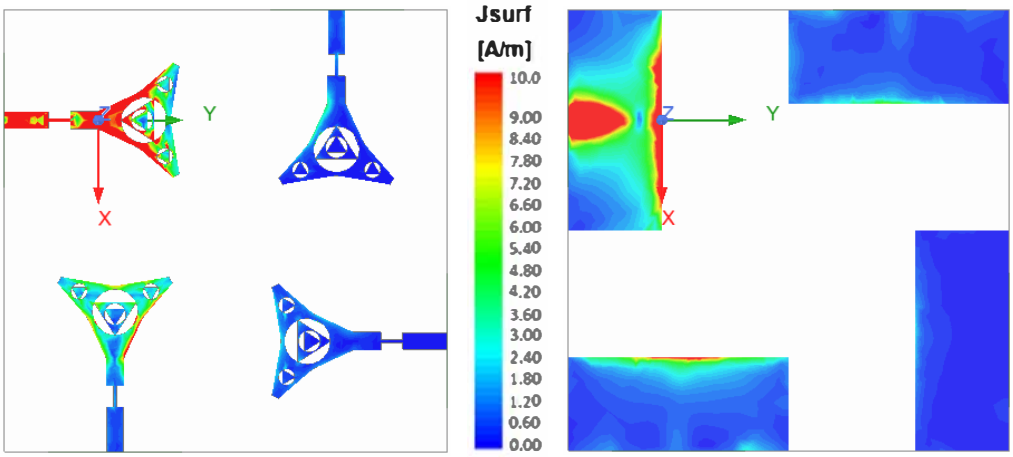

(a) Top layer (c) Bottom layer

Figure 5.10 : Current distribution of the Apollonian fractal antenna.

indicating that it can effectively convert electrical signals into radiated energy with minimal loss. In conclusion, the stable gain and efficiency are essential factors that determine the antenna's functionality and reliability in practical applications.

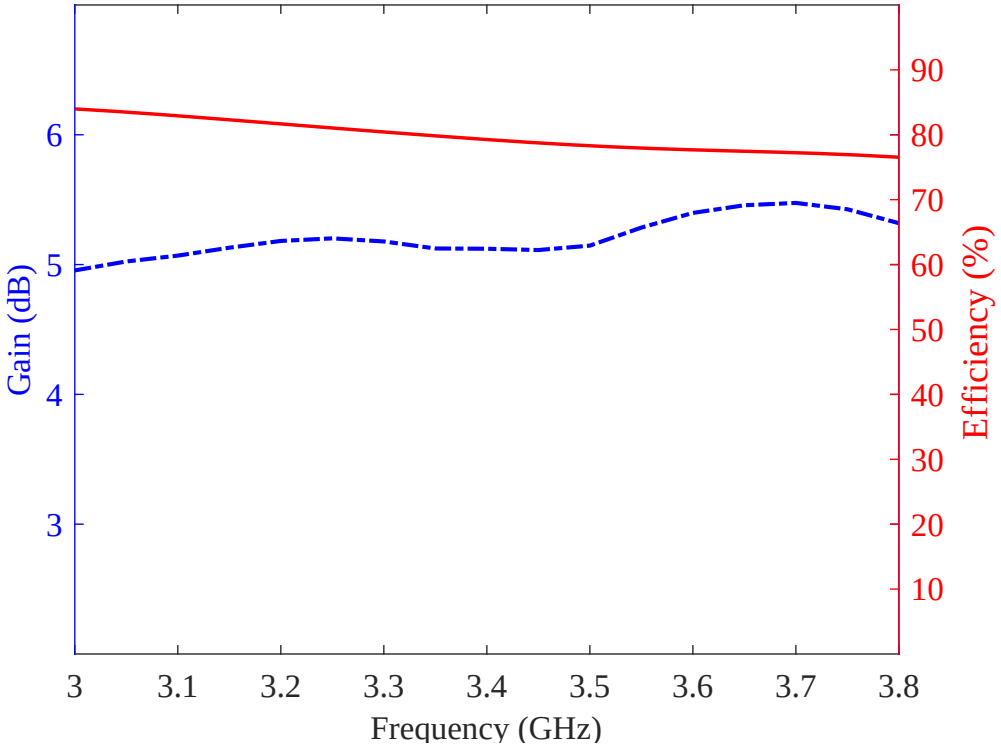

Figure 5.11 : Efficiency and gain of the Apollony fractal antenna.

The radiation patterns of the electromagnetic waves emitted by the antenna in the co- and cross-polarization are presented in Figure 5.12, covering the examined frequencies of 3.4, 3.6, and 3.8 GHz. The results confirm that the antenna's radiation patterns are in good agreement, which is consistent with the values obtained from the CST and HFSS simulations. Notably, the observed radiation patterns in the actual antenna closely match those predicted by the simulations.

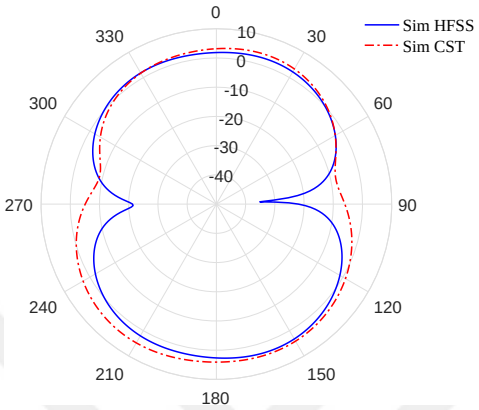

(a) co-polarization @ 3.4 GHz.

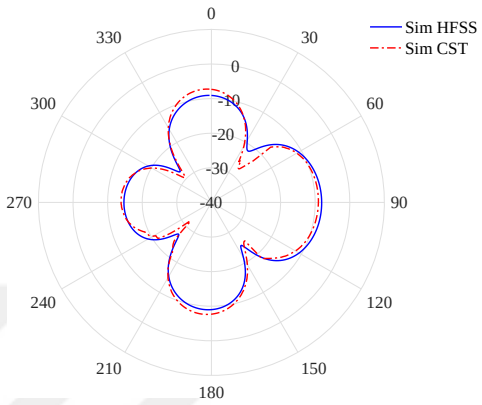

(b) cross-polarization @ 3.2GHz.

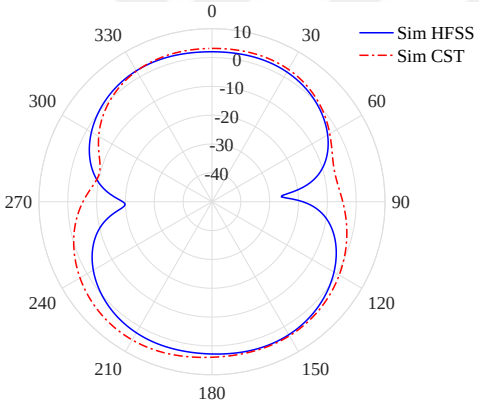

(c) co-polarization @ 3.6 GHz.

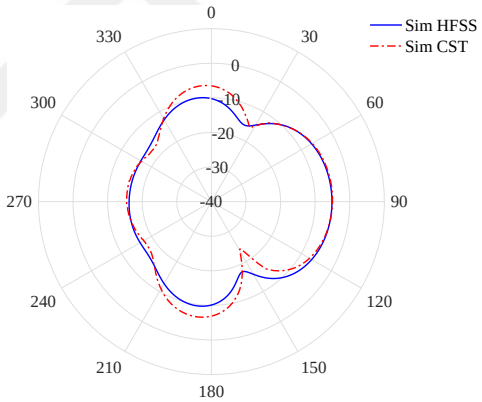

(d) cross-polarization @ 3.6GHz.

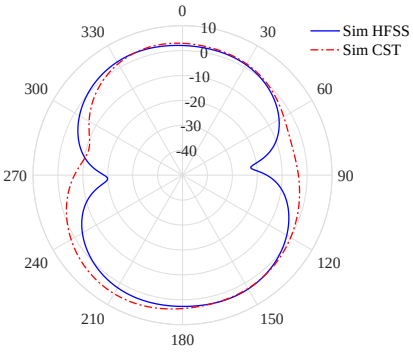

(e) co-polarization @ 3.8 GHz.

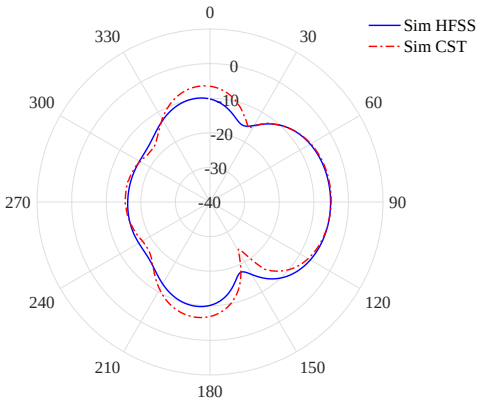

(f) cross-polarization @ 3.8GHz.

Figure 5.12 : Radiation patterns of the Apollony fractal-shaped antenna.

5.1.5 Characterisation of Apollony-Shaped MIMO Antenna

The envelope correlation coefficient (ECC) measures how well the neighboring radiating antenna elements correlate with every MIMO element [50] - [51]. Experimental ECC measurements are displayed in Figure 5.13, and they are found to be in fairly good agreement with the simulation results. The ECC values between adjacent and diagonal antenna elements were found to be less than 0.05 and 0.03, respectively. This indicates better overall diversity performance of the Apollonian-shaped fractal MIMO antenna.

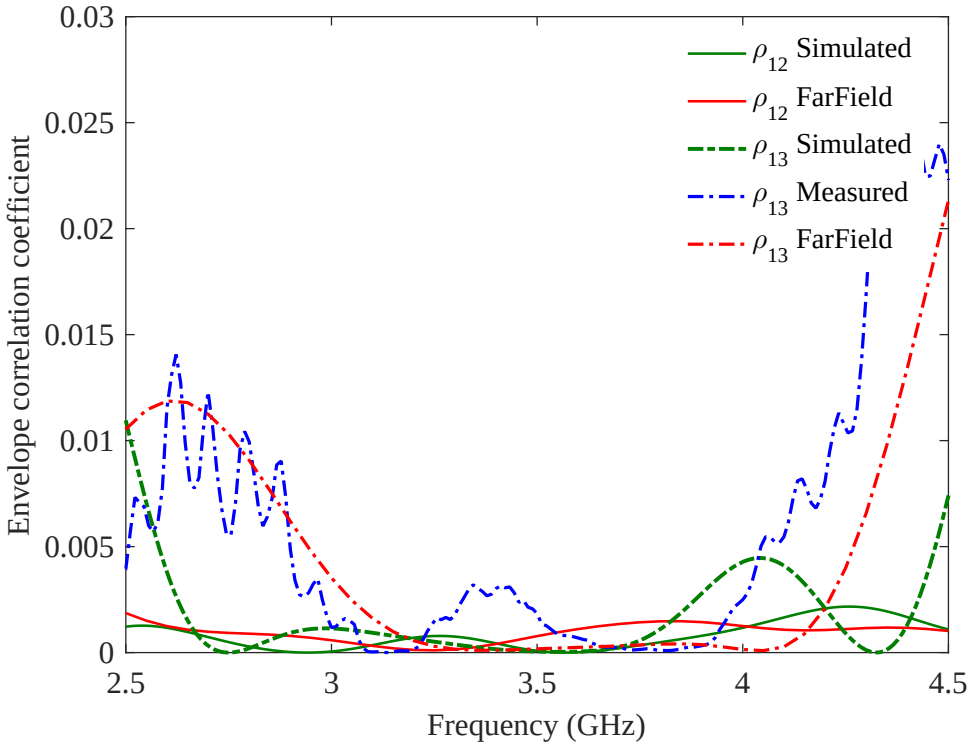

Figure 5.13 : ECC of the Apollony-shaped antenna.

The channel capacity loss (CCL) refers to the maximum data rate that a signal can be safely transmitted without significant errors [52, 53]. To calculate the CCL for the proposed antenna, S-parameters were used based on simulations and observations. Figure 5.14 shows the highest value across the entire operational bandwidth, which is less than 0.6, indicating satisfactory diversity performance of the MIMO antenna system. However, there were some inaccuracies in the simulated and measured CCL results due to manufacturing errors and welding.

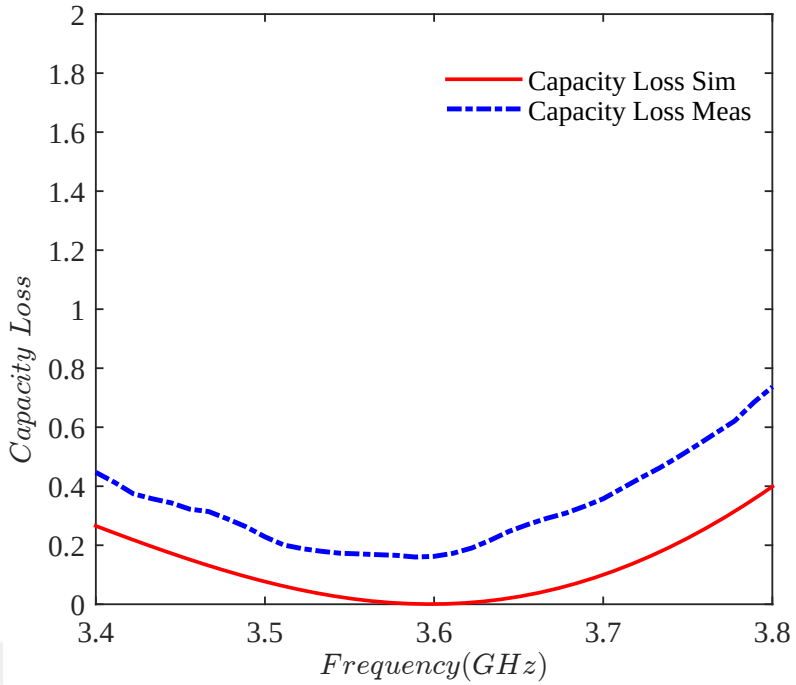

Figure 5.14 : Capacity loss of the Apollony antenna.

The comparison of the ergodic channel capacity for a MIMO antenna over Rayleigh fading is shown in Figure 5.15, using simulated and measured correlated 4x4 matrices based on scattering parameters. The results show that the simulated and measured correlated channel capacities are reasonably comparable to the capacity of the i.i.d. model. The optimal capacity is achieved when there is lower correlation between the elements in the channel matrix. Thus, reducing the correlation leads to the ideal capacity of a MIMO system.

Based on the methodology and analyses shown above, the channel capacities of SISO, 2x2, and 4x4 MIMO are modeled and compared. Assuming that the transmit and receive antennas are correlated, a Monte Carlo method is used to simulate the Rayleigh fading channel. By utilizing 100,000 channel realizations, the capacities were calculated in an environment that displayed isotropic scattering.

The simulated ergodic channel capacities of the proposed 4x4 MIMO system are 27 bps/Hz and 25.75 bps/Hz with correlation and with efficiency and correlation, respectively. The simulated channel capacity of the proposed 4x4 MIMO system is 22 bps/Hz with an IID channel capacity. The measured channel capacities of the proposed 4x4 MIMO system are 26.5 bps/Hz and 25.75 bps/Hz with correlation and with efficiency and correlation, respectively, at an SNR of 25 dB. The peak ergodic

channel capacity reached 27 bps/Hz, which is twice the value of 14 bps/Hz achieved by a 2x2 MIMO system.

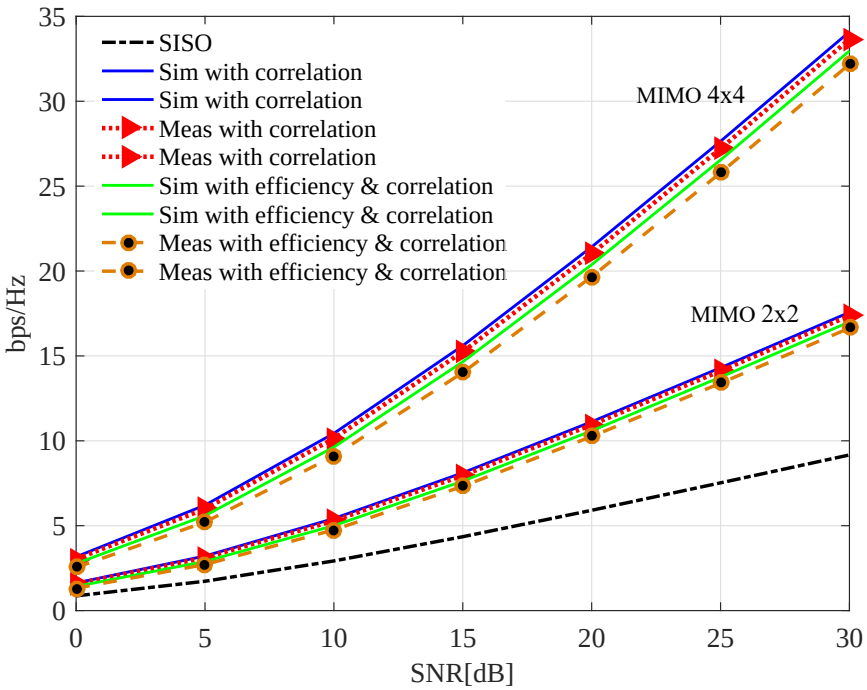

Figure 5.15 : Capacity of the MIMO system over a Rayleigh fading channel

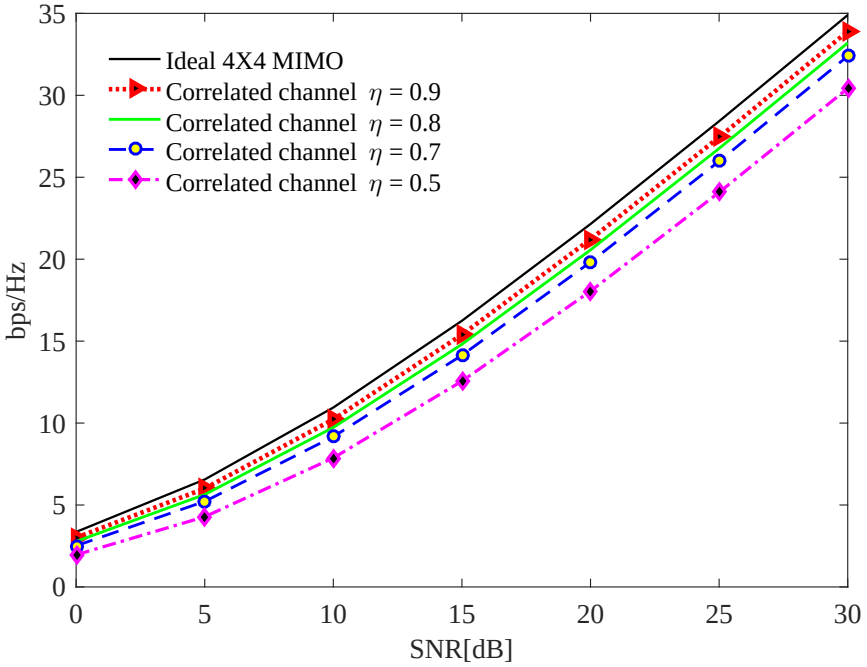

Figure 5.16 : Comparison of capacity versus efficiency.

As shown in this Figure 5.16, when the efficiency (η) increases, the channel capacity increases. Figure 5.16 shows the ergodic channel capacities of the proposed array when changing efficiency from 0.5 to 0.9.

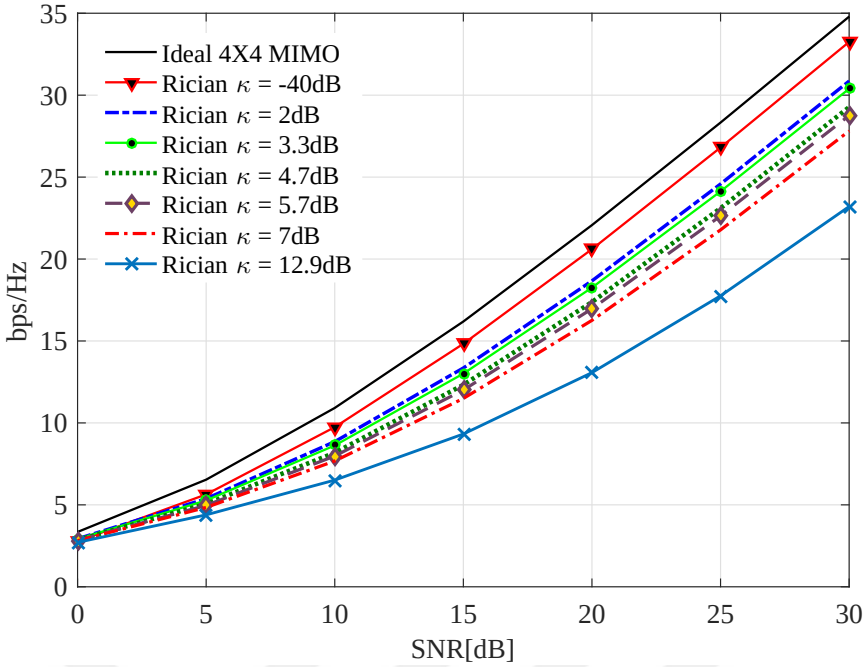

Figure 5.17 : Capacity of the MIMO system over Rican fading channel.

In Figure 5.17, the ergodic capacity of a wireless communication system decreases as the Rician K-factor increases. However, the impact of the K-factor depends on the specific application and environment. In some cases, a higher K-factor may actually be beneficial. For instance, in LOS environments, a high K-factor can lead to a stronger and more LOS.

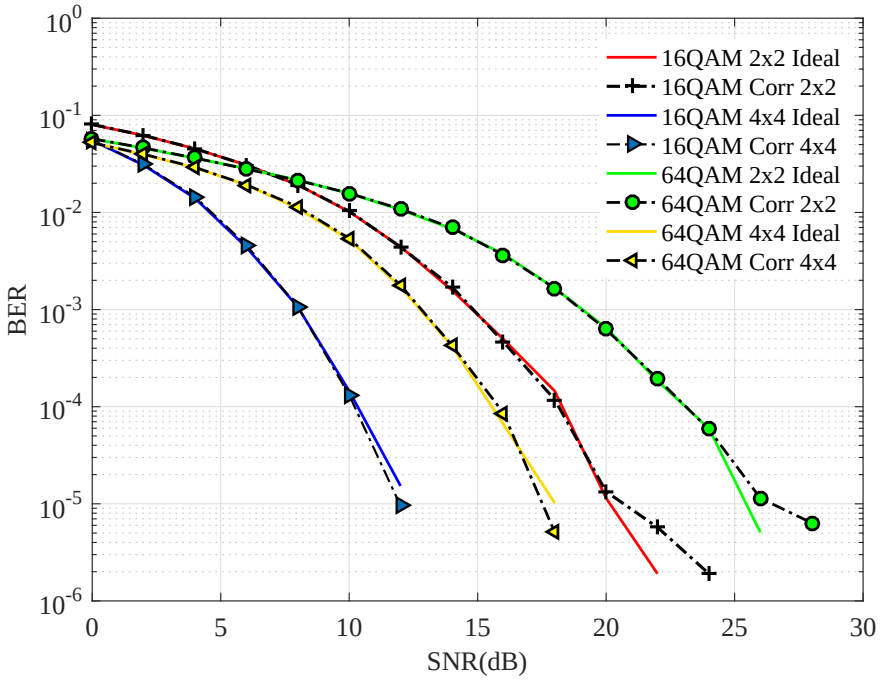

Figure 5.18 : BER of the MIMO system.

In Figure 5.18, the BER of a wireless communication system is affected by various factors, including the MIMO configuration, SNR, and modulation scheme. At 2x2 MIMO antennas with QAM modulation, good performance is obtained at moderate to high SNR levels. However, at lower SNR levels, the BER increases. For instance, the graph shows that 64-QAM requires an SNR of 25 dB to obtain a BER of 10^{-5}, while 16-QAM only requires roughly 20 dB SNR for the same BER. While at 4x4 MIMO antennas with QAM modulation, good performance improves the BER performance, particularly at lower SNR values. At higher SNR values, the improvement is less significant due to the diminishing returns of higher-order modulation and MIMO configuration. The graph shows that 64-QAM requires an SNR of 17.5 dB to obtain a BER of 10^{-5}, while 16-QAM only requires roughly 12 dB SNR for the same BER.

Table 5.2 : Comparing the intended MIMO antenna to previously released studies

Ref.	**Size** mm^2	**BW** GHz	**Isolation** dB	**Peak Gain** dBi	**ECC**
[54]	$140X140$	1.8-2.9	> 15	5.5	< 0.1
[55]	$100X150$	2.4-4.8	> 10	5	$-$
[56]	81×87	3.01 - 12.5	> 18	4	< 0.05
[57]	80×80	3.18 - 11.5	> 19	4	< 0.15
Proposed Antenna	80×80	3.30 - 3.80	> 22	5.4	< 0.01

Table 5.2 compares the proposed MIMO antenna to comparable four-port planar MIMO antennas mentioned in the literature. The factors indicated in this table are the number of radiating components, gain, isolation, ECC, and the antenna size. According to Table 5.2, the Apollony MIMO antenna has a smaller footprint and higher isolation compared to the other antennas mentioned in the literature. Specifically, the Apollony antenna has 22 dB of isolation, significantly higher than the 19 dB isolation of the other antennas. Consequently, the suggested antenna's performance characteristics outperform those previously described in References [47], [58] - [57].

5.2 Dual Sub-6 Band using Quad-Tapered Slot for 5G MIMO Antenna

Fifth-generation (5G) wireless communication systems, with their fast speed, low latency, and high data rates, are the latest release in this field [59]. As the development of wireless devices and networks continues to grow, emerging technologies such as MIMO antennas are being applied to improve performance in 5G applications and achieve higher data rates [60,61]. Among the various MIMO antennas, the tapered slot antenna has received the most study due to its broad bandwidth, high gain, low cross polarization, and constant radiation properties [62]. The tapered slot Vivaldi MIMO antennas have been extensively studied for their high gain, broadband capability, and ease of fabrication [63]. Vivaldi antennas are considered a good choice for wideband communication systems.

In this section, we propose a quad-port antenna with a tapered slot that can be used for 5G wireless applications. The tapered slot elements are positioned orthogonally to take advantage of the intended MIMO antenna's diversity. Furthermore, in order to improve the impedance bandwidth, a tapered transformer is utilized in the microstrip line feeding an exponentially tapered slot. As a result, the intended antenna offers better inter-element isolation and lower ECC. The proposed antenna layout and simulation were conducted using a commercial CST simulator. To validate the design method, a MIMO antenna was fabricated and measured.

5.2.1 Design of a quadruple tapered-slot antenna

The antenna configuration that has been designed is shown in Figure 5.19, while Table 5.3 displays the optimal sizes for the proposed MIMO antennas. Essentially, the design of the antenna involves an exponentially tapered slot and a feed line. The MIMO antenna was fabricated and modeled using a substrate made of FR-4 measuring 120 x 120 mm, with a height of 1.6 mm and a tangent loss of 0.025. To ensure that the antenna operates at a characteristic impedance of 50 Ω, a feed line width of 3.05 mm was selected. The antenna was implemented on a PCB board, with quadruple identical exponentially tapered slots etched orthogonally on the upper copper cladding layer.

Additionally, symmetrical tapered slots were positioned perpendicularly to capitalize on the diversity in the MIMO antennas.

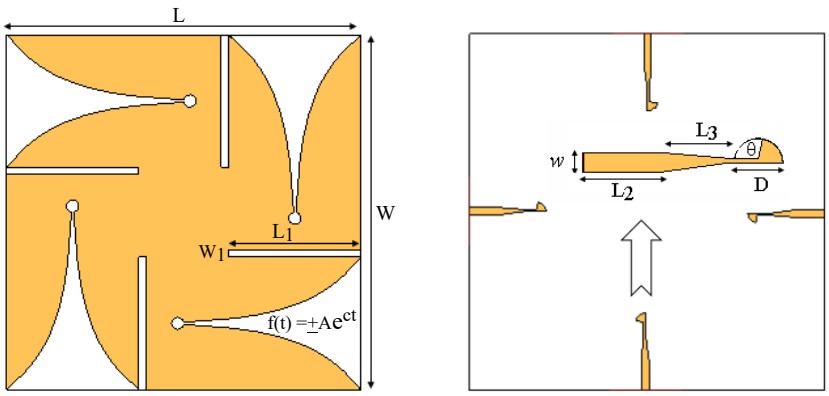

(a) Front view (b) Back view

Figure 5.19 : The configuration of the quad tapered-slot antenna.

Table 5.3 : Optimum dimensions for a quad tapered-slot antenna

Parameter	Value (mm)	Parameter	Value (mm)	Parameter	Value (mm)
W	120	W1	3	A	0.65
L	120	L1	44	c	0.05
L2	8.7	L3	8	W5	2.6
D	7.6	w	3.05	-	-

5.2.2 Tapered-Slot MIMO Antennas: Results and Discussion

The Vivaldi antenna, as depicted in Figure 5.20, was designed and subjected to experimental testing for its viability in wireless applications in the 5G NR bands n78 and n79. Utilizing a spectrum analyzer, the scattering parameter values were calculated, and the signal behavior was analyzed. During the experiment, two ports of the MIMO antenna were stimulated, while the remaining ports were loaded with a 50-ohm terminating load. Figure 5.21 illustrates the simulation and measurement of the reflection coefficients for the Vivaldi-shaped MIMO antenna. The intended quadruple radiating antenna functions within the impedance bands of 3.3-3.8 GHz and 4.4-5.0 GHz with a reflection coefficient that is less than -10dB. This finding demonstrates that the experimental measurements are significantly consistent with the simulated reflection coefficient values.

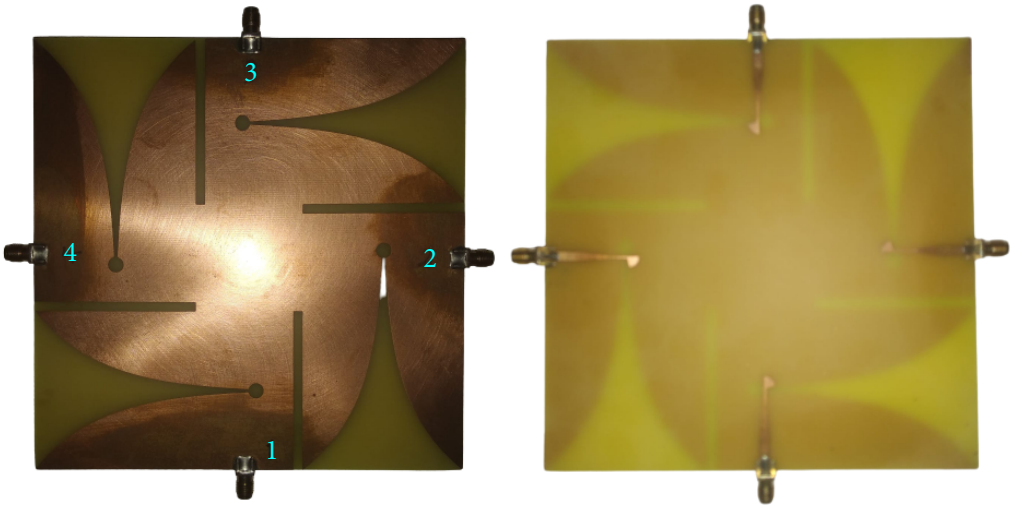

(a) Top layer (b) Bottom layer

Figure 5.20 : The manufactured quad tapered-slot antenna.

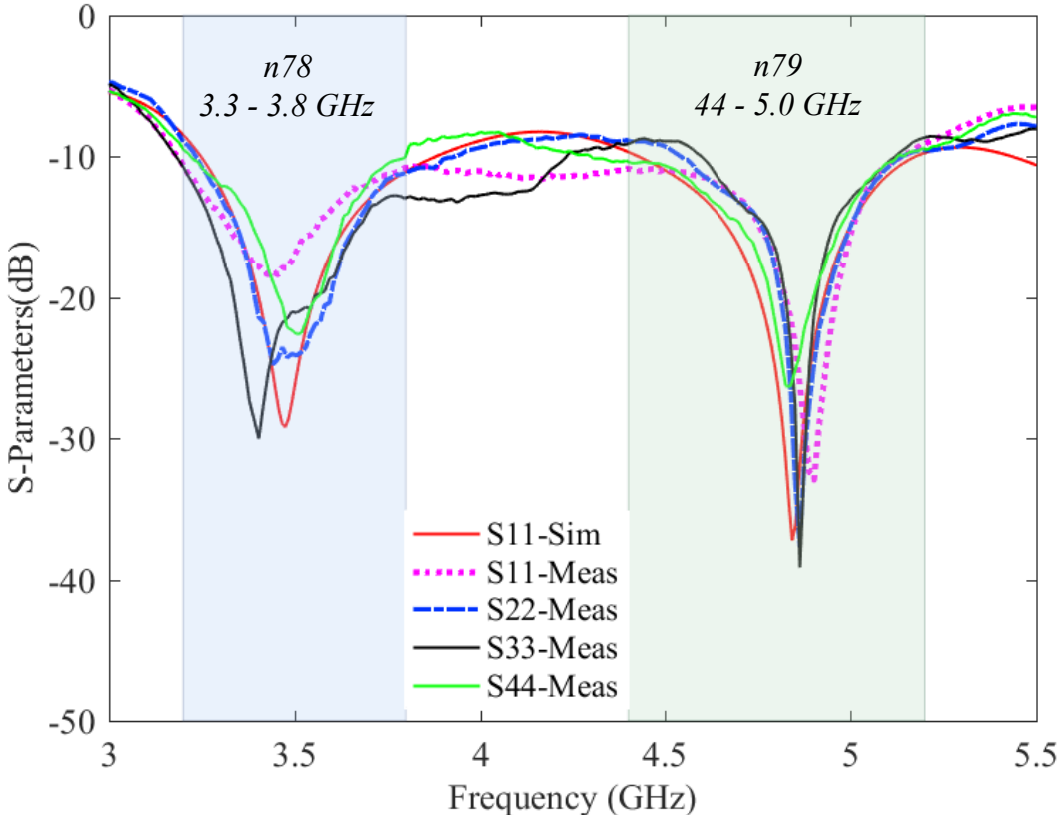

Figure 5.21 : Reflection coefficients for the quad tapered-slot antenna

The tapered-shaped antenna's optimal terminal model was achieved by preliminary simulations, which focused on achieving high isolation and proper impedance

matching. The experimental and simulation-based results, as presented in Figure 5.22, shows that isolation between the adjacent elements (S21 and S41) were obtained to be less than -25dB. However, the mutual coupling between the diagonal element and S31 was determined to be less than -30dB over the operating frequency range. These findings imply that the experimental data isolation measures are reasonably compatible with the modeling results. The figure shows a slight effect on the measurement findings. Because of manufacturing inaccuracy, welding, and the utilization of lossy dielectric material, there is a little discrepancy among the experimental and simulated results.

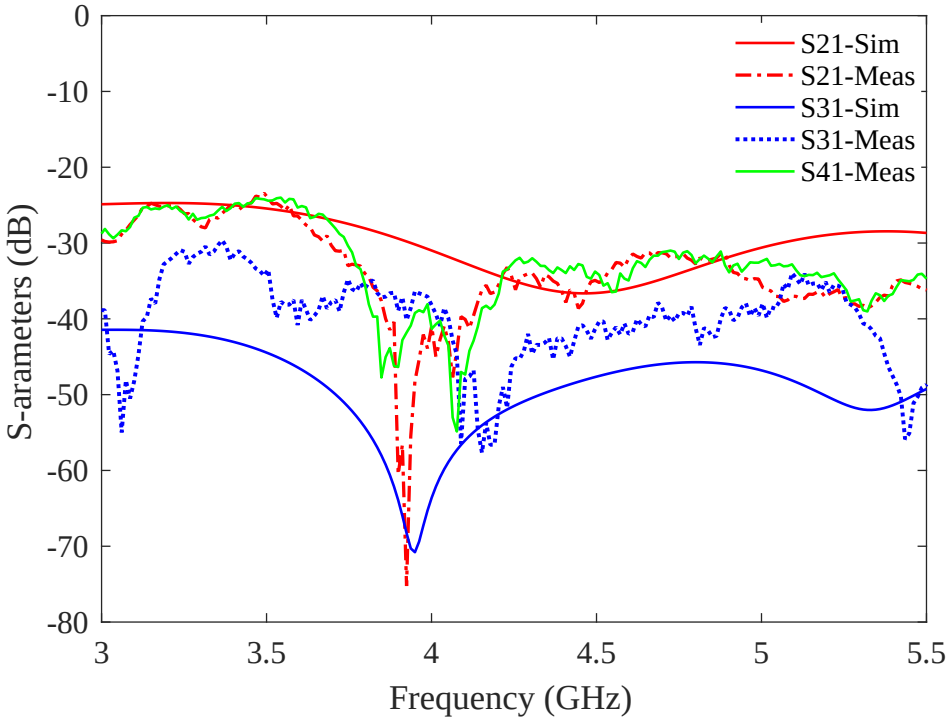

Figure 5.22 : The Isolation of quad tapered-slot for 5G MIMO Antenna..

Figure 5.23 demonstrates the input impedance using the Smith chart with a normalized impedance of 50 Ω. It is clear that the slots have an impact on the impedance matching process, resulting in an enhanced overall performance of the antenna. The slots cause an inductive effect on the antenna impedance, and this effect is directly related to the expansion of the slots. Therefore, it can be concluded that slots have the potential to function as impedance matchers, which can lead to a superior performance of the antenna.

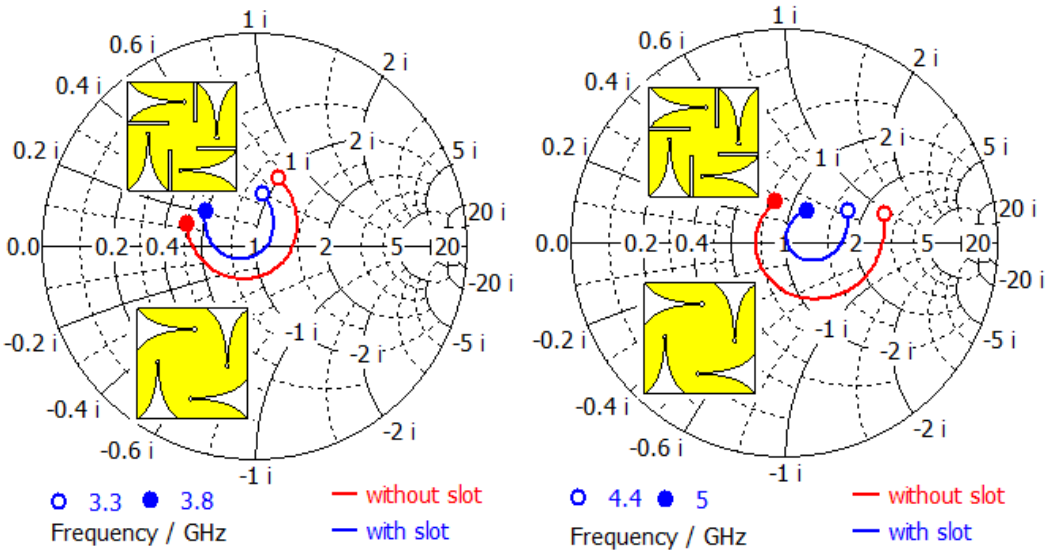

(a) (b)

Figure 5.23 : The impact of a slot on impedance matching is illustrated on the Smith chart.

The peak gain and antenna radiation efficiency at dual-band frequencies are plotted in Figure 5.24. The proposed and developed MIMO antennas exhibit considerable potential, having achieved a maximum gain in the range of 6 to 7 dBi. Moreover, the plot generated shows that these MIMO antennas demonstrate a sustained and high level of radiation efficiency, surpassing 75 % throughout all dual-band frequencies. The 3D patterns simulated at a frequency of 3.5 GHz are displayed in Figure 5.25. These results imply that the proposed isolation techniques do not significantly impact the radiation properties of the MIMO antennas. Therefore, these antennas are a suitable choice for various UE communication applications due to their notable gain and radiation efficiency.

Figures 5.26 and 5.27 show the E- and H-planes for linearly polarized waves at 3.5 GHz and 4.8 GHz, respectively. Figure 5.25 illustrates the 3D radiation patterns for port 1 excitation at 3.5 GHz, which exhibit both pattern and polarization diversity. Port 1 corresponds to mutual orthogonality between ports 2 and 4, whereas Port 3 represents the opposite-directed pattern.

The current distribution shown in Figure 5.28 corresponds to the excitation of port 1 while the other ports are loaded. The surface current distribution indicates that the adjacent exponentially tapered slot elements have less effect during MIMO operation because they are slotted onto the radiating element.

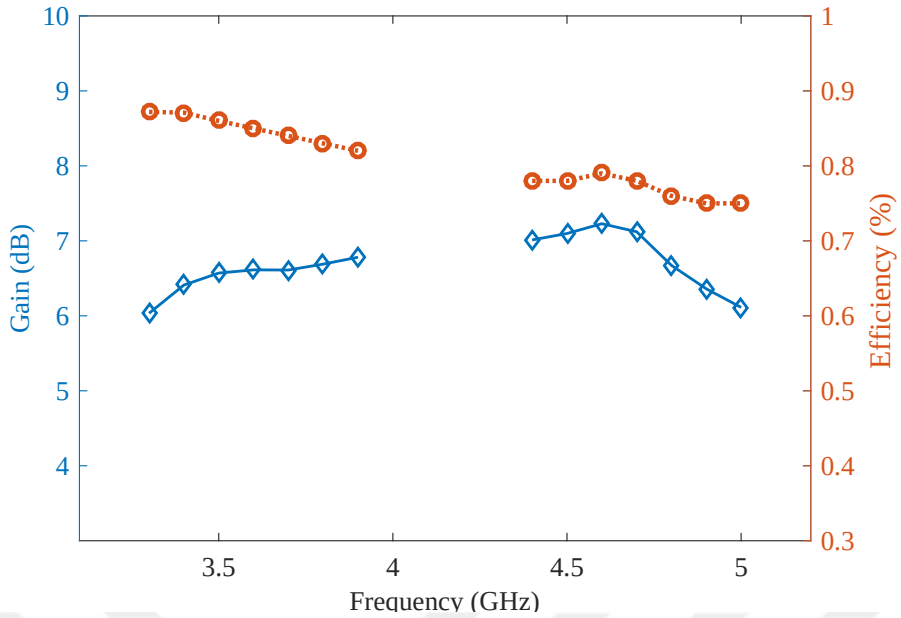

Figure 5.24 : Gain and efficiency of a quad tapered-slot antenna.

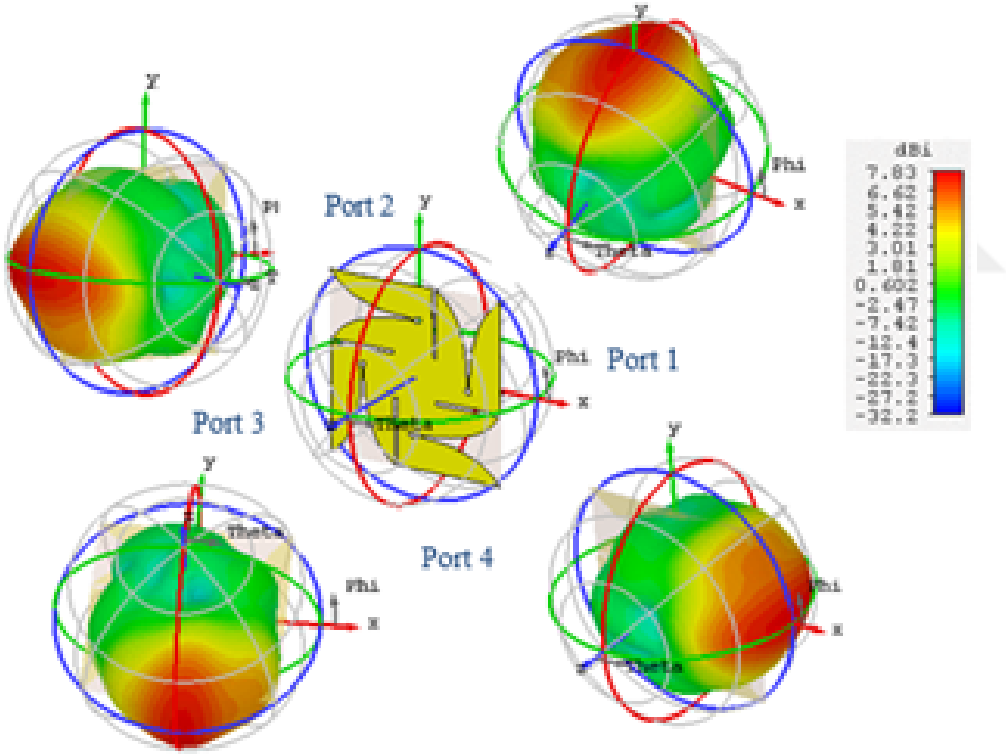

Figure 5.25 : The 3D radiation pattern at 5.8 GHz of a quad tapered-slot antenna

5.2.3 Characterization of MIMO Antenna

The ECC is the metric used to assess the effectiveness of MIMO antennas in wireless communication. The ECC determines the correlation betwixt the two adjacent tapered

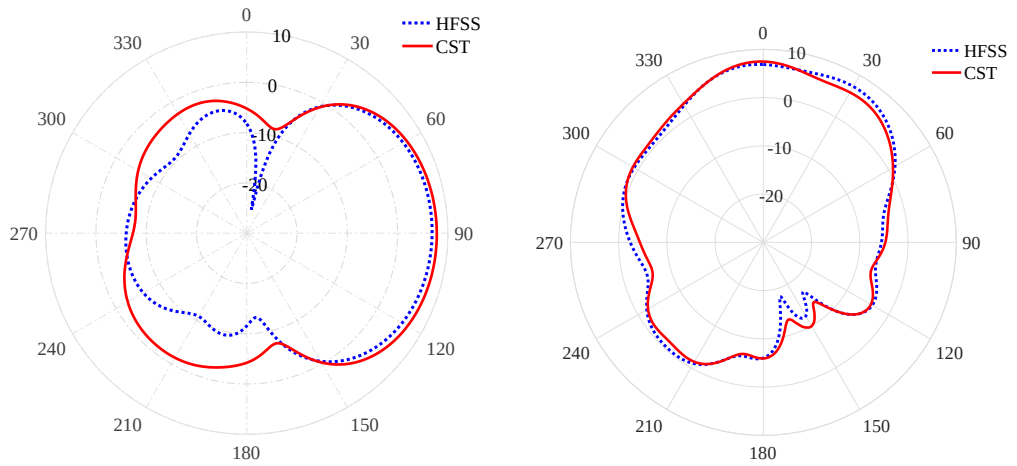

(a) E-Plane (b) H-Plane

Figure 5.26 : The 2D radiation patterns at 3.7 GHz of the tapered shaped antenna.

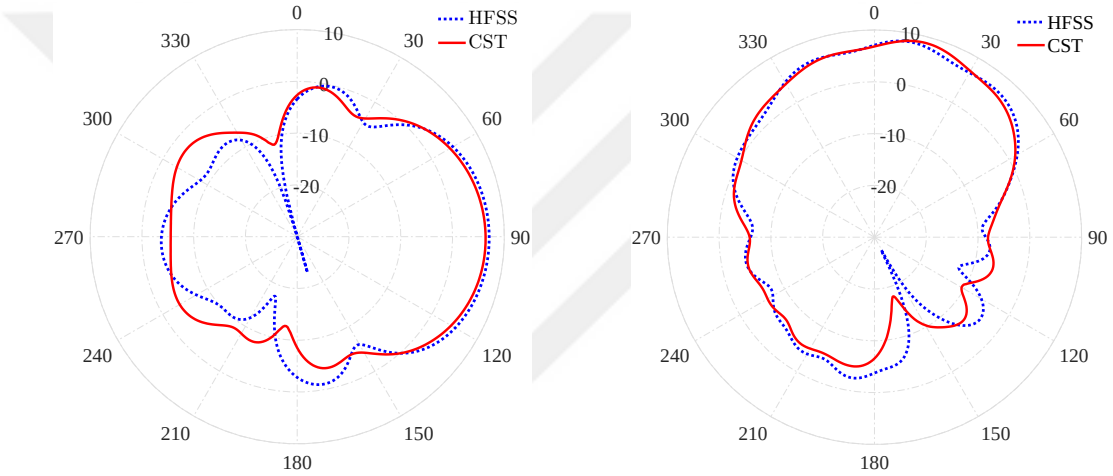

(a) E-Plane (b) H-Plane

Figure 5.27 : The 2D radiation patterns at 4.8 GHz of the tapered shaped antenna.

slot elements of the antenna. Two approaches could be applied to figure out the ECC of a MIMO antenna [50]. The first technique is based on the antenna's S-parameters, while the second approach on is using the antenna's far-field pattern. Equations (1) and (2), which are depending on the S-parameters and the field pattern respectively, which are used to compute the correlation of the proposed antenna [51]. The results are shown in Figure 5.29, where the red line represents the value calculated using simulated and measured S parameters, and the other lines represent the value estimated by applying antenna pattern. Measured values are exhibited to be in fair agreement with the simulated and field pattern values in Figure 5.29. The ECC result between neighboring antenna elements are less than 0.01.

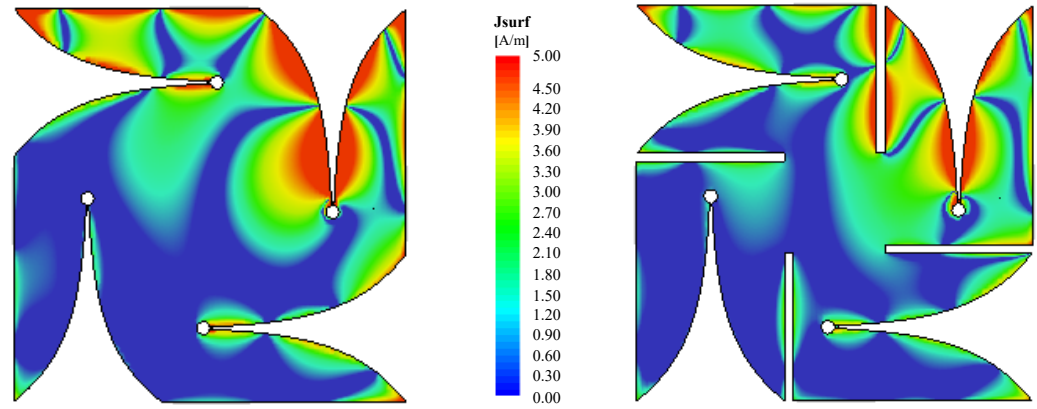

(a) with out slot @ 3.5GHz. (c) with slot @ 3.5GHz.

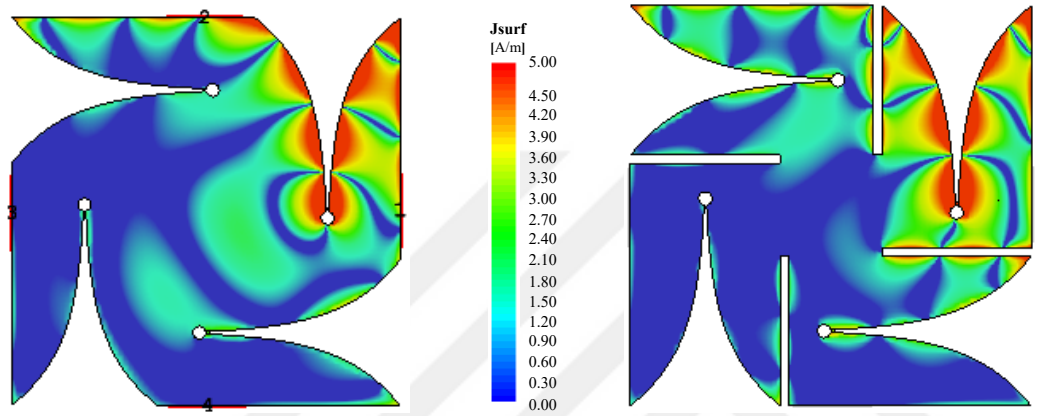

(d) with out slot @ 4.8GHz. (f) with slot @ 4.8GHz.

Figure 5.28 : Current density distribution of the tapered shaped antenna at 3.7 GHz.

Generally speaking, the total active reflection coefficient (TARC) can be used as a dependable indicator of stability in resonant frequency, even if the phase difference between the antenna elements is altered. Equation (3.2) was used to calculate TARC by maintaining the input signal phase of port one constant and gradually changing port two from 0 degrees to 180 degrees with 30-degree increments. Figure 5.30 displays the variation of TARC in relation to frequency. The results demonstrate that the TARC values for all three frequency bands are below -10 dB, indicating optimal radiation performance.

Figure 5.31 compares the ergodic channel capacity of a MIMO antenna over Rayleigh fading using simulated and measured correlated 4x4 matrices based on scattering parameters. Figure 5.31 displays the average capacity of the MIMO system obtained through Monte Carlo simulations over 100,000 random channel realizations. The graph shows that the simulated and measured correlated channel capacities agree reasonably well with the capacity of the i.i.d. model. The optimal capacity can be

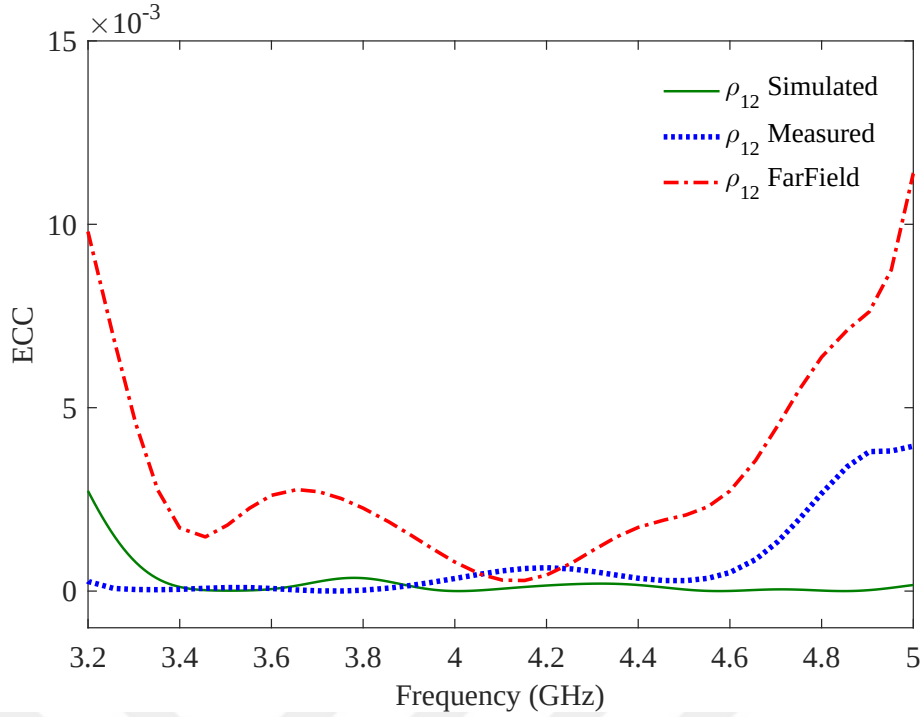

Figure 5.29 : The ECC of quad tapered-slot for 5G MIMO Antenna..

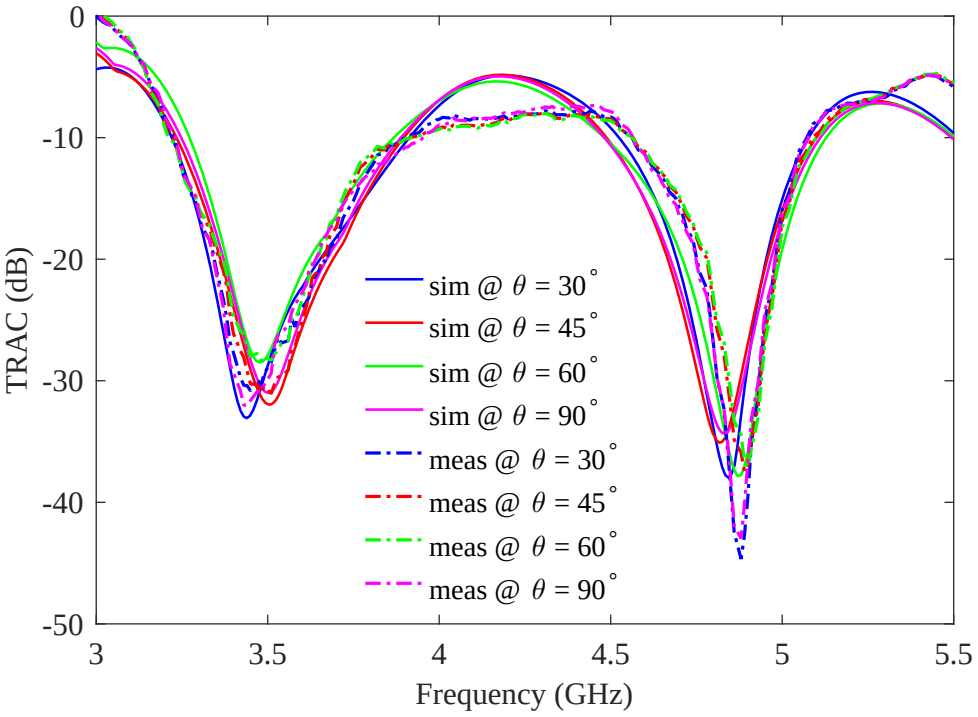

Figure 5.30 : The TARC of quad tapered-slot antenna

achieved when there is less correlation between the elements in the channel matrix. Therefore, reducing the correlation can lead to the ideal capacity of a MIMO system.

As shown in this Figure 5.32, when the efficiency (η) increases, the channel capacity increases. Figure 5.32 shows the ergodic channel capacities of the proposed array when changing efficiency from 0.5 to 0.9.

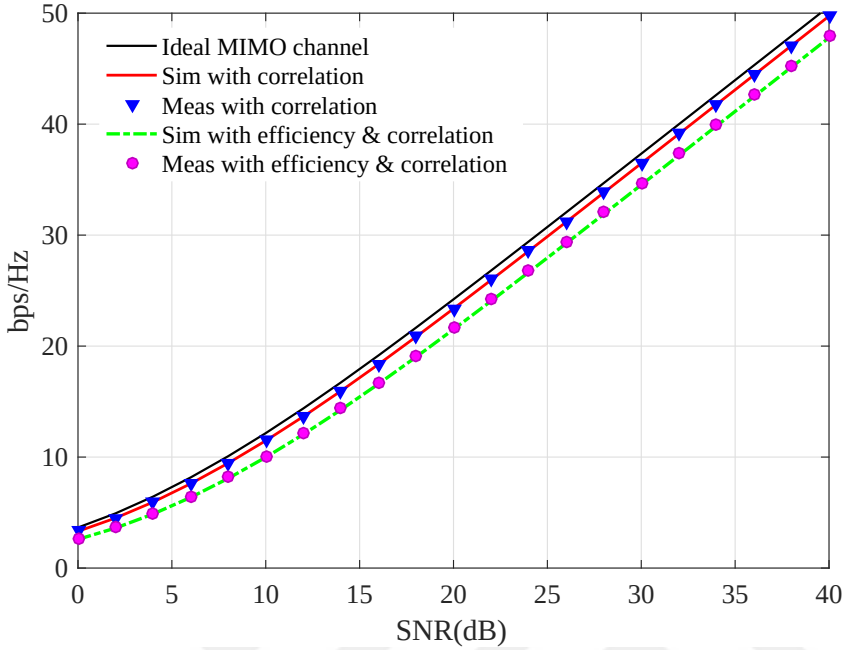

Figure 5.31 : The Capacity of of quad tapered-slot for n79 5G MIMO Antenna.

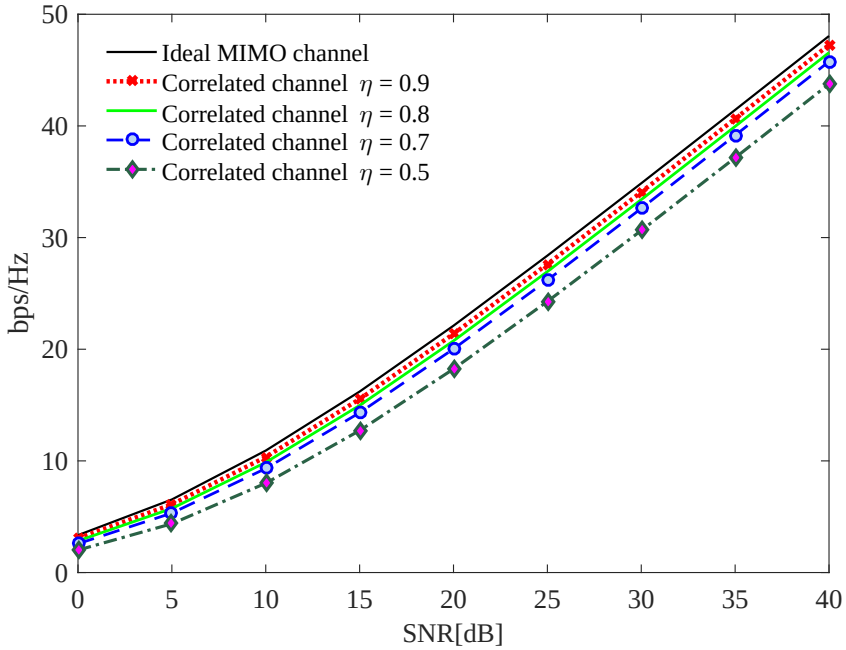

Figure 5.32 : The Capacity of quad tapered-slot for n78 5G MIMO Antenna.

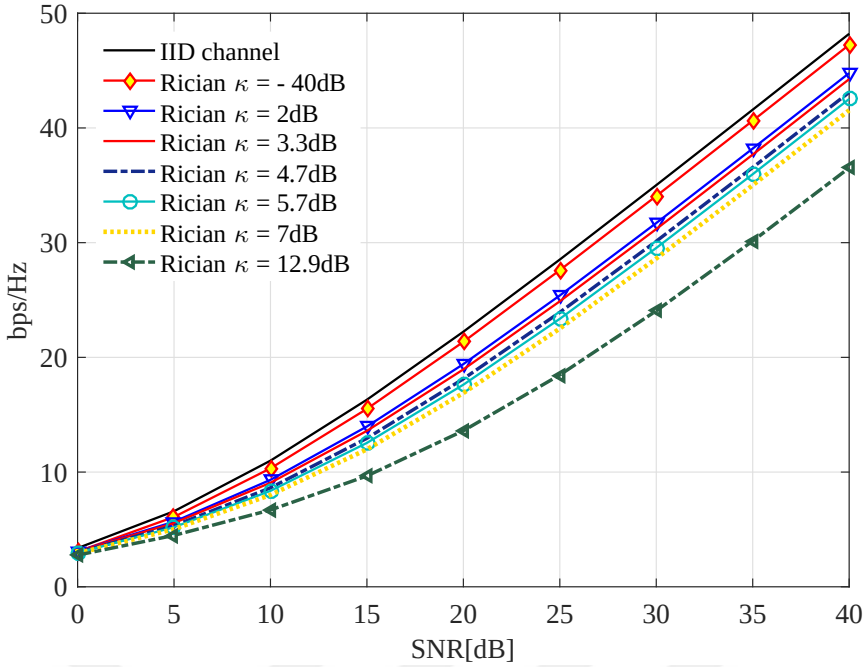

Figure 5.33 : The Capacity of of quad tapered-slot for n79 5G MIMO Antenna.

In Figure5.33, the ergodic capacity of a wireless communication system decreases as the Rician K-factor increases. However, the impact of the K-factor depends on the specific application and environment. In some cases, a higher K-factor may actually be beneficial. For instance, in LOS environments, a high K-factor can lead to a stronger and more LOS.

In Figure 5.34, the BER of a wireless communication system is affected by various factors, including the MIMO configuration, SNR, and modulation scheme. At 2x2 MIMO antennas with QAM modulation, good performance is obtained at moderate to high SNR levels. However, at lower SNR levels, the BER increases. For instance, the graph shows that 64-QAM requires an SNR of 25 dB to obtain a BER of 10^{-5}, while 16-QAM only requires roughly 20 dB SNR for the same BER. While at 4x4 MIMO antennas with QAM modulation, good performance improves the BER performance, particularly at lower SNR values. At higher SNR values, the improvement is less significant due to the diminishing returns of higher-order modulation and MIMO configuration. The graph shows that 64-QAM requires an SNR of 17.5 dB to obtain a BER of 10^{-5}, while 16-QAM only requires roughly 12 dB SNR for the same BER.

Table 6.3 compares the isolation, gain, and bandwidth of the MIMO antenna developed in this research with four-element MIMO antennas from the literature. While the

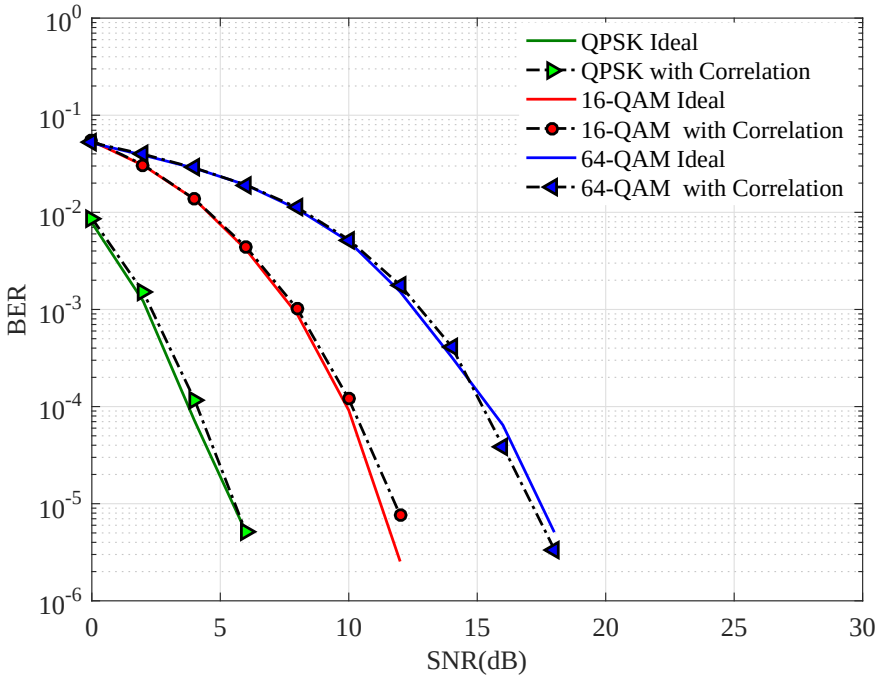

Figure 5.34 : The BER of of quad tapered-slot for n79 5G MIMO Antenna.

antenna size is greater than the one suggested in this research, the antennas in [37, 38] offer a higher gain than the designed antenna. Nonetheless, the designed MIMO antenna has the smallest dimensions and provides more than 17 dB of isolation across the operational frequency spectrum (2.3–2.7 GHz).

Table 5.4 : Comparison of the designed MIMO antenna with earlier publications.

Ref.	Size (mm^2)	BW (GHz)	Isolation (dB)	Peak Gain (dBi)	ECC
[37]	$120X120$	3.1-11.36	> 18	6.0	< 0.1
[38]	$137X137$	2.0 - 6.0	> 17	4.8	
[39]	$140X120$	1.8-2.9	> 15	5.5	< 0.1
[40]	$114X114$	2.4-4.8	> 10	5	
Proposed Antenna	$120X120$	3.30-3.8 4.40-5.0	> 25	7.4	< 0.01

6. MIMO ANTENNA FOR SPECTRUM SHARING OF LTE-NR DEVICE

MIMO antennas are suitable for deployment in User Equipment (UE) devices to achieve high data rates and increase channel capacity [31]. This chapter specifically focuses on two planar antenna designs: the wideband antenna and the concentric octagonal antenna. These designs are applicable for deploying spectrum sharing in the LTE-NR band, which includes frequencies from 1.8 GHz to 3.2 GHz. Moreover, they offer notable impedance matching, which is crucial to ensure the quality of transmitted and received signals. Despite having dual or quad ports sharing a single radiating antenna element, these antennas demonstrate reasonable performance in terms of frequency diversity and minimal ECC. This allows them to handle signals across a range of frequencies while maintaining signal quality. In conclusion, incorporating MIMO antennas, particularly the wideband and concentric octagonal designs, can be a beneficial solution for enhancing channel capacity, achieving high data rates in UE devices, managing spectrum sharing, and maintaining linear polarization.

6.1 Wideband MIMO Antenna for User Equipment Devices

In this chapter, the focus is on the design and manufacture of a MIMO antenna with a quad port that can operate within a wide frequency range of 2.0 to 3.0 GHz. The antenna consists of a quad symmetric microstrip feed point, a radiating element designed in the shape of a square step, and a base plate that is frame-shaped. In order to improve the performance of the MIMO antenna and to decrease coupling between the ports, steps were integrated into the radiating edge while slots were added to the frame-shaped ground edges. The chapter delves into the detailed process of developing, simulating, optimizing, constructing, and testing the MIMO antenna. The results of the simulations and measurements are examined to identify the performance characteristics of the MIMO antenna system, and this information is then used to evaluate its performance indicators.

6.1.1 Design and fabrication of antennas

Figure Figure 6.1 illustrates the MIMO antenna designed for wideband operation. The antenna consists of a single-radiating-element patch antenna, four balanced microstrip feedlines, square metal elements, and a ground plane in the shape of a frame. We used Computer Simulation Technology (CST) electromagnetic software to design the MIMO antenna before fabricating and measuring it on a FR-4 printed circuit board (PCB). The dielectric substrate used in the construction of the PCB possesses a relative permittivity of 4.4, a thickness of 1.6 mm and a loss tangent of 0.025. The dimensions of the substrate are L = 108 mm and W = 108 mm. A patch antenna, consisting of a monopole radiator and partial ground plane, is situated on the top and bottom layers of the substrate, respectively. This configuration enhances the radiation characteristics of the antenna by improving its gain and reducing its side lobes. In order to broaden the bandwidth, the defective ground copper layer located beneath the ground plane was removed. This alteration resulted in an increase in the effective size of the ground plane and a reduction in interference with neighboring components, leading to a wider frequency response.

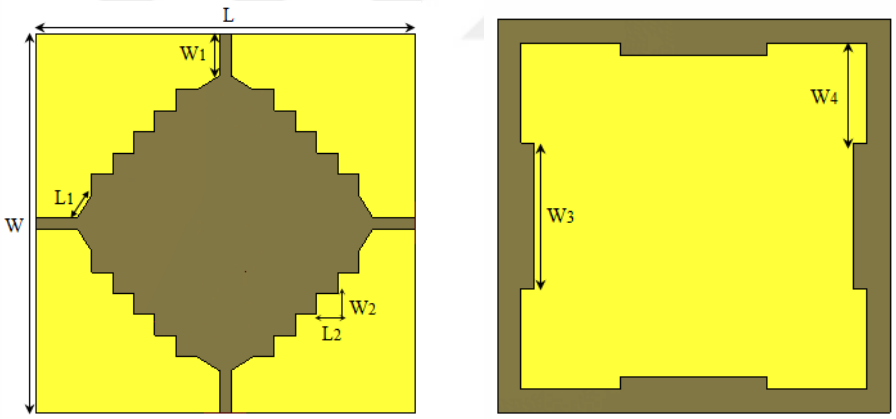

(a) Top layer (b) Bottom layer

Figure 6.1 : Quad-port solitary radiating antenna layout

Table 6.1 : The optimum size for a MIMO antenna

Parameter	Value	Parameter	Value	Parameter	Value
L	108	W	108	L2	6
L1	7.5	W1	7.05	W2	6
W3	40	W4	27.5		

The solitary radiating antenna comes with a ground plane and square steps that reduce the mutual interaction between its two ports. Its compact and broad frequency range design makes it highly suitable for use on a printed circuit board. Following its estimated optimal design dimensions through modeling, the antenna was constructed and tested. The feedline, which had a width of 3.30 mm, contributed to a characteristic impedance of 50Ω. Table 6.2 shows the optimal dimensions of the proposed antenna.

6.1.2 Result of solitary radiating MIMO antenna

In this section, it is explained that the prototype for the proposed MIMO antenna has been fabricated, and its design is shown in Figure 6.2. Additionally, the measured and simulated reflection coefficients of the antenna have been presented in Figure 6.3, and they have been considered satisfactory. However, the measurement process was carried out with only two of the feedline ports excitations active, while the other two were terminated with a 50Ω load match. This setup caused a slight discrepancy between the actual performance of the antenna and its intended design due to the use of a lossy material and soldering. Nevertheless, Figure 6.3 indicates that the MIMO antenna has a wideband characteristic between 2 to 3 GHz frequencies, and its reflection coefficient is below -10 dB.

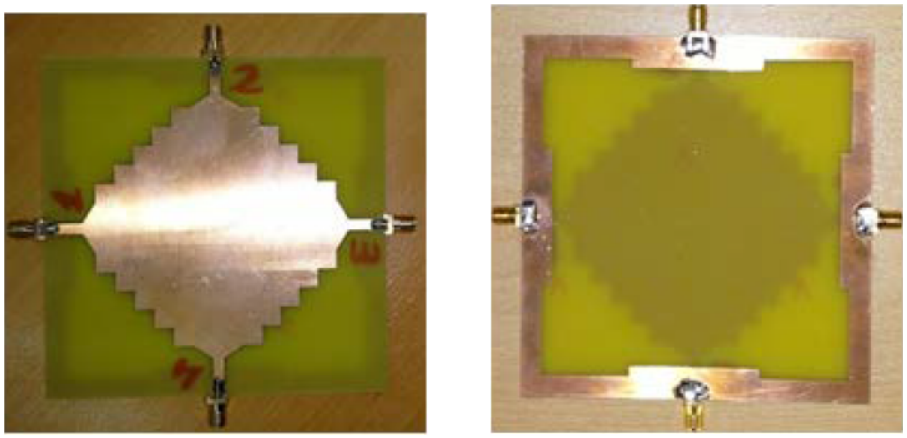

(a) Top layer (b) Bottom layer

Figure 6.2 : Prototype of quad-port solitary MIMO antenna.

According to Figure 6.4, the mutual coupling coefficients of the wideband MIMO antennas have been measured and modeled. The results indicate that the values are reasonably similar, and the design operates in the frequency range of 2 to 3 GHz

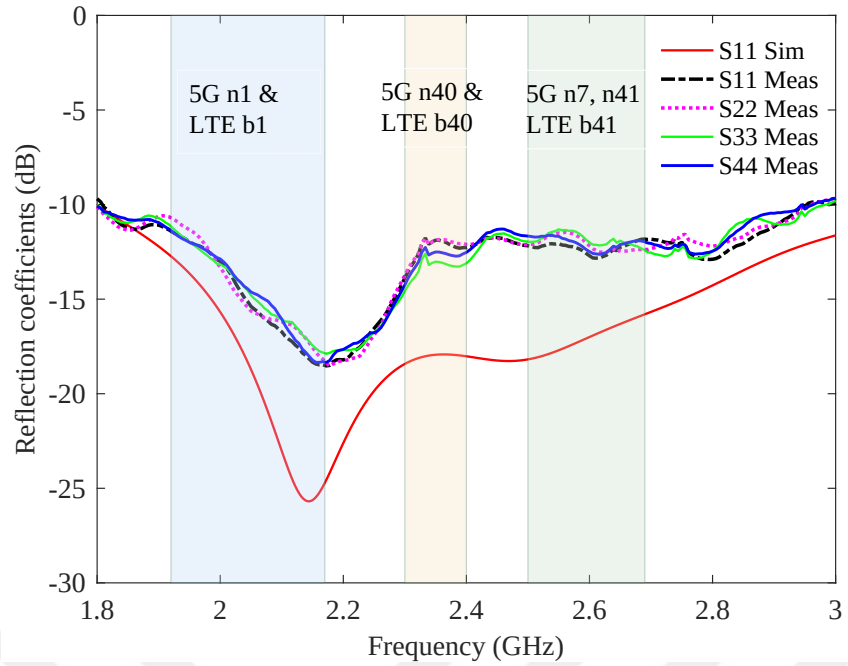

Figure 6.3 : The reflection coefficients of solitary MIMO antenna.

while ensuring that the isolation level remains below -12 dB. Although there are minor discrepancies in the mutual coupling coefficients between ports (1 and 3) and ports (2 and 4) during both simulation and measurement, the overall outcome is considered acceptable. However, it should be noted that the measured isolation coefficients are lower than the simulated values due to various factors such as material, solder, and cable losses.

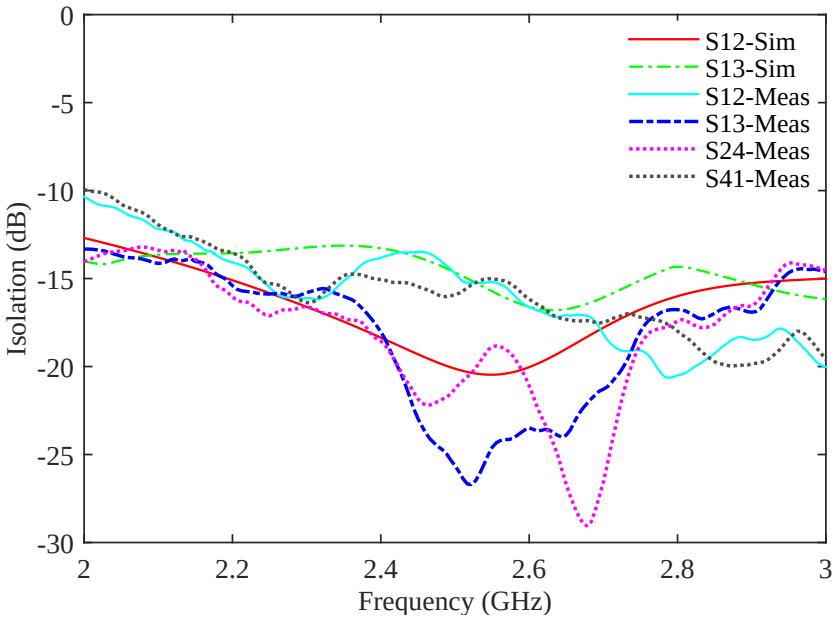

Figure 6.4 : The isolation of solitary MIMO antenna.

6.1.3 Performance metrics of quad-port MIMO antenna

The ECC plays a crucial role in determining the level of independence of an antenna from its neighboring elements. It is a key parameter used to compute the radiation pattern and S-parameters between any two ports of MIMO antennas. As shown in Figure 6.5, the minimum correlation between antennas is depicted, which enhances isolation. The ECC is calculated numerically for the antenna ports and is exceedingly low, approaching zero.

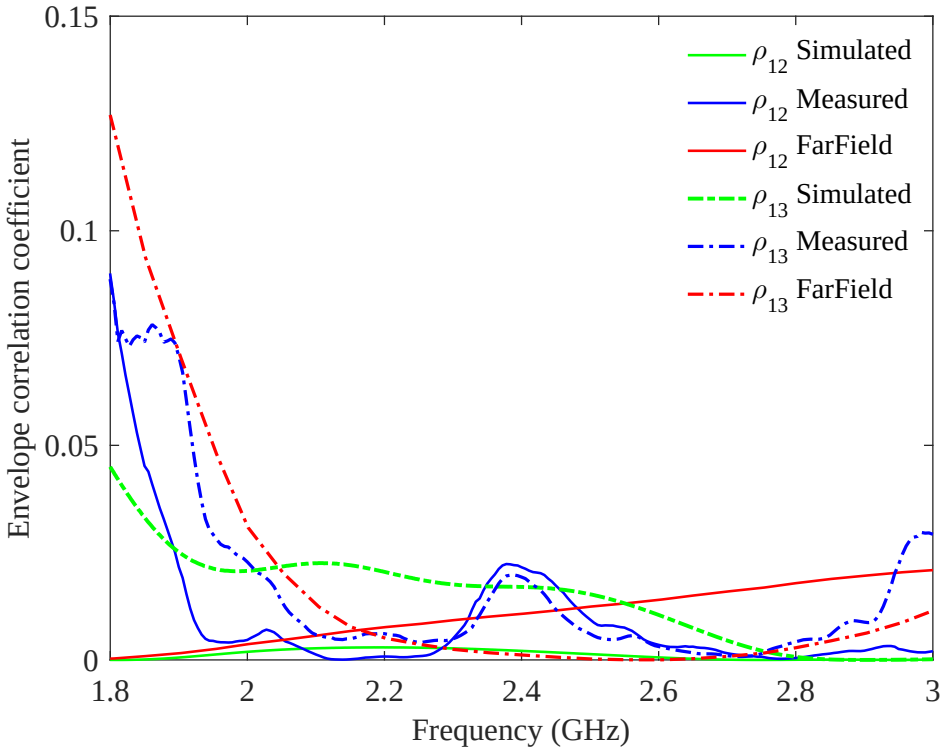

Figure 6.5 : The ECC of a solitary radiating MIMO antenna.

The results of the current distribution across the solitary radiating monopole at two resonant frequencies are presented in Figure 6.6. To obtain these results, an experiment was conducted where port 1 was excited, while the other ports were terminated with a matching load. The current flow through the monopole antennas was measured at 2.1 GHz, which indicated that the induced current in feeding line ports 2 and 4 was highly dense. This, in turn, contributed to the formation of impedance matching over 5G n1. Comparatively, at 2.6 GHz, the current distribution was different. The current density was light around port 1, whereas there was a light current density

across ports 2 and 4, as shown in Figure 6.7. These results have led us to conclude that the monopole plays a crucial role in impedance matching across 5G n41 bands, which reduces mutual coupling. In summary, the experiment and the corresponding results presented in Figures 6.6 and 6.7 demonstrate that the current distribution across the solitary radiating monopole at different frequencies can improve the performance of the antenna system. These findings could have significant implications for the development of 5G networks and other communication technologies.

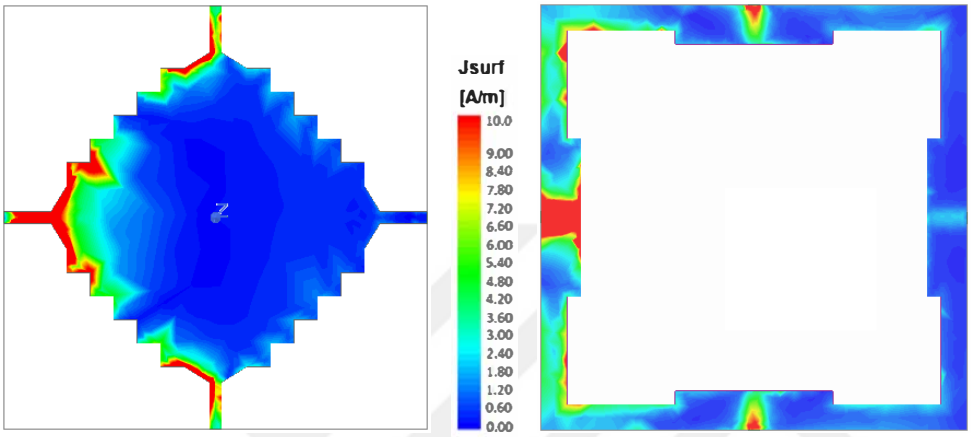

(a) Top layer (c) Bottom layer

Figure 6.6 : Radiation distribution of solitary radiating MIMO antenna @2.1GHz.

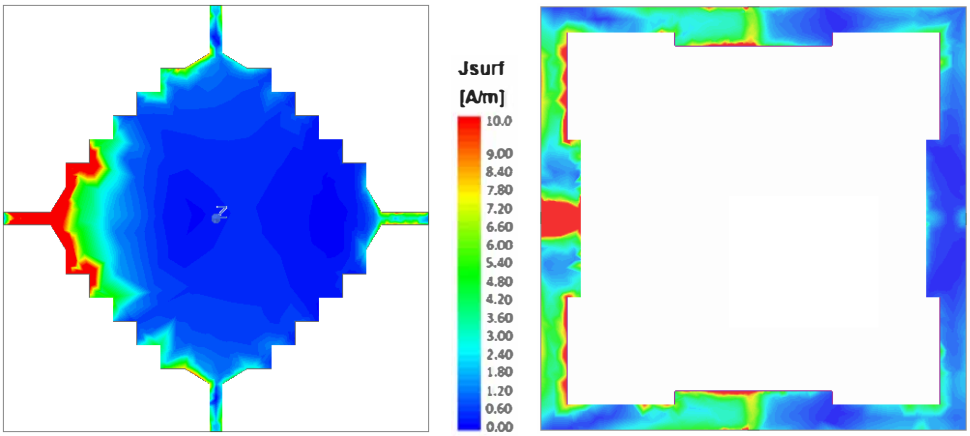

(a) Top layer (c) Bottom layer

Figure 6.7 : Radiation distribution of solitary radiating MIMO antenna @2.6GHz.

The realized gain and total efficiency at the low-frequency band are shown in Figure 6.8. Assessing the gain and efficiency of the proposed antenna is crucial to obtain additional data on its performance. According to Figure 6.8, the antenna design provides maximum gains of 5.8 dB and 6.2 dB at 2.1 GHz and 2.6 GHz, respectively.

Additionally, the radiation efficiencies of the produced antenna reach 82% and 89% in the frequency bands of n1 and n41, respectively, as demonstrated in Figure 6.8.

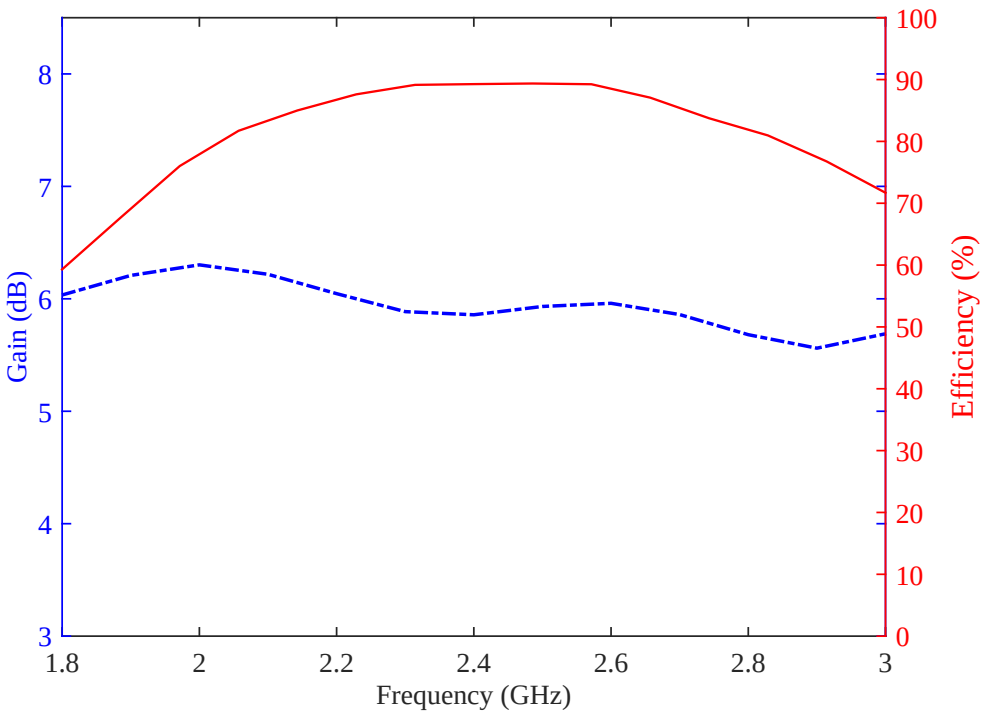

Figure 6.8 : The gain and efficiency of solitary radiating MIMO antenna.

Figure 6.9 display the radiation pattern in the E- and H-planes for linear polarization at 2.1, 2.3, and 2.6GHz. The antenna exhibits a consistent omnidirectional pattern across the entire operational spectrum. Additionally, the results show a high degree of agreement between the CST and HFSS simulations.

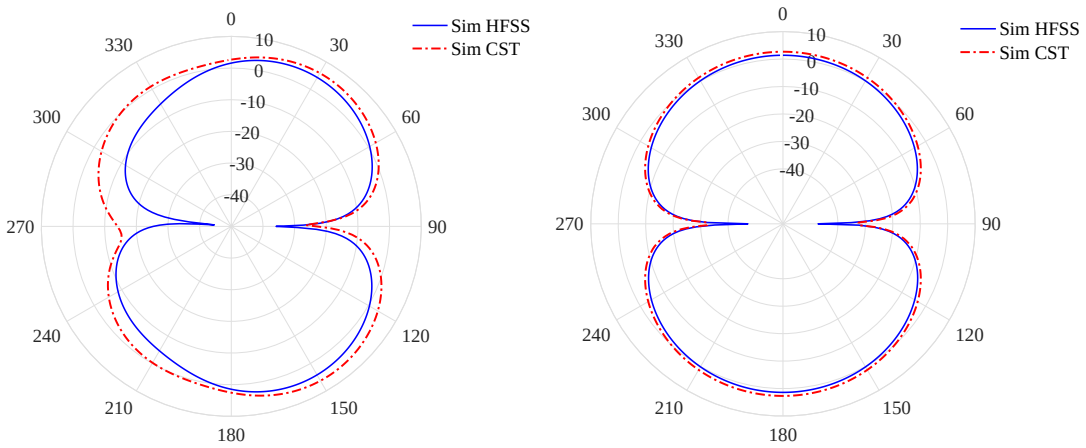

(a) E-Plane (b) H-Plane

Figure 6.9 : Radiation pattern of a solitary radiating antenna at 2.1GHz.

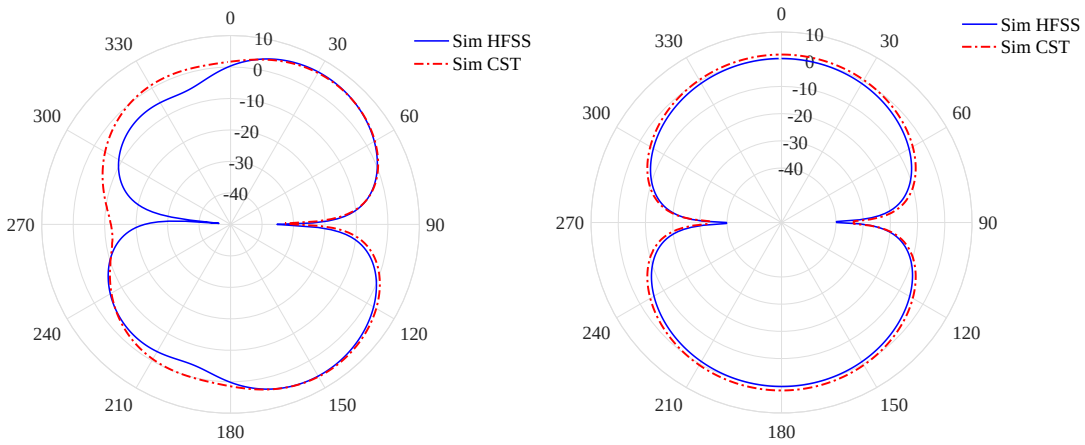

(a) E-Plane (b) H-Plane

Figure 6.10 : Radiation pattern of a solitary radiating antenna at 2.3GHz.

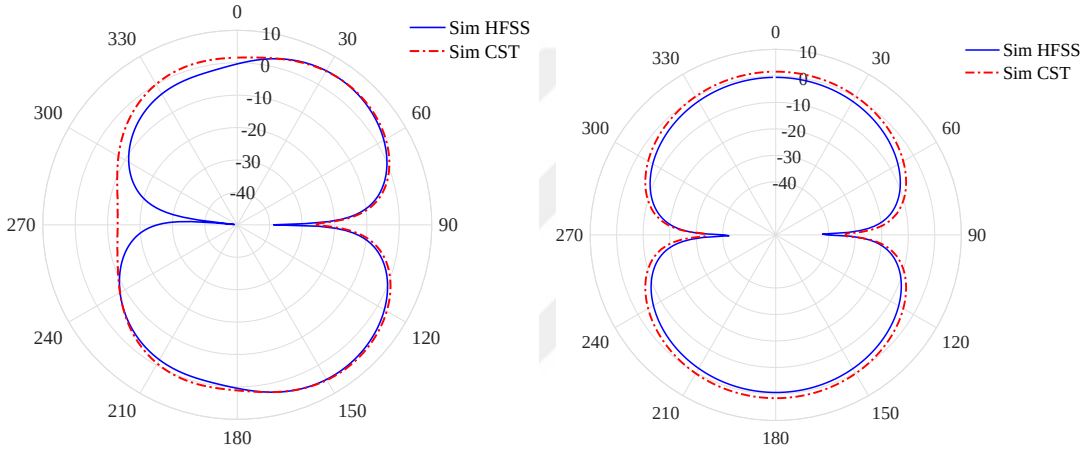

(a) E-Plane (b) H-Plane

Figure 6.11 : Radiation pattern of a solitary radiating antenna at 2.6GHz.

Decoupling network synthesis using transmission lines

The design of solitary radiating MIMO antenna systems poses various challenges, including mutual coupling between antenna ports, which leads to poor system performance and lower efficiency. Decoupling networks synthesized using transmission lines represent one potential method for reducing mutual coupling. Design a preliminary decoupling network using lumped components such as capacitors and inductors. Next, simulate this network using CST Microwave Studio to evaluate its performance. Then, using ADS, redesign the lumped components with transmission lines that have the appropriate length and characteristic impedance. This improves the decoupling network to make it more broadband and realistic. Thus, the transmission

line network synthesis approach verifies an effective way to design a decoupling network for a quad-port single-radiator MIMO antenna. This requires the design of a decoupling network that can effectively isolate the ports from each other. Figure 7.9 illustrates the decoupling network topology in ADS. Figure 7.10 shows the S-parameters of the four-port antenna after incorporating the synthesized transmission line based decoupling network, with the transmission line branches of the network having distinct characteristic impedances and electrical lengths.

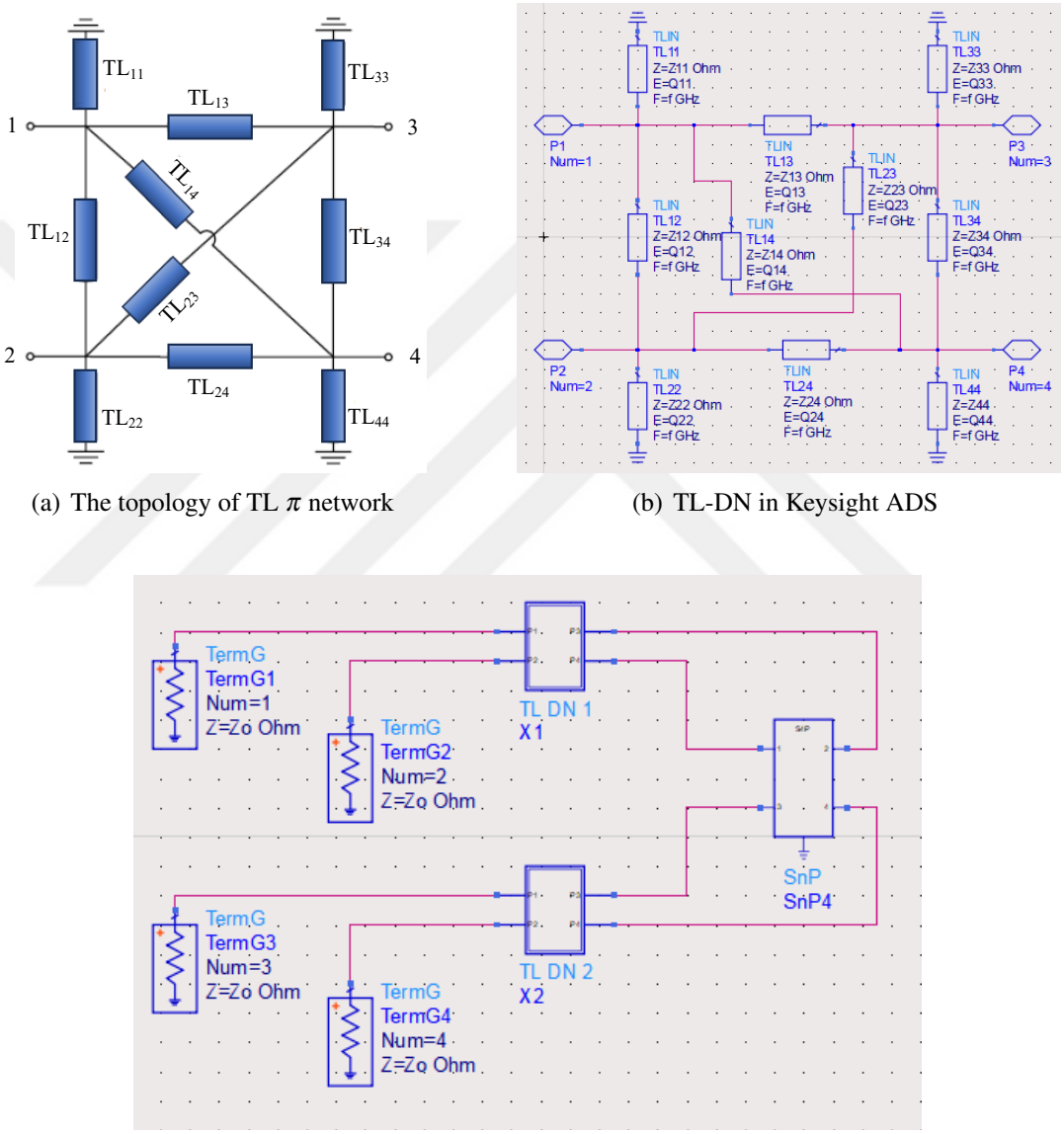

(a) The topology of TL π network

(b) TL-DN in Keysight ADS

(c) TL-DN in Keysight ADS

Figure 6.12 : The synthesized TL-based decoupling network topology in ADS.

Channel capacity refers to the maximum achievable data rate through a MIMO system with minimal errors. The relationship between channel capacity and MIMO antenna

Table 6.2 : Characteristic Impedance and Electrical Length of the TL

Transmission Line	Characteristic Impedance	Electrical Length
TL_n	$Z_n\ (dB)$	$E_n\ (^\circ)$
TL_{11}	150	54
TL_{12}	60.75	81
TL_{13}	72	92
TL_{14}	95	100
TL_{22}	60.75	81
TL_{23}	72	92
TL_{24}	95	100
TL_{33}	60.75	81
TL_{34}	72	92
TL_{44}	95	100

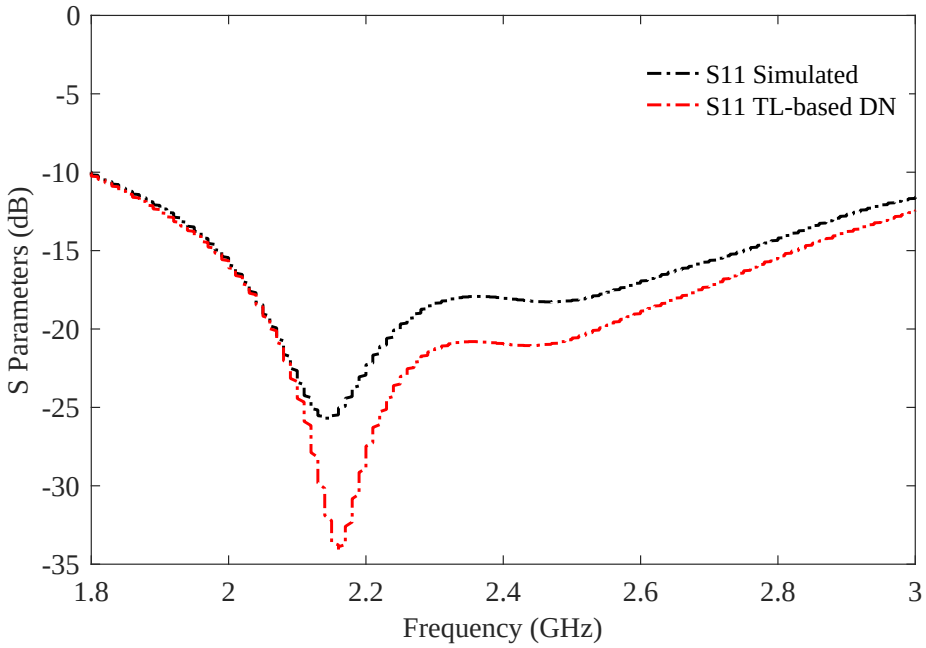

Figure 6.13 : The S-parameters of the quad-port MIMO antenna using the TL-based DN

characteristics is not as intuitive as in a single antenna system. This is because various factors can concurrently affect capacity in MIMO antenna networks, as investigated in studies like [1]-[4]. One method to characterize the multiplexing efficiency of a MIMO array is to compute the reduction in power efficiency needed to attain the same channel capacity as a reference multi-antenna system under similar channel conditions If the transmitter has no channel information, the M x K channel matrix can be expressed as:

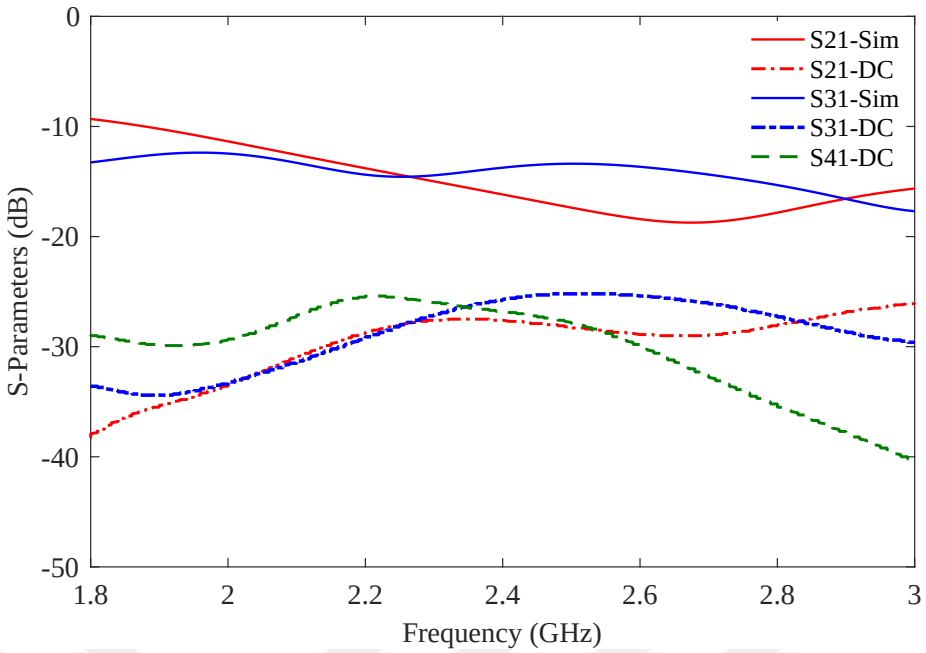

Figure 6.14 : The S-parameters of the quad-port MIMO antenna using the TL-based DN

The Ergodic channel Capacity can be calculated using the following formula, where E represents the expectation over different channel realizations, I denotes the identity matrix, $\frac{P}{\sigma_n^2}$ represents the average SNR at the receiving end, N is the number of transmitting antennas, $(.)^{\dagger}$ denotes the Hermitian operation, and the channel matrix H is given by:

$$C_k = E\left[\log_2 det\left\{I + \frac{P}{\sigma_n^2 N} HH^{\dagger}\right\}\right] \tag{6.1}$$

$$H = R^{\frac{1}{2}} H_w \tag{6.2}$$

Where R_r and R_t are the correlation matrices of the receive and transmit antenna, respectively, and channel matrix H_w is a matrix with independent Gaussian elements with unity variance.

$$R = \begin{bmatrix} \eta_1 & \rho_{12}\sqrt{\eta_1\eta_2} & \cdots & \rho_{1i}\sqrt{\eta_1\eta_i} \\ \rho_{12}^{\dagger}\sqrt{\eta_1\eta_2} & \eta_2 & \cdots & \rho_{2i}\sqrt{\eta_2\eta_i} \\ \vdots & \vdots & \ddots & \vdots \\ \rho_{1i}^{\dagger}\sqrt{\eta_1\eta_i} & \rho_{2i}^{\dagger}\sqrt{\eta_2\eta_i} & \cdots & \eta_i \end{bmatrix}$$

$$\eta_i = \eta_{i,rad}(1 - |S_{ii}|^2 - \sum_{i \neq j} |S_{ij}|^2) \tag{6.3}$$

Where $\eta_{i,rad}$ is the radiating efficiency of the nth port, which is computed as the ratio of the transmitted power to the received power.

For the proposed 4x4 MIMO system, 10,000 independent and identically distributed (i.i.d.) channel realizations were generated to compute the ergodic channel capacity. Figure 9.7 shows the ergodic capacities for 4 x 4 MIMO channels without utilizing CSI at the transmitter side. The simulated channel capacities for the 4x4 MIMO system are 21 bps/Hz with correlation and 20.5 bps/Hz with a transmission line-based decoupling network (TL-based DN). In comparison, independent and identically distributed (iid) channels achieve a simulated capacity of 22 bps/Hz. When the system is measured at an SNR of 20 dB, the actual channel capacities of the proposed 4x4 MIMO system were found to be 19.5 bps/Hz for both correlation scenarios.

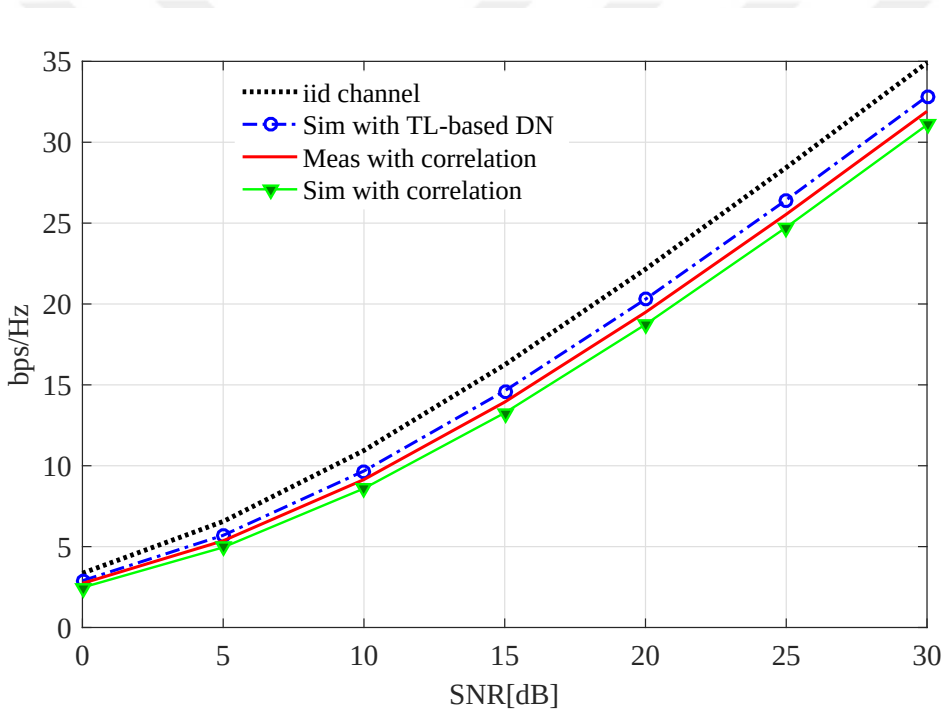

Figure 6.15 : Capacity of a quad-port solitary radiating antenna at 2.1 GHz.

In addition, Figure 1.22 provides a visual representation of an example of the channels in a 4x4 MIMO system. The power is 21 bps/Hz with communication and 20.5 bps/Hz with TL-based DN, while the iid channels achieve a simulated power of 22 bps/Hz Notably, when measuring system has an SNR of 20 dB, the actual channel power of the proposed 4x4 MIMO system is 19.5 bps for both communication conditions.
The results highlighted in Figure 1.23 reaffirm the previously mentioned conclusions regarding the simulated channel capabilities of 4x4 MIMO systems. In particular, the

powers are 21 bps/Hz with communication and 20.5 bps/Hz with TL-based DN, while the simulated power of iid channels reaches 22 bps/Hz when measured at SNR of 20 dB and the actual method of the proposed 4x4 MIMO system is 19.5 bps for both communication conditions.

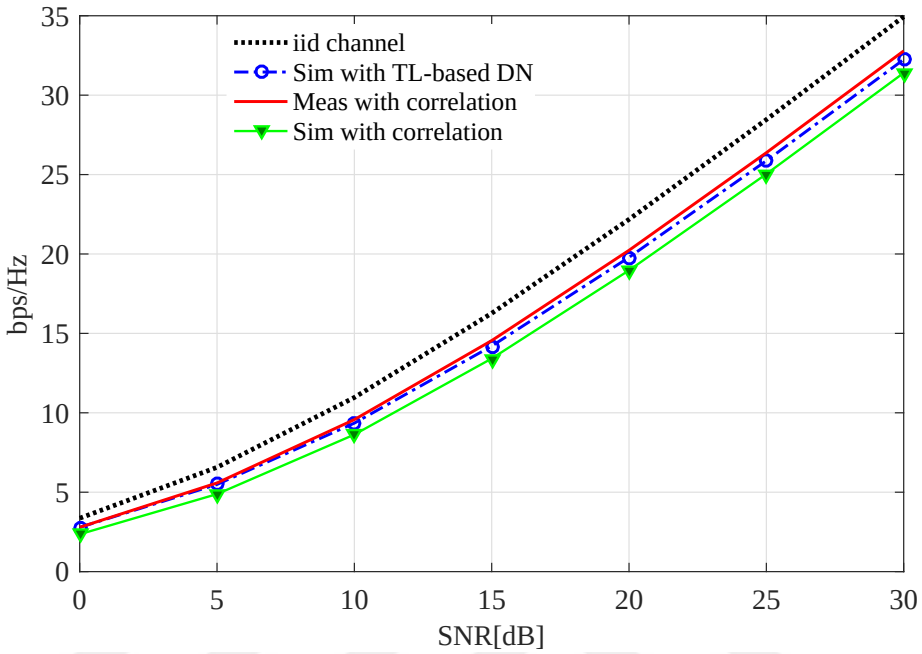

Figure 6.16 : Capacity of a quad-port solitary radiating antenna at 2.3 GHz.

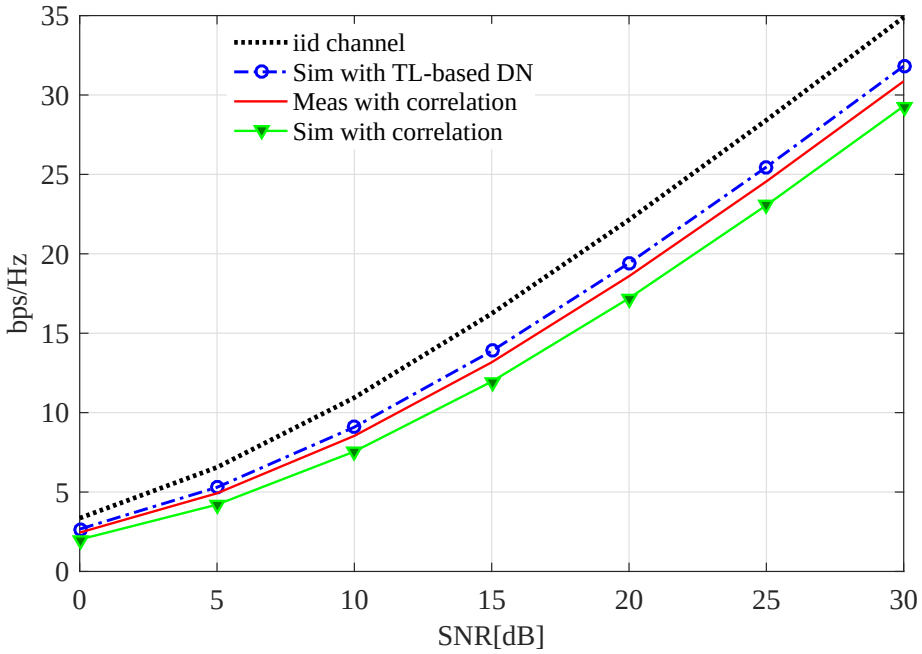

Figure 6.17 : Capacity of a quad-port solitary radiating antenna at 2.6 GHz.

Table 6.3 compares the MIMO antenna and the solitary radiating quad-port antenna based on existing literature in terms of correlation, gain, and isolation. It should be noted that while the antennas reported in [37, 38] have a higher gain than the proposed antenna, their physical size is larger. However, the proposed MIMO antenna design is both cost-effective and capable of providing up to 17 dB of isolation throughout the operational frequency range of 2.0-3.0 GHz, which ensures consistent signal quality free from interference in this frequency range. Additionally, the cost-effectiveness of the proposed MIMO antenna design makes it an attractive option for a wide range of applications where cost is a major consideration. Overall, the results of this comparison demonstrate the superior performance of the proposed MIMO antenna design over other existing antenna designs.

Table 6.3 : A comparison of the MIMO antennas proposed and published.

Ref.	Size (mm^2)	BW (GHz)	Isolation (dB)	Peak Gain (dBi)	ECC
[64]	$137X137$		> 17	4.8	
[54]	$140X140$	1.8-2.9	> 15	5.5	< 0.1
[55]	$100X150$	2.4-4.8	> 10	5	
[65]	$114X114$	2.4-4.8	> 10	5	
[66]	$110X110$	1.95-3.27	> 20	5	
Proposed Antenna	$108X108$	1.8-3.0	> 25	7.4	< 0.01

6.2 Design of a Concentric Octagon MIMO Antenna

With the increasing number of antennas on LTE and 5G NR wireless communication devices, UE device sizes are becoming more compact. Thus, achieving low mutual coupling is a design issue for miniature MIMO antennas in proximity space. To attain spatial diversity, MIMO antenna systems require the separation of antenna elements. An alternative technique to alleviate the space constraint is to leverage polarization and pattern diversity between several antenna elements. Due to the proximity of the antenna components, these antennas display significant coupling between the elements. As stated in Chapter 2, several isolation measures have been introduced to minimize mutual coupling between closely packed antenna elements. Numerous methods for reducing coupling among collocated antenna ports have been described, such as DGS, CSRR, and metamaterial techniques. A DGS consists of a series of slots etched into the ground, which act as a stop band to attain the desired frequency isolation [67]. The CSRR was utilized in [68] to mitigate mutual coupling as non-periodic sub-wavelength features between symmetrically polarized antenna components etched on the ground. However, these designs significantly increase back radiation due to their defective ground. The metamaterial technique includes a sequence of via holes in the design using the confined patch and ring resonance [69]. As a result, the mutual coupling among the quad-input ports has been reduced. These structures are complex, challenging to produce, and suffer from losses caused by the resonance.

In this section, to achieve an optimal antenna design, the first step is to identify the geometry that provides the widest bandwidth. Once the most efficient geometry is established, the next step is to determine the optimal feed positions that ensure good matching and isolation. In this design, an octagonal annular radiating plane was added to minimize mutual coupling, which is a parasitic technique used to reduce interference between adjacent antennas. The antenna is planar and includes a ground plane, making it suitable for integration into a wireless device terminal.To evaluate antenna performance characteristics, such as scattering parameters, ECC, TARC, and channel capacity, simulations and measurements are employed.

6.2.1 Design evaluation of concentric octagon antenna

The concentric octagonal monopole antenna design evaluation is illustrated in Figure 6.18, which involves four stages aimed at verifying the design by adjusting the frequency response n38 band (2.57 – 2.62 GHz) using the antenna topology to determine the geometry. The physical aperture determines the frequency band in each mode in terms of modeling. To streamline the process, a circular shape was initially employed for a single patch design in the first stage, resulting in a frequency response of 2.6 GHz. In the second stage, an octagonal-shaped antenna was matched to the 50 Ω feed line, as shown in Figure 6.18b, to enhance the antenna's impedance bandwidth over Ant 1. In the subsequent design stage, a slotted octagon with radii of 3.2 mm was inserted in the center of the solid concentric octagonal-shaped antenna, as depicted in Figure 6.18c. By exploring the impact of modifying fractal geometry on the monopole antenna input impedance, the slots provide capacitive loading to the radiating components at Ant 3. Moreover, Figure 6.19 demonstrates that the parasitic components generate inductive loading to the concentric octagonal antenna. Consequently, the capacitive loading reduces when the octagonal parasitic elements are added to the octagonal radiating element, and the plot switches to inductive at Ant 4.

The optimum dimensions for achieving the finest impedance matching over the n38 band (2.57 – 2.62 GHz) were used to design a concentric octagonal-shaped antenna with a microstrip feed line for 5G applications. This design enhanced bandwidth and ensured compatibility with the desired frequency range.

6.2.2 Concentric octagon MIMO antenna configuration

The proposed antenna utilizes octagonal patches that resonate in various transverse modes. This design was initiated with a single radiating element in the two basic orthogonal modes for ports 1 and 2 to achieve compactness and collocation. A concentric octagonal ring strip is inserted around the radiating element to act as a parasitic decoupling for enhanced impedance bandwidth and good isolation. Furthermore, the feed positions have been adjusted to P1 (5 mm, 0) and P2 (0 mm, 5 mm) to achieve accurate input impedance matching. Despite the slightly

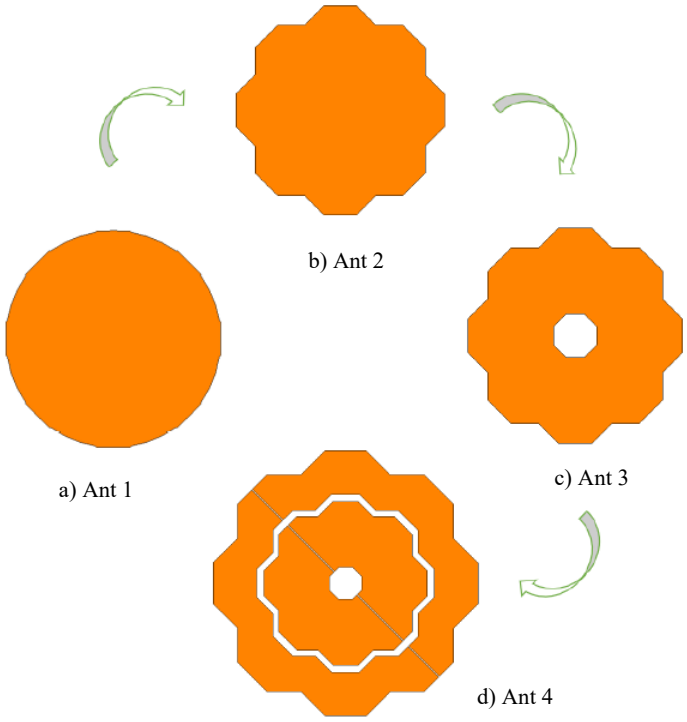

Figure 6.18 : The evolution of concentric octagon antenna.

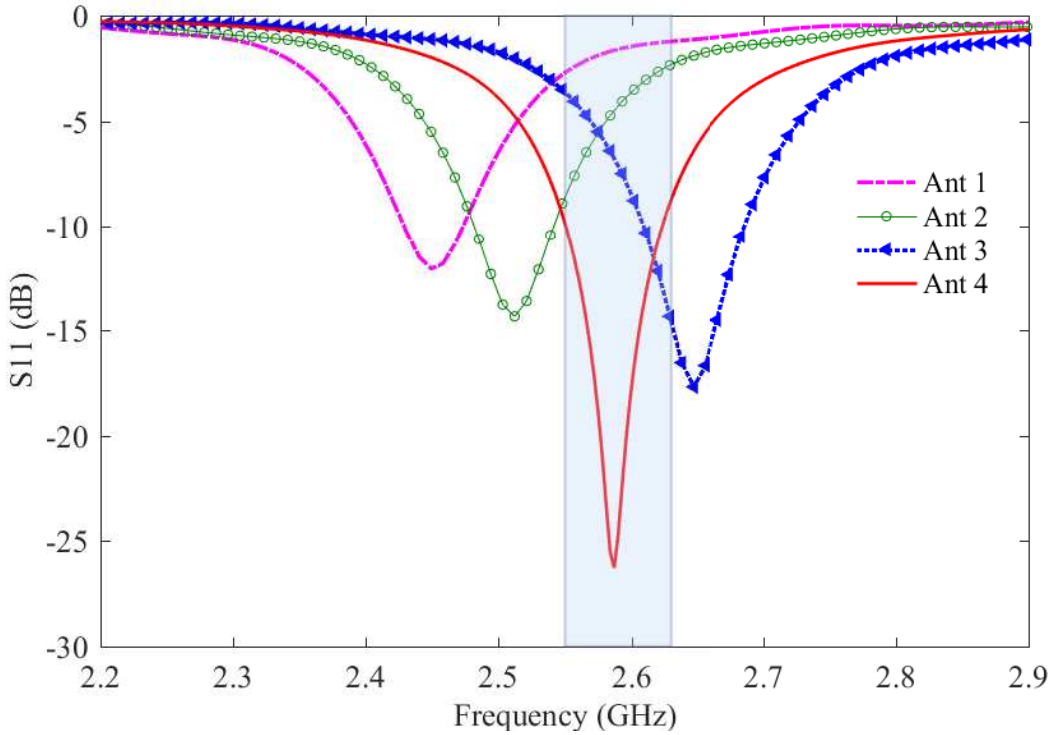

Figure 6.19 : S_{11} of concentric octagon antenna.

altered frequency band, the antenna's overall behavior seems quite close to the desired resonance in the 5G band at 2.6 GHz. Figure 6-3 depicts the intended antenna's layout, and the following table displays the optimum sizes in Table 6-1.

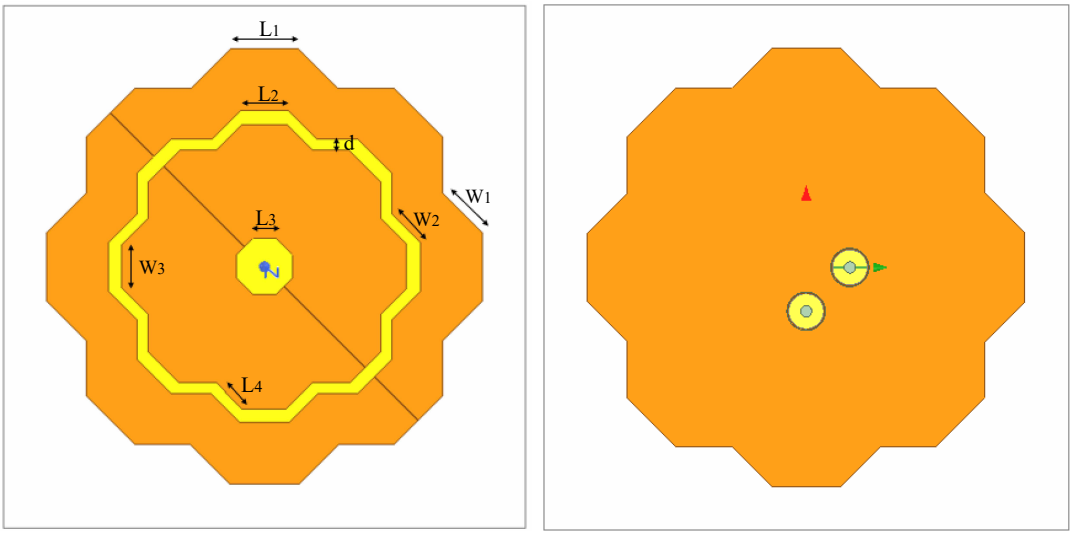

(a) Top layer. (b) Bottom layer.

Figure 6.20 : Dual-port concentric octagon layout.

Table 6.4 : Optimum dimensions of concentric octagon antenna.

Parameters	Value (mm)	Parameters	Value (mm)
L1	7.81	W1	6.46
L2	5.60	W2	4.60
L3	2.67	W3	5.10
L4	4.20	d	1.38
L	60	L	60
w	2.85	L3	9.5

6.2.3 The Result of concentric octagon MIMO antenna

Figure 6.21 illustrates the concentric octagonal radiating prototype, which was produced and tested to validate the suitability of the antenna design. To accommodate the proximity of the two ports, the prototype utilizes right-angle SMA connectors as feeds, while SMA adapters are used for calibration and measurement. The Spectrum Analyzer was used to measure the S-parameters of the paired port antenna, as presented in Figure 6.22. The figure displays the reflection coefficient of the fabricated antenna, which closely resembles the simulation results, with a slight deviation across the operating frequency from the CST simulation outcome. Despite using a conventional fabrication process, the variance between measurement and simulation results is acceptable.

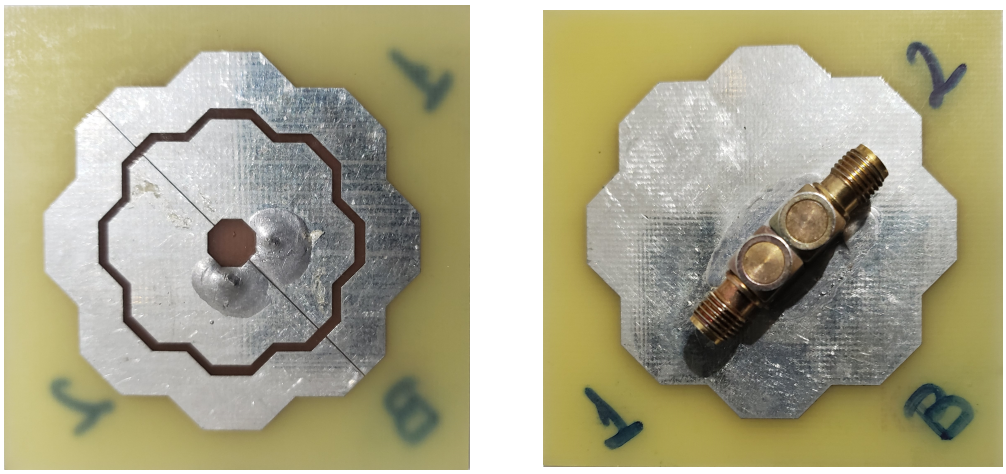

(a) Top layer. (b) Bottom layer.

Figure 6.21 : Concentric octagon dual-port antenna fabrication

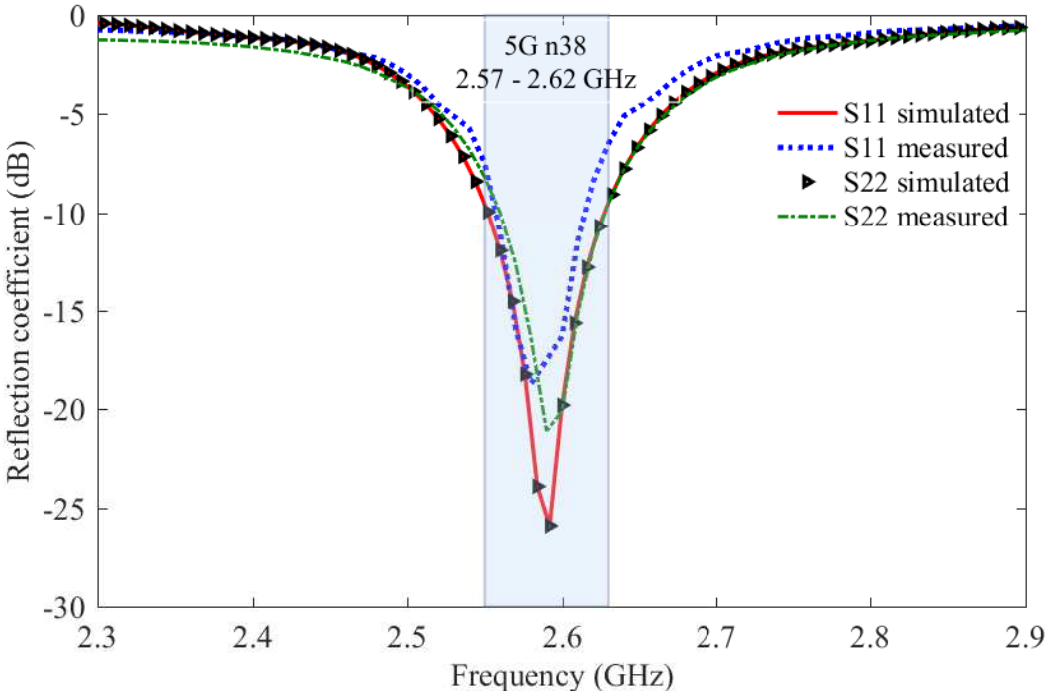

Figure 6.22 : The reflection coefficients of concentric octagon MIMO antenna.

The previous simulations provided the optimal design for the concentric octagon-shaped antenna based on good isolation and proper impedance matching. The simulations also achieved an optimal terminal model for the antenna with high isolation and proper impedance bandwidth. Figure 6.23 presents the experimental and simulation-based results, which show that the isolation between adjacent elements was less than -20dB throughout the operating frequency band. This result implies that the experimental isolation is consistent with the simulated results. The plot shows minimal

discrepancy in the measured results, despite manufacturing inaccuracies, welding, and the use of lossy dielectric material.

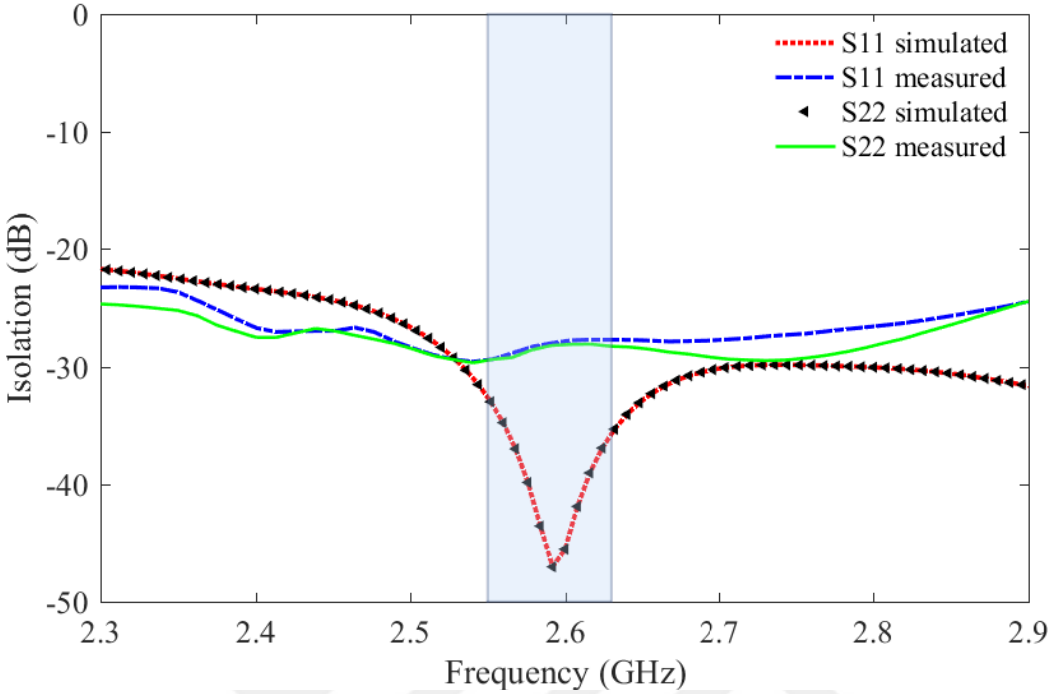

Figure 6.23 : The isolation of concentric octagon MIMO antenna.

In Figure 6.24, surface current distributions in the frequency bands being used are depicted. It is apparent from the illustration that the majority of the currents are concentrated on the octagonal annular, effectively enhancing isolation between antennas. The closeness effect causes a redistribution of electric current in radiating elements that are in close proximity, leading to a concentration of current distribution on the side and opposite of the excited ports. Despite this, the parasitic elements specifically designed for decoupling serve a vital purpose in achieving high isolation by preventing induced currents from reaching the unexcited antenna.

Figure 6.25 displays the radiation pattern of the antenna in both co- and cross-polarization at 2.57, 2.6, and 2.62 GHz for both the E- and H-planes. The plots demonstrate that the cross-polarization is significantly lower than the co-polarization, with a difference of approximately 35 dB, which is desirable for reducing interference and leading to clearer and more reliable communication. Furthermore, the antenna maintains a consistent broad pattern throughout its entire operational spectrum.

As shown in Chapter 2, the ECC (Envelope Correlation Coefficient) is an important element in MIMO (Multiple Input Multiple Output) antenna systems. Two distinct

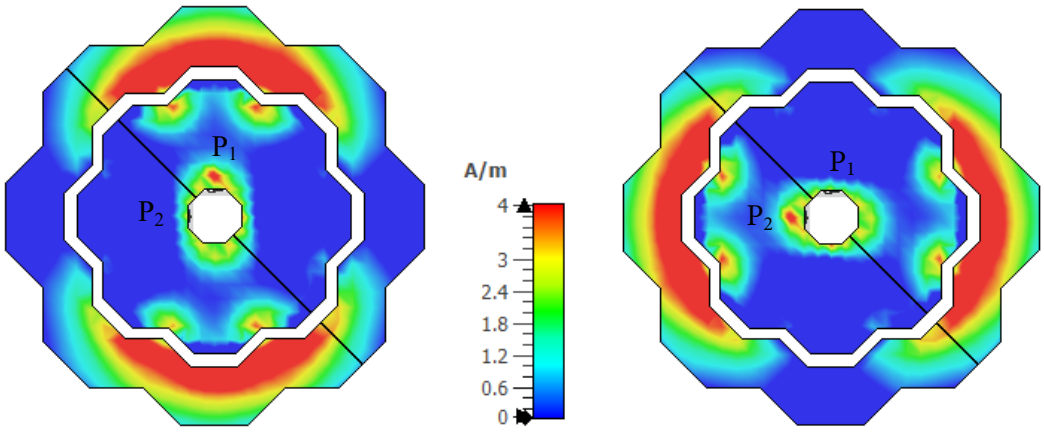

(a) Port 1 is excited (c) Port 2 is excited

Figure 6.24 : Radiation distribution of solitary radiating MIMO antenna @2.1GHz.

methods exist for determining the ECC of a MIMO antenna. The first technique relies on the antenna's far-field radiation pattern [23, 24], while the second uses the antenna's S parameters [25]. The correlation coefficient of the proposed MIMO antenna was calculated using equation (3.1), which is based on the scattering parameter displayed in Figure 6.26. The plot shows that the ECC value is 0.002, which is much less than the maximum value permitted for MIMO antenna applications, which is 0.3 [5].

TARC, which stands for Total Active Reflection Coefficient, is a key parameter in multiple antennas used to properly evaluate the system's bandwidth and efficiency. The ratio of the total incident power to total reflected power is known as TARC [23]. In the two-port multi-antenna system, TARC is calculated using Equation (3.2) [28]. TARC values for the current design are computed using Equation (3.2) and displayed in Figure 6.27. The TARC curves cover the phase range from 0o to 90o in 45o increments. The bands are clearly visible at TARC values smaller than -10 dB.

Channel capacity refers to the maximum achievable data rate through a MIMO system with minimal errors. The relationship between channel capacity and MIMO antenna characteristics is not as intuitive as in a single antenna system. This is because various factors can concurrently affect capacity in MIMO antenna networks, as investigated in studies like [1]-[4]. One method to characterize the multiplexing efficiency of a MIMO array is to compute the reduction in power efficiency needed to attain the same channel capacity as a reference multi-antenna system under similar channel conditions. MIMO technology, in combination with orthogonal frequency division multiplexing

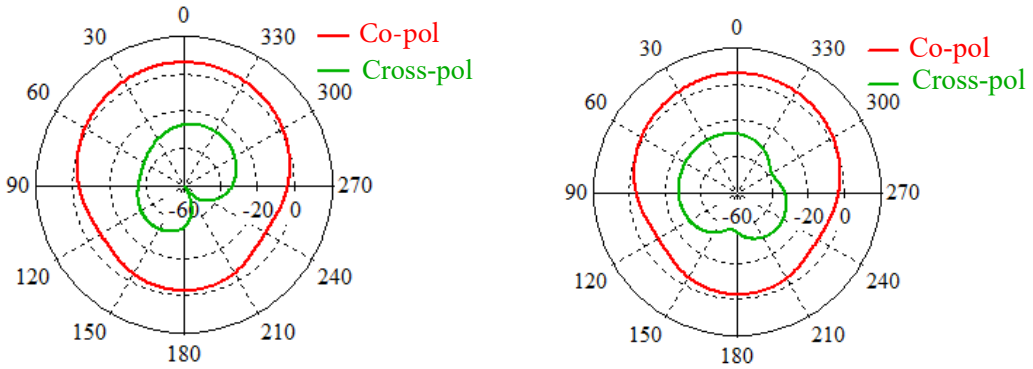

(a) E-plane @ 2.57 GHz (b) H-plane @ 2.57 GHz

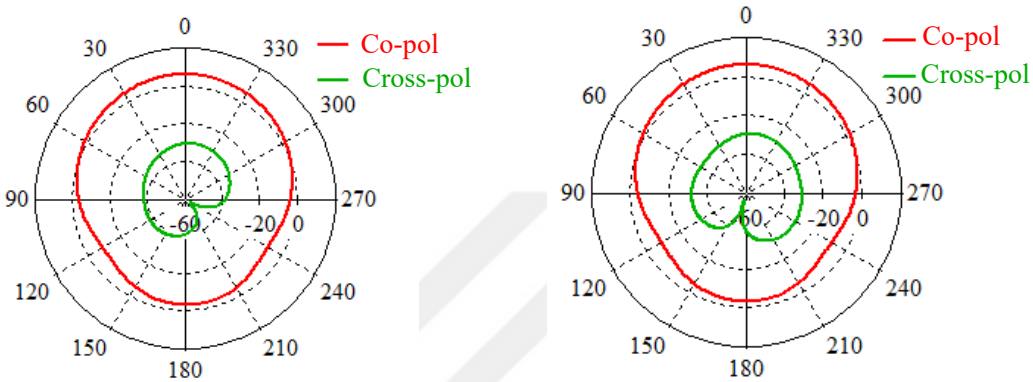

(c) E-plane @ 2.60 GHz (d) H-plane @ 2.60 GHz

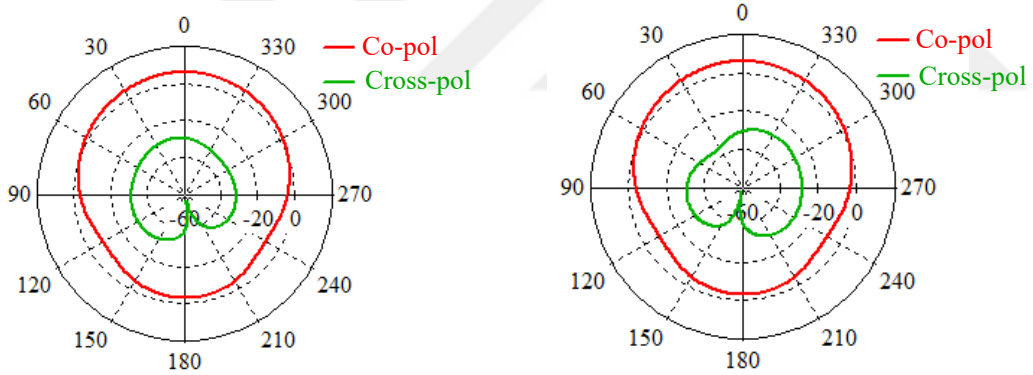

(e) E-plane @ 2.62 GHz (f) H-plane @ 2.62 GHz

Figure 6.25 : Radiation patterns of the proposed antenna in two principle plane.

(OFDM), has emerged as a crucial enabler for high data rate wireless communication systems. MIMO-OFDM incorporates MIMO spatial diversity with OFDM spectrum efficiency to attain performance and reliability. The ergodic capacity of a MIMO channel characterizes the maximum achievable average transmission rate for reliable communication over the fading channel realizations. The capacity C on each sub-band is determined using the standard MIMO channel Ergodic capacity in Equation 2.21.

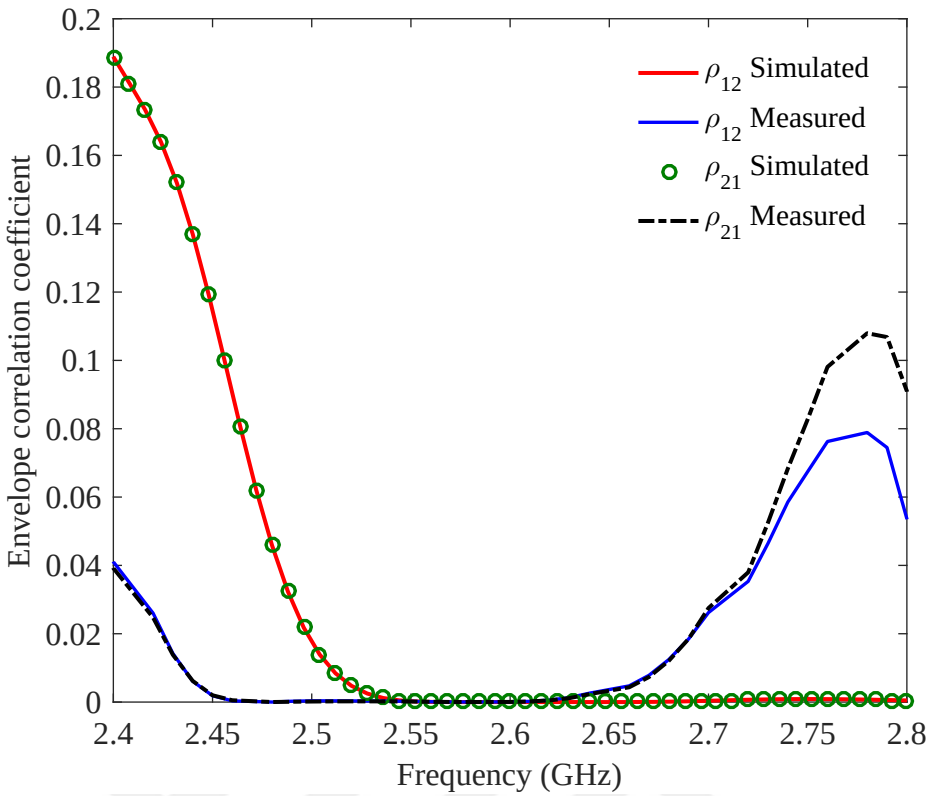

Figure 6.26 : The ECC concentric octagon MIMO antenna.

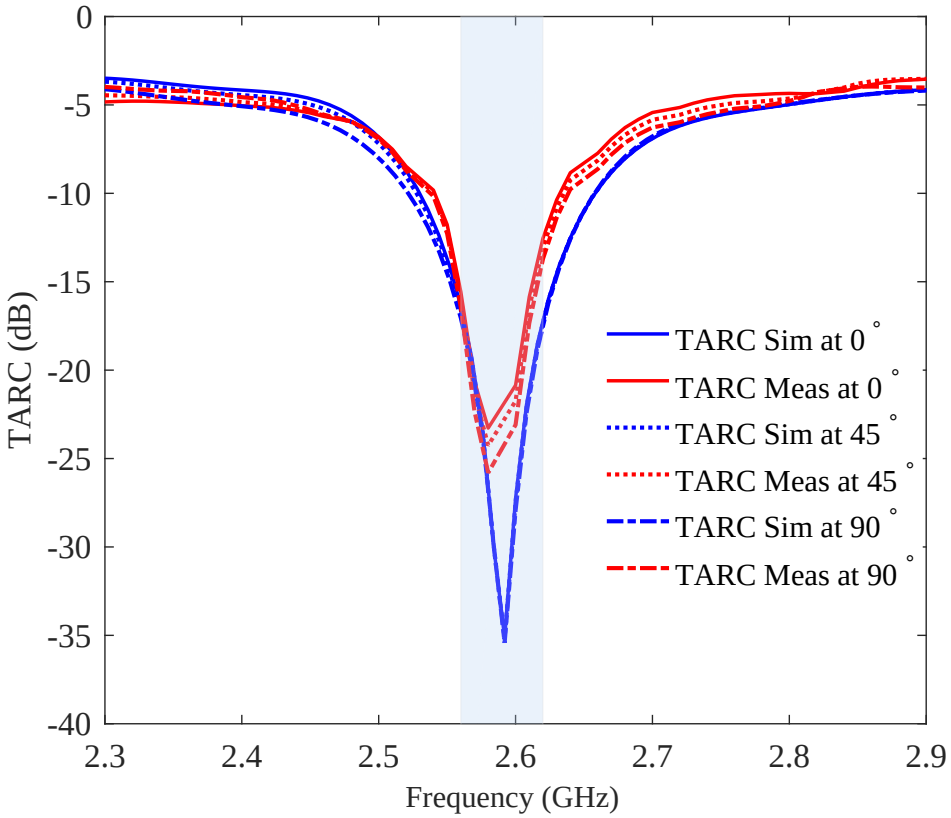

Figure 6.27 : The TARC concentric octagon MIMO antenna.

The broadband capacity of the MIMO-OFDM system is determined as the weighted sum of the capacities across all K sub-bands. Let w_k represent the capacity obtained on sub-band k. Then, the broadband capacity C is given by:

$$C = \frac{1}{K}\sum_{k=1}^{K}\mathbb{E}\left[\log_2 det\left\{I + \frac{P}{\sigma_n^2 N}HH^{\dagger}\right\}\right] \tag{6.4}$$

where E represents the expectation over different channel realizations, I denotes the identity matrix, $\frac{P}{\sigma_n^2}$ represents the average SNR at the receiving end, N is the number of transmitting antennas, $(.)^{\dagger}$ denotes the Hermitian operation.

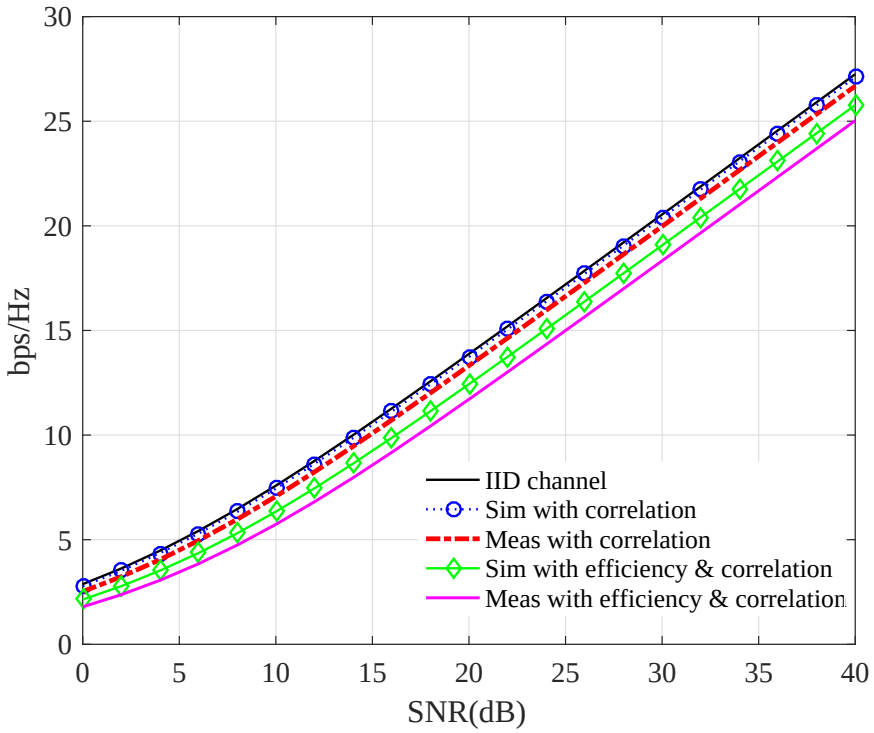

Figure 6.28 : The capacity concentric octagon MIMO antenna.

The proposed antenna design offers several advantages over previously published studies. Compared to Ref. [67], the proposed antenna boasts a higher gain of 5.0 dB while maintaining comparable isolation (-25 dB). Compared to Ref. [68], the proposed antenna offers a higher gain of 5.0 dB and a lower envelope correlation coefficient (ECE) of 0.01, compared to 0.4. Additionally, the proposed antenna avoids back-lobe radiation, which can reduce antenna gain. Compared to Ref. [69], the proposed antenna offers a higher gain of 5.0 dB and a lower ECE of 0.01, along with a simpler design and easier fabrication. In conclusion, the single concentric octagonal-shaped MIMO antenna design emerges as a compact and effective solution

for 5G n38 applications, offering excellent isolation, proper impedance matching, and high gain.

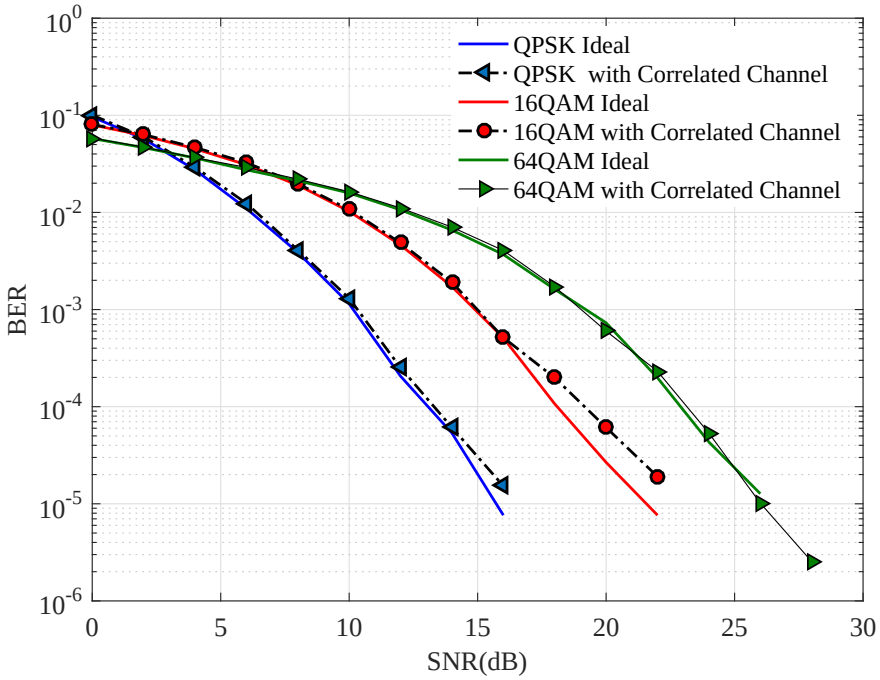

Figure 6.29 : The BER of concentric octagon MIMO antenna.

Table 6.5 : Comparing the intended MIMO antenna to previously published studies.

Ref.	Dimensions (mm)	Isolation (dB)	ECE	Gain (dB)	Technique	Remarks
[67]	60.2x60.2	-25 at 2.45	0.1	2.1	Square ring DGS	Back-lobe radiation Reduces antenna gain.
[68]	60.0x60.0	-22 at 2.45	0.4	4.0	CSRR loaded ground	used as band stop filter. Back radiation
[69]	38.5x39.5	-20 at 5.25	0.05		shorting vias	Complex
Proposed antenna	60×60	-25 at 2.6	0.01	5.0	parasitic element	Compact easy fabrication.

7. CONCLUSIONS AND RECOMMENDATIONS

The research in this thesis focused on developing a new antenna design methodology based on MIMO performance metrics, mutual coupling, and defining antenna parameters for sub-6GHz frequencies for user equipment (UE). The research involved the design and analysis of five different types of MIMO antennas, including a dual-band elliptically tapered slot Vivaldi MIMO antenna, a single concentric octagonal-shaped MIMO antenna, a dual elliptically tapered MIMO antenna, a wideband MIMO antenna for UE devices, and a quad-element MIMO antenna using a modified Apollony fractal. The proposed design methodology for MIMO antennas is based on a systematic approach that takes into account MIMO performance metrics such as ECC, DG, TARC, capacity loss and capacity. The methodology also considers decoupling techniques such as antenna placement and orientation, etching slots, parasitic elements, neutralization, and synthesized pi-networks TL-based decoupling network topology to reduce mutual coupling and improve MIMO performance. The proposed methodology was evaluated through simulations and measurements, and was found to significantly improve MIMO antenna performance for sub-6GHz frequencies compared to existing antenna designs.

The dual-elliptically tapered MIMO antenna was designed for user equipment (UE) and consists of four elements arranged in a compact configuration. Various decoupling techniques were employed to mitigate mutual coupling between closely spaced antenna elements. These techniques included parasitic elements, antenna placement and orientation, annular stripes on the ground, and an overall size of 66 mm x 66 mm. To effectively mitigate mutual coupling between the closely spaced antenna elements, various decoupling techniques were employed. These techniques included strategically placing and orienting the radiators, as well as incorporating parasitic structures such as a cross-shaped stub parasitic on top of the substrate and a partial ground plane with ring-shaped stripes parasitic on the bottom. These parasitic elements induce coupling currents to suppress undesired coupling effects among the radiating elements,

enhancing isolation in close proximity. In summary, the dual-elliptically tapered MIMO antenna was designed for the 5G n40, n41 band and also suitable for LTE (2.3-2.4GHz, 2.496-2.69GHz) and Wi-Fi (2.412-2.484GHz) applications. The MIMO antenna exhibited desirable performance characteristics, with a capacity loss lower than 0.6 b/s/Hz and an ECC value of 0.04, making it well-suited for LTE and Wi-Fi applications.

The quad-element MIMO antenna using a modified Apollonian fractal was designed for the 5G n78 band. The antenna configuration consists of a quad Apollonian fractal antenna and a decoupling technique utilizing physical placement and orientation, as well as quarter-wave impedance matching to provide a match between the antenna and the transmission line for maximum power transfer and minimizing reflections. The decoupling techniques are employed to reduce the strength of the coupling fields and to minimize coupling through polarization mismatch. The design and characterization of an Apollonian-shaped fractal MIMO antenna with an inter-element spacing of $0,5\lambda$ were also investigated. The overall size of the antenna is 80 mm x 80 mm. The performance of the antenna was evaluated through simulations using the full-wave electromagnetic simulator. Subsequently, a prototype of the Apollonian fractal antenna was fabricated, and the scattering parameters were measured to assess the diversity performance of the MIMO antenna system. The measured reflection coefficient of the Apollonian-shaped MIMO antenna ranged from 3.2 GHz to 3.8 GHz, with an S11 of -10dB. This frequency range aligns with the operating frequencies of 5G networks. Additionally, the mutual coupling between neighboring antenna elements was observed to be lower than -20dB, indicating a significant reduction in interference. The measured results of the fabricated antenna closely matched the simulated results. The diversity performance, characterized by the ECC and capacity loss, demonstrated favorable values of lower than 0.04 and 0.5, respectively. Based on these findings, it can be concluded that the proposed Apollonian-shaped MIMO antenna is a promising candidate for 5G portable communication devices. Its compactness, combined with its excellent performance parameters, makes it well-suited for meeting the demands of 5G communication systems.

The dual-band elliptically tapered slot Vivaldi MIMO antenna is designed for the 5G n78 and n79 bands. It features a configuration consisting of four elliptically

tapered slot Vivaldi antennas on a shared radiator antenna with four ports. The antenna design incorporates a decoupling technique to enhance isolation between the antenna elements. This technique involves strategic placement and orientation of antenna slots and tapered slots. The overall size of the antenna is 108 mm x 108 mm. The Vivaldi-shaped dual-band MIMO antenna is specifically designed for 5G applications and covers the 5G NR bands n78 (3.3-3.8 GHz) and n79 (4.4-5.0 GHz). The antenna aims to achieve a gain of at least 7.63 dBi and 8.5 dBi for the respective frequency bands, with mutual coupling below -30 dB. Simplicity was prioritized in the antenna design by avoiding complex multilayer and via configurations. To evaluate the performance of the proposed antenna, various performance metrics were used, including S-parameters, ECC, and channel capacity. Experimental measurements were conducted to validate the antenna's performance. The evaluation demonstrated an ECC value lower than 0.01, indicating a high level of diversity between the MIMO antenna elements. The findings from the measurements are in agreement with the simulation results, providing validation to support the performance of the proposed antenna design.

A single-layer concentric octagonal-shaped MIMO antenna was designed for 5G user equipment (UE) applications. The design achieves compactness and collocation by utilizing a concentric octagon configuration with two coaxial feed ports. The antenna operates in the 5G n38 band, and a decoupling technique utilizing parasitic octagonal-ring elements, slot and slit structures, optimized feed placement, and an overall size of 60 mm x 60 mm was employed. The design was explored and optimized using Hyperstudy. The design focuses on optimizing the antenna element for operation in the n38 5G frequency band, which spans from 2.57 GHz to 2.62 GHz. A notable feature of this design is that it uses only a single layer, which simplifies the manufacturing process and reduces manufacturing costs. CST software was used to simulate the antenna's electromagnetic performance, which indicates that the antenna achieves a peak gain of 5.5 dBi, with mutual coupling maintained below -25 dB. Additionally, the antenna exhibits an exceptionally low ECC value of 0.003 across the entire frequency band. These simulation results were further verified by measurements taken from a fabricated prototype, which demonstrated good agreement with the simulated performance.

The wideband MIMO antenna for UE devices was designed to operate in the LTE b1, b40, b41, n1, n7, n40, n41 bands. The antenna configuration consists of a single radiating element with a rhombus structure patch antenna, four balanced microstrip feedlines, and a neutralize line within a partial ground plane. A decoupling technique utilizing neutralization, antenna placement and orientation, 4 strip steps edge between the ports, and the synthesized pi-networks TL-based decoupling network topology in ADS was employed. The overall size of the antenna is 108 mm x 108 mm. The proposed single element MIMO antenna with four ports for wideband wireless communication applications is composed of a symmetrical four feedline microstrip patch antenna with a single radiating element, accompanied by a frame-shaped partially grounded plane. The designed MIMO antenna demonstrates a favorable -10 dB reflection coefficient and a bandwidth of approximately 1.2 GHz, spanning from 2.0 GHz to 3.0 GHz. Additionally, it achieves an acceptable level of isolation, with values lower than -12 dB across the covered frequency band.

Future work in this area could include developing AI-based optimization algorithms for more efficient and automated antenna design processes, investigating the integration of the antenna design with other components of 5G user equipment for a complete system solution, and collaborating with industry partners to validate the proposed antenna designs in real-world scenarios and commercialize them for use in 5G and beyond wireless communication systems.

In conclusion, the research presented in this thesis has demonstrated the feasibility and effectiveness of the proposed methodology for designing compact MIMO antennas that offer improved performance metrics. The prototype four-port MIMO antenna, as well as the Apollony-shaped fractal MIMO antenna, Vivaldi-shaped dual-band MIMO antenna, and quad-ports single element MIMO antenna, all exhibited favorable performance characteristics that make them well-suited for use in 5G and beyond wireless communication systems. Further research in this area is recommended to fully realize the potential of the proposed methodology and antenna designs.

REFERENCES

[1] **Liu, Y.**, **Yang, X.**, **Jia, Y. and Guo, Y.J.** (2019). A low correlation and mutual coupling MIMO antenna, *IEEE Access*, *7*, 127384–127392.

[2] **Alkhateeb, A.**, **Leus, G. and Heath, R.W.** (2015). Limited feedback hybrid precoding for multi-user millimeter wave systems, *IEEE Transactions on Wireless Communications*, *14*(11), 6481–6494.

[3] **Hong, W.**, **Jiang, Z.H.**, **Yu, C.**, **Zhou, J.**, **Chen, P.**, **Yu, Z.**, **Zhang, H.**, **Yang, B.**, **Pang, X.**, **Jiang, M. and et al.** (2017). Multibeam Antenna Technologies for 5G Wireless Communications, *IEEE Transactions on Antennas and Propagation*, *65*(12), 6231–6249.

[4] **Sultan, K.S.**, **Abdallah, E.A. and Hennawy, H.E.** (2020). A multiple-input-multiple-output on-chip Quasi-Yagi-Uda antenna for multigigabit communications: Preliminary study, *Engineering Reports*.

[5] **Aboelleil, H.**, **Ibrahim, A.A. and Khalaf, A.A.M.** (2022). Four-radiator ultra-wideband multiple-input multiple-output antenna with high performance and dual-band rejection features for high-speed communications, *International Journal of Communication Systems*.

[6] **Biswas, S.**, **Ghosh, C.K.**, **Banerjee, S.**, **Mandal, S. and Mandal, D.** (2020). High port isolation of a dual polarized microstrip antenna array using DGS, *Journal of Electromagnetic Waves and Applications*, *34*(6), 683–696.

[7] **Pasumarthi, S.R.**, **Kamili, J.B. and Avala, M.P.** (2019). Design of tri-band MIMO antenna with improved isolation using DGS and vias, *Wireless Personal Communications*, *110*(3), 1523–1532.

[8] **Li, J.F.**, **Chu, Q.X. and Huang, T.G.** (2012). A compact wideband MIMO antenna with two novel bent slits, *IEEE Transactions on Antennas and Propagation*, *60*(2), 482–489.

[9] **Luo, C.M.**, **Hong, J.S. and Zhong, L.L.** (2015). Isolation enhancement of a very compact UWB-MIMO slot antenna with two defected ground structures, *IEEE Antennas and Wireless Propagation Letters*, *14*, 1766–1769.

[10] **Ali Sehrai, D.**, **Muhammad, F.**, **Hassan Kiani, S.**, **Haq Abbas, Z.**, **Tufail, M. and Kim, S.** (2020). Gain-enhanced metamaterial based antenna for 5G communication standards, *Computers, Materials and Continua*, *64*(3), 1587–1599.

[11] **Singh, H.**, **Gupta, A.**, **Bakshi, S. and Mittal, N.** (2021). Designing and analysis of non-symmetric dual layer CRLH metamaterial, *Journal of Magnetism and Magnetic Materials*, *538*, 168269.

[12] **Tirado-Mendez, J.A.**, **Jardon-Aguilar, H.**, **Flores-Leal, R.**, **Rangel-Merino, A.**, **Vasquez-Toledo, L.A.**, **Rodriguez-Colina, E.**, **Marcelin-Jimenez, R. and Pascoe-Chalke, M.** (2022). Metamaterial split-ring resonators applied as reduced-size four-port antenna array for MIMO applications, *AEU - International Journal of Electronics and Communications*, *154*, 154338.

[13] **Li, M.**, **Jiang, L. and Yeung, K.L.** (2020). A General and Systematic Method to Design Neutralization Lines for Isolation Enhancement in MIMO Antenna Arrays, *IEEE Transactions on Vehicular Technology*, *69*(6), 6242–6253.

[14] **Singh, H.V.**, **Tripathi, S. and Mohan, A.** (2021). Closely-coupled MIMO antenna with high wideband isolation using decoupling circuit, *AEU - International Journal of Electronics and Communications*, *138*, 153833.

[15] **Li, M.**, **Wu, D.**, **Xiao, B.**, **Yeung, K.L. and Jiang, L.** (2020). A novel calculation method to design parasitic decoupling technique for two antennas, *IEEE Access*, *8*, 116041–116051.

[16] **Bird, T.S.** (2021). Basics of antenna mutual coupling, *Mutual Coupling Between Antennas*, 9–26.

[17] **Hao, C.**, **Zheng, H.**, **Gu, Y. and Sun, X.b.** (2021). Mutual coupling reduction of MIMO antenna array using meta-FCRR, *Wireless Personal Communications*, *119*(4), 3435–3445.

[18] **Radhi, A.H.**, **Nilavalan, R.**, **Al-Raweshidy, H.S. and Aziz, N.A.** (2017). High isolation planar UWB antennas for wireless application, *2017 IEEE MTT-S International Microwave Workshop Series on Advanced Materials and Processes for RF and THz Applications (IMWS-AMP)*.

[19] **Li, X.L.**, **Yang, G.M. and Jin, Y.Q.** (2019). Isolation enhancement of wideband vehicular antenna array using fractal decoupling structure, *IEEE Antennas and Wireless Propagation Letters*, *18*(9), 1799–1803.

[20] **Ren, Z.**, **Zhao, A. and Wu, S.** (2019). MIMO antenna with compact decoupled antenna pairs for 5G Mobile Terminals, *IEEE Antennas and Wireless Propagation Letters*, *18*(7), 1367–1371.

[21] **Wen, D.**, **Hao, Y.**, **Wang, H. and Zhou, H.** (2019). Design of a MIMO antenna with high isolation for smartwatch applications using the theory of characteristic modes, *IEEE Transactions on Antennas and Propagation*, *67*(3), 1437–1447.

[22] **Blanch, S.**, **Romeu, J. and Corbella, I.** (2003). Exact representation of antenna system diversity performance from input parameter description, *Electronics Letters*, *39*(9), 705.

[23] **Chae, S.H.**, **Oh, S.k. and Park, S.O.** (2007). Analysis of Mutual Coupling, Correlations, and TARC in WiBro MIMO Array Antenna, *IEEE Antennas and Wireless Propagation Letters*, *6*, 122–125.

[24] **Tran, H.H. and Nguyen-Trong, N.** (2021). Performance enhancement of MIMO patch antenna using parasitic elements, *IEEE Access*, *9*, 30011–30016.

[25] **Xu, K.D.**, **Zhu, J.**, **Liao, S. and Xue, Q.** (2018). Wideband Patch Antenna Using Multiple Parasitic Patches and Its Array Application With Mutual Coupling Reduction, *IEEE Access*, *6*, 42497–42506.

[26] **Wei, K.**, **Li, J.Y.**, **Wang, L.**, **Xing, Z.J. and Xu, R.** (2016). Mutual coupling reduction by novel fractal defected ground structure bandgap filter, *IEEE Transactions on Antennas and Propagation*, *64*(10), 4328–4335.

[27] **Wei, K.**, **Li, J.**, **Wang, L.**, **Xing, Z. and Xu, R.** (2016). S-shaped periodic defected ground structures to reduce microstrip antenna array mutual coupling, *Electronics Letters*, *52*(15), 1288–1290.

[28] **Tiwari, R.N.**, **Singh, P.**, **Kanaujia, B.K. and Srivastava, K.** (2019). Neutralization technique based two and four Port High Isolation Mimo Antennas for UWB Communication, *AEU - International Journal of Electronics and Communications*, *110*, 152828.

[29] **Yang, Y.**, **Chu, Q. and Mao, C.** (2016). Multiband MIMO Antenna for GSM, DCS, and LTE Indoor Applications, *IEEE Antennas and Wireless Propagation Letters*, *15*, 1573–1576.

[30] **Banerjee, J.**, **Ghatak, R. and Karmakar, A.** (2018). A compact planar UWB MIMO diversity antenna with Hilbert fractal neutralization line for isolation improvement and dual band notch characteristics, *2018 Emerging Trends in Electronic Devices and Computational Techniques (EDCT)*, pp.1–6.

[31] **Malik, J.**, **Patnaik, A. and V. Kartikeyan, M.** (2018). *Compact Antennas for High Data Rate Communication: Ultra-wideband (UWB) and Multiple-Input-Multiple-Output (MIMO) Technology*, Springer International Publishing.

[32] **O. Katie, M.**, **Jamlos, M.F.**, **S.Alqadami, A. and Jamlos, M.A.** (2017). Isolation enhancement of compact dual-wideband MIMO antenna using flag-shaped stub, *Microwave and Optical Technology Letters*, *59*, 1028–1032.

[33] **Malviya, L.**, **Panigrahi, R. and Kartikeyan, M.** (2017). MIMO antennas with diversity and mutual coupling reduction techniques: a review, *International Journal of Microwave and Wireless Technologies*, *9*, 1763–1780.

[34] **Ali, W.A. and A.Ibrahim, A.** (2017). A compact double-sided MIMO antenna with an improved isolation for UWB applications, *AEU - International Journal of Electronics and Communications*, *82*, 7–13.

[35] **Sharma, Y.**, **Sarkar, D.**, **Saurav, K. and Srivastava, K.V.** (2017). Three-Element MIMO Antenna System With Pattern and Polarization Diversity for WLAN Applications, *IEEE Antennas and Wireless Propagation Letters*, *16*, 1163–1166.

[36] **Kumar, A.**, **Ansari, A.Q.**, **Kanaujia, B.K. and Kishor, J.** (2019). A novel ITI-shaped isolation structure placed between two-port CPW-fed dual-band MIMO antenna for high isolation, *AEU - International Journal of Electronics and Communications*, *104*, 35–43.

[37] **Malviya, L.**, **Panigrahi, R.K. and Kartikeyan, M.V.** (2016). A 2 x 2 Dual-Band Mimo Antenna With Polarization Diversity For Wireless Applications, *Progress In Electromagnetics Research C*, *61*, 91–103.

[38] **Sharawi, M.S.**, **Khan, M.U.**, **Numan, A.B. and Alo i, D.N.** (2013). A CSRR Loaded MIMO Antenna System for ISM Band Operation, *IEEE Transactions on Antennas and Propagation*, *61*, 4265–4274.

[39] **K. Ding**, **Gao, C.**, **D. Qu and Yin , Q.** (2017). Compact Broadband MIMO Antenna With Parasitic Strip, *IEEE Antennas and Wireless Propagation Letters*, *16*, 2349–2353.

[40] **Malviya, L.**, **Kartikeyan, M. and Panigrahi, R.** (2018). Multi-standard, multi-band planar multiple input multiple output antenna with diversity effects for wireless applications, *International Journal of RF and Microwave Computer-Aided Engineering*, *29*.

[41] **Dahlman, E.**, **Parkvall, S. and Johan, S.** (2021). *5G nr: The next generation wireless access technology*, Academic Press.

[42] **Holma, H.**, **Toskala, A. and Nakamura, T.** (2020). *5G technology 3GPP New Radio*, John Wiley & amp Sons, Inc.

[43] **Enescu, M.** (2020). *5G new radio a beam-based air interface*, Wiley.

[44] **Gurjar, R.**, **Upadhyay, D.K.**, **Kanaujia, B.K. and Sharma, K.** (2018). A novel compact self-similar fractal UWB MIMO antenna, *International Journal of RF and Microwave Computer-Aided Engineering*, *29*(3).

[45] **Bhattacharya, A.**, **Roy, B.**, **Chowdhury, S.K. and Bhattacharjee, A.K.** (2019). Computational and experimental analysis of a low-profile, isolation-enhanced, band-notch UWB-MIMO antenna, *Journal of Computational Electronics*, *18*(2), 680–688.

[46] **Das, S.**, **Chattopadhyay, K. and Bhadra Chaudhuri, S.R.** (2019). Bandwidth enhancement of a wide slot antenna using fractal geometry for UWB application with multiple notched bands, *Wireless Personal Communications*, *110*(2), 677–698.

[47] **Tripathi, S.**, **Mohan, A. and Yadav, S.** (2017). A performance study of a fractal UWB antenna for on-body WBAN applications, *Microwave and Optical Technology Letters*, *59*(9), 2201–2207.

[48] **Balanis, C.A.** (2016). *Antenna theory*, Hoboken, NJ:Wiley.

[49] **Bourke, P.** (2006). An introduction to the Apollonian fractal, *Computers and Graphics*, *30*(1), 134 –136.

[50] **Blanch, S.**, **Romeu, J. and Corbella, I.** (2003). Exact representation of antenna system diversity performance from input parameter description, *Electronics Letters*, *39*(9), 705.

[51] **Malviya, L.**, **Panigrahi, R.K. and Kartikeyan, M.V.** (2017). MIMO antennas with diversity and mutual coupling reduction techniques: A Review, *International Journal of Microwave and Wireless Technologies*, *9*(8), 1763–1780.

[52] **Sharma, Y.**, **Sarkar, D.**, **Saurav, K. and Srivastava, K.V.** (2017). Three-element MIMO antenna system with pattern and polarization diversity for WLAN applications, *IEEE Antennas and Wireless Propagation Letters*, *16*, 1163–1166.

[53] **Ali, W.A. and Ibrahim, A.A.** (2017). A compact double-sided MIMO antenna with an improved isolation for UWB applications, *AEU - International Journal of Electronics and Communications*, *82*, 7–13.

[54] **Sim, C.Y.D.** (2012). Conical Beam Array Antenna With Polarization Diversity, *IEEE Transactions on Antennas and Propagation*, *60*(10), 4568–4572.

[55] **Addaci, R.**, **Diallo, A.**, **Luxey, C.**, **Le Thuc, P. and Staraj, R.** (2012). Dual-Band WLAN Diversity Antenna System With High Port-to-Port Isolation, *IEEE Antennas and Wireless Propagation Letters*, *11*, 244–247.

[56] **Srivastava, K.**, **Kumar, A.**, **Kanaujia, B.K.**, **Dwari, S. and Kumar, S.** (2018). A CPW-fed UWB MIMO antenna with integrated GSM band and dual band notches, *International Journal of RF and Microwave Computer-Aided Engineering*, *29*(1).

[57] **Hasan, M.N.**, **Chu, S. and Bashir, S.** (2019). A DGS monopole antenna loaded with u-shape stub for UWB MIMO applications, *Microwave and Optical Technology Letters*, *61*(9), 2141–2149.

[58] **Malviya, L.**, **Panigrahi, R. and Kartikeyan, M.** (2017). A low profile planar MIMO antenna with Polarization Diversity for LTE 1800/1900 applications, *Microwave and Optical Technology Letters*, *59*(3), 533–538.

[59] **Dahlman, E.**, **Parkvall, S. and Johan, S.** (2021). *5G nr: The next generation wireless access technology*, Academic Press, an imprint of Elsevier.

[60] **Elfergani, I.**, **Hussaini, A.S.**, **Rodriguez, J. and Abd-Alhameed, R.** (2019). *Antenna Fundamentals for legacy mobile applications and beyond*, SPRINGER.

[61] **Malik, J.**, **Patnaik, A. and Kartikeyan, M.V.** (2018). *Compact antennas for high data rate communication*, Springer.

[62] **Bhattacharjee, A.**, **Bhawal, A.**, **Karmakar, A.**, **Saha, A. and Bhattacharya, D.** (2020). Vivaldi antennas: A historical review and current state of art, *International Journal of Microwave and Wireless Technologies*, *13*(8), 833–850.

[63] **Yao, Y.**, **Liu, M. and Feng, Z.** (2008). Analysis and design of ultra-wideband planar tapered slot antenna arrays, *2008 Asia-Pacific Microwave Conference*.

[64] **Zhai, G.**, **Chen, Z.N. and Qing, X.** (2015). Enhanced Isolation of a Closely Spaced Four-Element MIMO Antenna System Using Metamaterial Mushroom, *IEEE Transactions on Antennas and Propagation*, *63*(8), 3362–3370.

[65] **Costa, J.R.**, **Lima, E.B.**, **Medeiros, C.R. and Fernandes, C.A.** (2011). Evaluation of a New Wideband Slot Array for MIMO Performance Enhancement in Indoor WLANs, *IEEE Transactions on Antennas and Propagation*, *59*(4), 1200–1206.

[66] **Sarkar, D.**, **Singh, A.**, **Saurav, K. and Srivastava, K.V.** (2015). Four-element quad-band multiple-input–multiple-output antenna employing split-ring resonator and inter-digital capacitor, *IET Microwaves, Antennas & Propagation*, *9*(13), 1453–1460.

[67] **Anitha, R.**, **Sarin, V.**, **Mohanan, P. and Vasudevan, K.** (2014). Enhanced isolation with defected ground structure in MIMO antenna, *Electronics Letters*, *50*(24), 1784–1786.

[68] **Ramachandran, A.**, **Valiyaveettil Pushpakaran, S.**, **Pezholil, M. and Kesavath, V.** (2016). A Four-Port MIMO Antenna Using Concentric Square-Ring Patches Loaded With CSRR for High Isolation, *IEEE Antennas and Wireless Propagation Letters*, *15*, 1196–1199.

[69] **Sarrazin, J.**, **Mahe, Y.**, **Avrillon, S. and Toutain, S.** (2010). Collocated Microstrip Antennas for MIMO Systems With a Low Mutual Coupling Using Mode Confinement, *IEEE Transactions on Antennas and Propagation*, *58*(2), 589–592.

CURRICULUM VITAE

Name Surname: Abubeker Abdulkerim YUSSUF

EDUCATION:

- **B.Sc.** **:** 2007, International Islamic University Malaysia (IIUM), Faculty of Electrical and Computer, Department of Communications Engineering
- **M.Sc.** **:** 2011, International Islamic University Malaysia (IIUM), Faculty of Electrical and Computer, Department of Communications Engineering

PROFESSIONAL EXPERIENCE AND REWARDS:

- 2011-2012 Malaysia-Japan International Institute of Technology (MJIIT)
  Research assistance Electronic System Engineering (ESE).
- 2009-2011 Research and teaching assistant at Department of Electrical and Computer Engineering (ECE),IIUM.
- 2007-2009 Research Assistant at RF design laboratory
  Department of Electrical and Computer Engineering (ECE),IIUM.

PUBLICATIONS, PRESENTATIONS AND PATENTS ON THE THESIS:

- Yussuf, A. A., Paker, S. (2019). Design of a compact quad-radiating element MIMO antenna for LTE/Wi-Fi Application. AEU - International Journal of Electronics and Communications, 111, 152893. https://doi.org/10.1016/j.aeue.2019.152893
- Yussuf, A. A., Paker, S. (2017). Design of wideband MIMO antenna for Wireless Applications. 2017 25th Signal Processing and Communications Applications Conference (SIU). https://doi.org/10.1109/siu.2017.7960203

  *Y*ussuf, A. A., Paker, S. (2020). A Quad-Element MIMO Antenna Design using Modified Apollony-shaped Fractal for 5G Application Paper ACCEPTANCE Notification for IEEE 2020 Texas Microwave Symposium at Baylor University in Waco, Texas, USA, on April 2–3, 2020.

  *Y*ussuf, A. A., Paker, S. (2024). Dual-Band Vivaldi MIMO Antennas Designed for Sub-6 GHz 5G Wireless Applications. ACCEPTANCE Notification for 2024 International Conference on Broadband Communications for Next Generation Networks and Multimedia Applications (CoBCom).

OTHER PUBLICATIONS, PRESENTATIONS AND PATENTS:

- Yussuf, A. A., Hassan, W. H., Issa, S. (2012). A review of VHD approaches in Next Generation Wireless Networks. 2012 Second International Conference on Digital Information and Communication Technology and It's Applications (DICTAP). https://doi.org/10.1109/dictap.2012.6215376

- Islam, M. R., Yussuf, A. A., Alam, A. H. M. Z., Ismail, A. F., Chebil, J., Khan, S. (2011). Design of a passive RFID tag antenna at 2.45 GHz for mounting on various platforms. 2011 IEEE International RF Microwave Conference. https://doi.org/10.1109/rfm.2011.6168752

- Yussuf, A. A., Islam, M. R., Alam, A. H., Khalifa, O. O., Chebil, J., AbdElRaouf, H. E., Haji, I. A. (2010). Design of Multiband passive RFID tag antenna. International Conference on Computer and Communication Engineering (ICCCE'10). https://doi.org/10.1109/iccce.2010.5556824

- Haji, I. A., Islam, M. R., Alam, A. H., Khalifa, O. O., Khan, S., Abdullah, K. A., Yussuf, A. A. (2010). Design and optimization of linear array antenna based on the analysis of direction of arrival (DOA) estimation and beamforming algorithms. International Conference on Computer and Communication Engineering (ICCCE'10). https://doi.org/10.1109/iccce.2010.5556828

- Nordin, M. A., Abd El-Raouf, H. E., Yussuf, A. A. (2008). Bandwidth enhancement of a compact antenna based on the composite right/left-handed (CRLH) transmission-line (TL). 2008 International Conference on Computer and Communication Engineering. https://doi.org/10.1109/iccce.2008.4580817